## **MATERIALS** CHEMISTRY







**FRONTIERS** 

## **REVIEW**

**View Article Online** 



Cite this: Mater. Chem. Front.. 2023, 7, 3298

Received 24th February 2023. Accepted 13th April 2023

DOI: 10.1039/d3qm00188a

rsc.li/frontiers-materials

# Covalent organic frameworks in heterogeneous catalysis: recent advances and future perspective

Ziad Alsudairy, Normanda Brown, Allea Campbell, Abrianna Ambus, Bianca Brown, Kayla Smith-Petty and Xinle Li \*\*

Catalysis is ubiquitous in  $\sim$ 90% of chemical manufacturing processes and contributes up to 35% of global GDP. Hence, the development of advanced catalytic systems is of utmost importance for academia, industry, and government. Covalent organic frameworks (COFs) are a rapidly emerging class of crystalline porous materials that precisely integrate organic monomer units into extended periodic networks, offering a propitious platform for heterogeneous catalysis due to salient structural merits of ultralow density, high crystallinity, permanent porosity, structural tunability, functional diversity, and synthetic versatility. The past decade has witnessed an upsurge of interest in COFs for heterogeneous catalysis and this trend is expected to continue. In this review, we briefly introduce COF chemistry concerning the design principles, growth mechanism, and cutting-edge advances in structural evolution, linkage chemistry, and facile synthesis. We then scrutinize four leading design strategies for COF catalysts, namely pristine COFs with catalytically active backbones, COFs as hosts for the inclusion of catalytic species, COF-based heterostructures, and COF-derived carbons for thermo-, photo-, and electrocatalysis. Next, we overview the most recent advances (mainly from 2020 to 2023) of COFs in heterogeneous catalysis, along with their fundamentals and advantages. Finally, we outline the current challenges and offer our perspectives on the future directions of COFs for heterogeneous catalysis.

#### 1. Introduction

Catalysis, which was first scientifically defined by Ostwald in 1894 as the "acceleration of a slow chemical process by the presence of a foreign material", holds paramount significance in both fundamental research and industrial applications.

Department of Chemistry, Clark Atlanta University, Atlanta, Georgia 30314, USA. E-mail: xli1@cau.edu

From an economic perspective, catalysis contributes to over 35% of the world's gross domestic product (GDP), and every major innovation in catalysis has profoundly advanced global economic success. From an environmental perspective, the urgent need to address the energy crisis and unprecedented global warming necessitates the development of novel catalytic technology to sustainably produce commodity chemicals and achieve carbon neutrality by the mid-21st century.2 From a scientific perspective, catalysis research remains at the



Ziad Alsudairy

Ziad Alsudairy received his BS degree in General Chemistry from Qassim University and his MS degree in Analytical Chemistry from Clark Atlanta University. He is currently a PhD student under the guidance of Prof. Xinle Li and Prof. Conrad Ingram at Clark Atlanta University. His research focuses the expeditious synthesis covalent of organic frameworks for applications in adsorption, separation, and heterogeneous catalysis.



Normanda Brown

Normanda Brown obtained her BS degree (2021) in Chemistry with a minor in Psychology from Tougaloo College. Shecurrently a PhD student under the supervision of Prof. Xinle Li at Clark Atlanta University. Her research focuses onmechanochemical synthesis of covalent organic frameworks for environmental remediation and heterogeneous catalysis.

forefront of chemistry, physics, biology, chemical engineering, and materials science, expanding scientific understanding and resulting in nearly 20 Nobel Prizes in the field of catalysis, from the first one on fundamental catalysis principles (Wilhelm Ostwald, 1909) to the most recent one on asymmetric organocatalysis (Benjamin List and David MacMillan, 2021).

At the core of catalysis science, heterogeneous catalysis has garnered enormous attention because of its low cost, ecobenignity, high activity, selectivity, and stability, enabling facile catalyst recovery, regeneration, and sustainable manufacturing.<sup>3</sup> As a result, it plays an integral role in producing over 80% of chemical products worldwide. In the pursuit of developing high-performing heterogeneous catalysts, a broad array of porous catalytic solids has been developed, such as zeolites, mesoporous silica, activated carbons, metal-organic frameworks (MOFs), molecular cages, polymers of intrinsic microporosity (PIM), and porous aromatic frameworks (PAFs). Decades of research on these materials have furnished numerous porous catalysts that are of substantial scientific and industrial interest.

Covalent organic frameworks (COFs) are two- or threedimensional (2D or 3D) crystalline porous solids solely composed of organic building blocks via strong covalent bonds. Since their discovery in 2005, COFs have been in the limelight due to their eminent structural merits, such as ultralow density, high crystallinity, permanent porosity, skeleton modularity, and synthetic versatility, which underpin their broad applications in catalysis, gas storage, separation, chemosensing, water harvesting, drug delivery, optoelectronics, and many more.5 The field of COFs has been rapidly expanding, as evidenced by the exponential increase in annual publications in recent years (blue bar in Fig. 1). The research on COF-based heterogeneous catalysis began in 2011, with the pioneering work on COF-supported Pd(II) for the Suzuki-Miyaura coupling reaction.6 This seminal work sparked a surge of research interest in the use of COFs for heterogeneous catalysis over

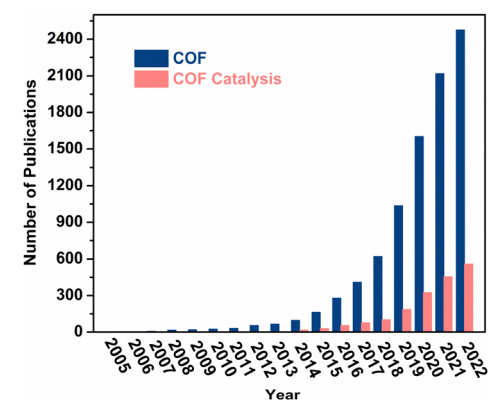


Fig. 1 Annual publications using the terms "covalent organic frameworks" and "covalent organic frameworks catalysis" from SciFinder. Data retrieved 31 December 2022

the past decade, as reflected by the steadily increasing annual publications (red bar in Fig. 1). Scheme 1 illustrates the timeline of notable advances in COF-based heterogeneous catalysis. The first thermocatalysis by pristine COF, metal nanoparticle/ COF, and 3D COF catalysts was initiated in 2011, January 2014, and February 2014, respectively. In 2014, the use of COFs was extended to asymmetric and tandem catalysis. Meanwhile, the first COF-mediated photocatalysis for hydrogen evolution was reported. With the pressing need to address the energy and environmental crisis, COFs emerged as promising catalysts for electrocatalytic CO2 reduction, biomass conversion, and biocatalysis in 2015. In 2017, COFs showed great promise in the photodegradation of water contaminants. Thereafter, the scope of catalytic reactions in COF-based thermo-, photo-, and electrocatalysis, as well as the structural diversity of COF catalysts, have expanded considerably, further underscoring the enormous potential of this rapidly evolving field.

Compared to other porous solids such as MOFs, carbons, and zeolites, COFs offer a unique set of advantages as



Allea Campbell

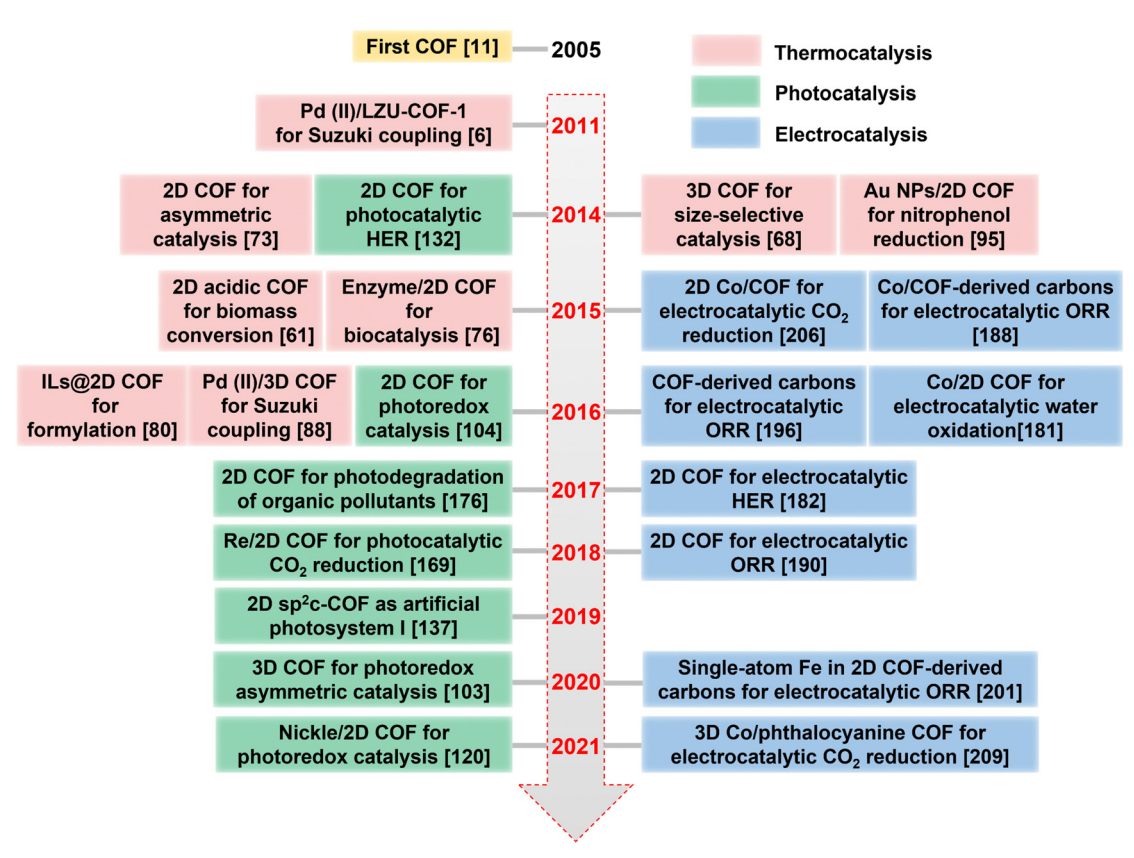
Allea Campbell received her BS degree (2017) in Inorganic Chemistry from Savannah State University. Sheis currently pursuing her PhD at Clark Atlanta University under the joint supervision of Prof. Xinle Li, Prof. Conrad Ingram, and Prof. Dinadayalane Tandabany. Her current research focuses on the synthesis of covalent organic frameworks for heterogeneous catalysis.



Xinle Li

Xinle Li earned his PhD degree (2016) from Iowa State University under the supervision of Prof. Wenyu Huang. Following this, he worked as a postdoctoral researcher in the group of Dr. Yi Liu at the Molecular Foundry in National Lawrence Berkeley Laboratory from 2017 to 2020. Не joined Clark Atlanta University in 2020 as an assistant inprofessor Department of Chemistry. His research interest currently

focuses on the synthesis of porous crystalline materials for applications in heterogeneous catalysis and environmental remediation.



Scheme 1 Timeline of noteworthy advances in COF-based heterogeneous catalysis over the past decade.

heterogeneous catalysts: (i) the exceptional structural tunability and synthetic versatility of COFs lead to a near-infinite variety of COF catalysts with high activity, selectivity, and durability; (ii) the atomically precise and regular structures of COFs enable the subtle modulation of catalytic properties at the atomic level and establish clear structure-catalysis relationships, thereby facilitating the mechanism-guided design and improvement of heterogeneous catalysts; (iii) the superb chemical stabilities of COFs ensure durable catalytic performance and catalyst recovery even under rigorous conditions; (iv) the permanent porosity and ordered nanochannels of COFs promote the mass diffusion of substrates and their ready access to active sites; (v) the conserved COF pores with amenable microenvironment such as molecular functionality, size, and chirality bestow catalytic reactions with high chemo-, size-, regio-, and enantioselectivity; (vi) the spatial arrangement of multiple catalytic sites within a single COF solid synergistically facilitate cooperative catalysis and/or tandem reactions; (vii) the ease of hybridizing COFs with other catalytically active materials allows the design of well-defined heterostructures with inherited merits from parent materials and enhanced catalytic efficiency; (viii) the ultralight COFs permit high gravimetric performance in catalysis. Taken together, these unparalleled structural merits collectively underpin the surging exploitations of COFs in heterogeneous catalysis.

To avoid duplicating several recent reviews on COF catalysis in 2020, <sup>7–10</sup> here we aim to spotlight the most recent advances in COF catalysis with a particular focus on novel COFs, outstanding catalytic performance, as well as advantages of COFs over benchmark porous solids and homogeneous catalysts. In doing so, we primarily review publications from 2020 to 2023 while acknowledging significant prior research. Firstly, we outline the design principles, growth mechanisms, and cutting-edge research frontiers of COFs. Next, we highlight the chronological milestones in the field of COF catalysis. We scrutinize leading design strategies of COF catalysts including manipulating COFs backbones, using COFs as hosts for the embedment of catalytic species, creating COF-based heterostructures, and pyrolyzing COFs into carbons. We then provide a brief overview of COFs in thermo-, photo- and electrocatalysis using up-to-date examples. Finally, we discuss current challenges and prospects for the application of COFs in heterogeneous catalysis. We anticipate that this review will stimulate further scientific endeavors in this intriguing field.

## 2. Chemistry of COFs

Assembling discrete molecular units into artificial high-ordered organic polymers has long been a substantial challenge. In 2005, Yaghi and co-workers overcame this impasse and successfully synthesized the first two COFs (COF-1 and COF-5) through the self-condensation of boronic acids or the cocondensation of boronic acids with catechols.11 COFs set them

apart from other established porous materials, such as carbons, zeolites, mesoporous silica, MOFs, and amorphous porous polymers, due to their hallmark features, including high crystallinity, ultralow density (e.g., 0.106 g cm<sup>-3</sup> for TUS-64), <sup>12</sup> large surface areas (e.g., 5083 m $^2$  g $^{-1}$  for DBA-3D-COF-1),  $^{13}$  adjustable pore aperture (e.g., 10.0 nm for TDCOF-3), 14 excellent thermal stability (e.g., 600 °C for COF-5),11 high carrier mobility (e.g., 35.4 cm<sup>2</sup> V<sup>-1</sup> s<sup>-1</sup> for NiPc-NH-CoPcF<sub>8</sub> COF), <sup>15</sup> bespoke structural backbones, and versatile synthesis methods. These unique features make COFs highly promising for diverse niche applications, particularly in heterogeneous catalysis.

#### 2.1 Design principles of COFs

COFs, often described as "Molecular Legos" and covalent analogs of MOFs, can be predicably designed by judiciously selecting geometrically defined monomers in terms of topology, dimensionality, and functionality. Depending on the extension of the covalent connectivity, COFs can be classified as 2D and 3D COFs. 2D COFs use rigid building blocks with reactive sites in a specific geometry to direct the growth of polygon skeletons via geometry matching, culminating in nine topologies, including trigonal, tetragonal, rhombic, hexagonal, and Kagome shapes. Hexagonal 2D COFs can be commonly designed using the  $[C_3 + C_2]$ ,  $[C_2 + C_2 + C_2]$ , and  $[C_3 + C_3]$ monomer combination, while tetragonal 2D COFs are generated using  $[C_4 + C_2]$  and  $[C_4 + C_4]$  combinations. To enhance the topological diversity and impart hierarchical porosity to 2D COFs, novel topologies such as heteropore COFs can be designed using desymmetrized monomers16 and multicomponent polymerization.<sup>17</sup> Unlike 2D COFs which typically demand planar building units, most 3D COFs require a tetrahedral  $(T_d)$  building block to extend the covalent connectivity in 3D. The assembly of a  $T_d$  unit with  $C_1$ ,  $C_2$ ,  $C_3$ ,  $C_4$ , and  $T_d$ symmetric building blocks yields various 3D COF topologies such as ctn (cubic-C<sub>3</sub>N<sub>4</sub>), dia (diamond), bor (boracite), pts (platinum sulfide), lon (lonsdaleite), ljh (Luojia hill), and rra topologies.<sup>18</sup> Beyond traditional T<sub>d</sub> monomers, highconnectivity monomers such as trigonal prism-shaped organic cage,  $^{19}$  6-connected  $(D_{3h})$  unit,  $^{20}$  octahedral unit,  $^{21}$  and 8connected B<sub>4</sub>P<sub>4</sub>O<sub>12</sub> cube<sup>22</sup> result in unusual 3D COF nets such as acs, stp, ceq, hea, soc, and bcu. A comprehensive topology diagram to guide the design of COFs is available in several prior reviews.23-25

#### 2.2 Growth mechanism of COFs: advancing the mechanistic understanding of COF formation

Despite enormous advances in the synthesis and application of COFs, in-depth mechanistic studies of COF formation far lag behind. It is generally accepted that dynamic covalent chemistry is essential to impart error-correction and defect-healing during COF crystallization, ultimately reaching the thermodynamic minimum of the system.<sup>26</sup> In 2014, Dichtel and coworkers conducted the first investigation into the COF growth mechanism using a prototypical boronate ester-linked COF-5 in a homogeneous solution. They found the nanocrystalline COF formed initially and then irreversibly precipitated. Later in

2016, they disclosed that imine COF first formed as an amorphous polyimine that gradually transformed into crystalline networks.<sup>27</sup> This amorphous-to-crystalline transformation was further corroborated by in situ X-ray scattering analysis and the facile synthesis of crystalline COFs from their amorphous counterparts.<sup>28</sup> In 2020, the groups of Dichtel and Marder further improved this mechanistic understanding. They demonstrated that certain 2D imine COFs formed as crystalline sheets within just 60 seconds and then rearranged into networks with greater 3D order.29 Recently in 2022, Zhao and coworkers investigated the growth process of 2D imine COFs using mass spectroscopy and density functional theory (DFT) calculations.<sup>30</sup> They proposed a template growth mechanism, in which existing COF surfaces direct the assembly and prearrangement of monomers/oligomers, which are crucial to the formation of crystalline 2D COFs. This clear mechanistic insight facilitated the growth and resolution of a singlecrystalline 2D COF by continuous rotation electron diffraction for the first time. However, most mechanistic studies have focused on boronate ester- or imine-linked COFs, while the growth mechanism of COFs with other linkage types remains scarcely explored.

#### 2.3 Structural evolution of COFs: moving from predominant 2D to 3D networks

2D COFs crystallize to form layered networks and stack through non-covalent forces, whereas 3D COFs are wholly held together by covalent bonds with interpenetrated channels. Despite the extensive study of 2D COFs, 3D COFs are of particular interest owing to ultralow density (as low as 0.106 g cm<sup>-3</sup>), large surface areas (up to 5083 m<sup>2</sup> g<sup>-1</sup>), hierarchical porosity, multifarious functionalities, and abundant open sites. However, the exploration of 3D COFs has been limited by major bottlenecks, such as limited building blocks, arduous structural determination, and crystallization issues, resulting in only ~120 structures since 2007.31 To expand the structural complexity and diversity of reticular chemistry, 3D COFs have become appealing synthetic targets in recent years and have been discussed in several latest reviews (2022).32,33 Enormous progress has been achieved in the following aspects: (i) diversifying topology of 3D COFs by using high-connectivity monomers and controlling the alignment of building units;34 (ii) rapid synthesis of 3D COFs at ambient temperature in ionic liquids (ILs);35 (iii) growing single-crystalline 3D COFs using the modulator approach<sup>36</sup> or supercritical fluid as reaction mediums;37 (iv) atomicresolution structural determination of 3D COFs with the aid of single-crystal X-ray diffraction, 3D electron diffraction, and cryo-continuous rotation electron diffraction;<sup>38</sup> (v) diverse applications in heterogeneous catalysis, polarized optics, selective gas adsorption, lithium-sulfur batteries, ion separation, and white light-emitting diodes. To fully realize the potential of 3D COFs, future research should focus on developing 3D COFs with easily accessible building blocks, unprecedented topologies, facile synthesis, minimal interpenetration, strong stability, and atomic-level structural elucidation.

# 2.4 Linkage chemistry of COFs: towards crystalline, robust, and $\pi$ -conjugated COFs

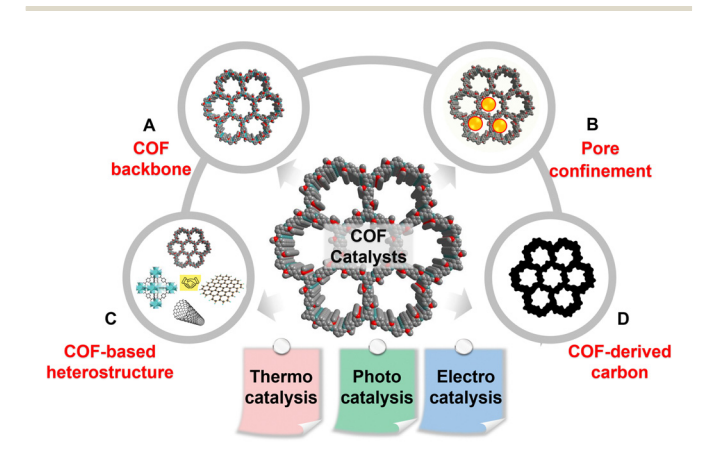
Linkages, which connect the discrete building blocks to form the extended framework, are immensely crucial for the emergent crystallinity, function, and stability of COFs. Reversible linkages, such as imine and boronate ester, have dominated the COF field due to their ability to ensure the dynamic healing of structural defects. However, dynamic linkages limit COF stability and hinder their practical implementations. Moreover, 2D COFs with imine and boronic ester linkages display inferior inplane  $\pi$ -conjugation, compromising their optoelectronic properties. To upend the stability-crystallinity dichotomy in COFs and enhance the in-plane  $\pi$ -conjugation, considerable efforts have been devoted to developing novel linkages that simultaneously impart COFs with high crystallinity, full  $\pi$ -conjugation, and superb chemical stability, 39 making linkage chemistry a frontier in the COF community. COF linkages have expanded rapidly and span boronate ester, triazine, imine, imide, hydrazone, imidazole, urea, ester, ether, aminal, pyrimidazole, indazole, cyanurate, etc. COFs with novel robust linkages are mainly developed via the following routes:40 (i) the confined synthesis of COFs on the metal surface or at the liquid-air and liquid/ liquid interfaces; 41 (ii) single-step reactions with limited reversibility; 42,43 (iii) reversible-irreversible multicomponent reactions; 44 (iv) postsynthetic modification (PSM) or exchange of labile imine linkages. 45,46 The booming linkage chemistry of COFs not only broadens the scope of reticular chemistry but also furnishes novel COFs with highly sought-after properties, including pronounced stability, improved optoelectronic properties, and unprecedented functionalities.

# 2.5 Synthetic strategy of COFs: towards rapid, facile, green, and ambient synthesis

COF synthesis has dominantly relied on the solvothermal protocol, which often involves lengthy reaction times (3-9 d), sealed pressurized vessels under vacuum or inert conditions, the use of hazardous organic solvents, and elevated synthetic temperatures (80-200 °C), all of which limit the full potential of COFs. As such, the rapid, facile, green, and ambient synthesis of high-quality COFs has been extensively pursued in recent years. These viable strategies mainly include: (i) employing new energy sources such as mechanical agitation,<sup>47</sup> ultrasound,<sup>48</sup> microwave, 49 and electron beam 50 to replace conventional thermal heating; (ii) developing novel catalysts such as metal triflates, 51,52 and Brønsted base 53 instead of traditional acetic acid; (iii) deploying new reaction mediums such as water,54 ILs, 35 CO<sub>2</sub>/water, 55 and ZnCl<sub>2</sub>/eutectic salt 66 in place of noxious organic solvents; (iv) restricting the bond rotation in monomers to minimize structural errors in COF formation;<sup>57</sup> (v) using supercritical CO2 instead of vacuum activation to minimize the structural collapse of COFs during the workup process.<sup>58</sup> Two recent reviews on the expeditious synthesis (2020),59 and ambient synthesis of COFs (2021)60 offer more details on these developments. The significant progress in COF synthesis calls for continued scientific efforts towards the rapid synthesis of COFs with broad generality, pronounced stability, scalability, mild reaction condition, and a clear growth mechanism.

# General design principles of COF catalysts

COFs offer a versatile material platform to design tailor-made heterogenous catalysts for thermo-, photo-, and electrocatalysis. The immense structural and functional diversity empowers the precise installation of targeted catalytic sites into COFs, resulting in solids with tailored catalytic activities. To date, four prevalent strategies exist for the fabrication of COF catalysts (Scheme 2). First, the COF backbone, including the linkage and functionalized pore walls, can serve as intrinsic catalytic centers for thermocatalysis. Additionally, the ordered columnar  $\pi$ arrays in 2D COFs facilitate the transport of exciton, electron, and charge carriers, enabling the design of metal-free COF catalysts in photo- and electrocatalysis (Scheme 2A). Second, the well-defined regular pores of COFs enable the inclusion of diverse catalysts, ranging from single atoms, metal complexes, and clusters, to metal nanoparticles and enzymes. Much more attractive, the atomically precise pore environment, such as pore size, shape, functionality, chirality, and wettability, can be accurately modulated to steer the catalytic behaviors of encapsulated catalysts at the atomic level, resulting in optimal catalytic performances (Scheme 2B). Third, COFs can be hybridized with diverse functional materials and combine the structural attributes of each component. The resultant COF-based heterostructures, exemplified by ILs/COF, MOF/COF, and graphene/COF hybrids, hold enormous prospects in heterogeneous catalysis due to their synergistically augmented properties over the catalytic individual components (Scheme 2C). Finally, to address the limitations of inferior stability and conductivity in pristine COFs, COF-derived carbons can be readily formed via pyrolysis and have gained growing popularity in electrocatalysis under aqueous acidic/ alkaline environments (Scheme 2D).



Scheme 2 Leading design principles of COF catalysts for thermo-, photo-, and electrocatalysis: (A) COF backbone, (B) pore confinement, (C) COF-based heterostructure, and (D) COF-derived carbon.

## 4. Thermocatalysis in COFs

#### Advantages of COF in thermocatalysis

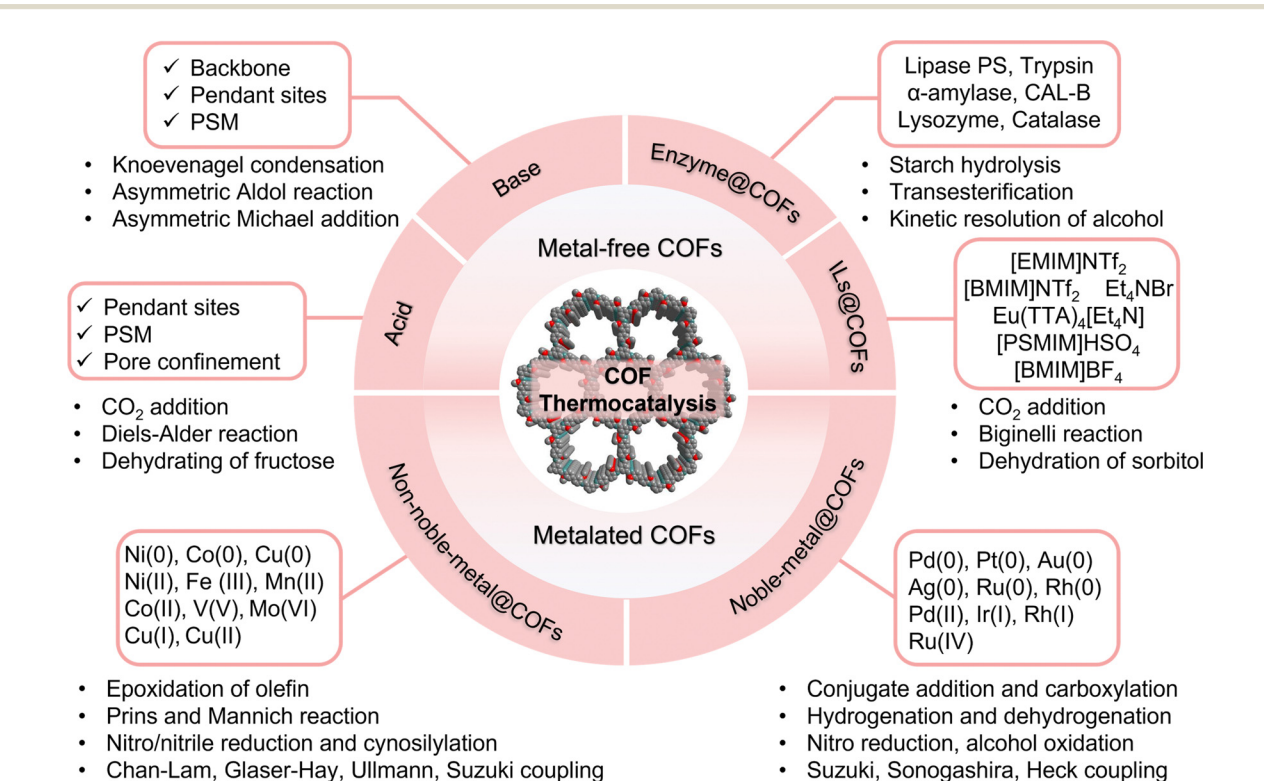
COFs have emerged as compelling heterogeneous catalysts for thermocatalysis due to their ability to combine the merits of both homogeneous and heterogeneous catalysts, resulting in high reactivity, selectivity, and recyclability. Notably, COF catalysts possess the following unique features: (i) the highly adaptable COFs enable the incorporation of target-specific active sites onto the backbone through de novo synthesis, PSM, and pore encapsulation, giving rise to a wide range of heterogeneous catalysts; (ii) the conserved pore spaces of COFs induce nano-confinement effects to enhance catalysis; (iii) the high porosity and regular nanochannels facilitate the adsorption and enrichment of substrates, promoting the catalytic site-reactant interaction and maximizing the catalytic efficiency; (iv) the thermal and chemical stability of COFs ensures durable catalytic performance, a prerequisite for real-world application; (v) the precise and tailorable structure of COFs enable the understanding of the underlying catalytic mechanism through structure-catalysis correlations, accelerating the design of on-demand heterogeneous catalysts.

In the following section, we have classified COF catalysts into three categories: metal-free COFs (acid, base, enzyme/COF, ILs/COF), non-noble metal/COFs, and noble metal/COFs, as illustrated in Scheme 3. We will briefly discuss the primary design strategies of COF catalysts in thermocatalysis and scrutinize pertinent examples reported recently.

#### 4.2 Metal-free COFs for thermocatalysis

4.2.1 COFs as solid acids. Acid-catalyzed reactions represent a vital paradigm of organic transformation in heterogeneous catalysis and have spurred enormous progress in the development of robust solid acid catalysts, which are vastly applied in an assortment of reactions such as biomass conversion, esterification, silvlation, acetylation, and more. COFs offer great potential as solids acid catalysts and their acidic sites can be introduced by three main routes: (i) de novo synthesis using monomers with intrinsic acidic sites, (ii) tethering acidic sites onto COF backbones via PSM, and (iii) encapsulating acids into COF pores. These strategies enable the customization of COF acidity to suit specific catalytic applications.

COF with intrinsic acidic backbones. COF catalysts with intrinsic acidic backbones can be synthesized de novo by using monomers containing acidic sites. The first example of using an acidic COF as a Brønsted acid solid catalyst was demonstrated by Zhao and co-workers in 2015, in which they synthesized a sulfonic acid-containing 2D COF for the dehydration of fructose to 5-hydroxymethylfurfural.<sup>61</sup> Following the analogous strategy, Dong and co-workers recently developed an acidic chiral 2D COF, (R)-CuTAPBP-COF, by linking an (R)-1,1'binaphthol (BINOL)-phosphate monomer bearing Lewis acidic BINOL and Brønsted phosphoric acid sites with a Cu(II)porphyrin monomer in 2022.62 Thanks to its inherent Brønsted/Lewis acidic sites and chiral pore confinement, the resulting COF displayed high activity (98%), enantioselectivity (95% ee), and broad substrate scope in the asymmetric



Scheme 3 Leading design strategies and notable examples of COF catalysts for thermocatalysis.

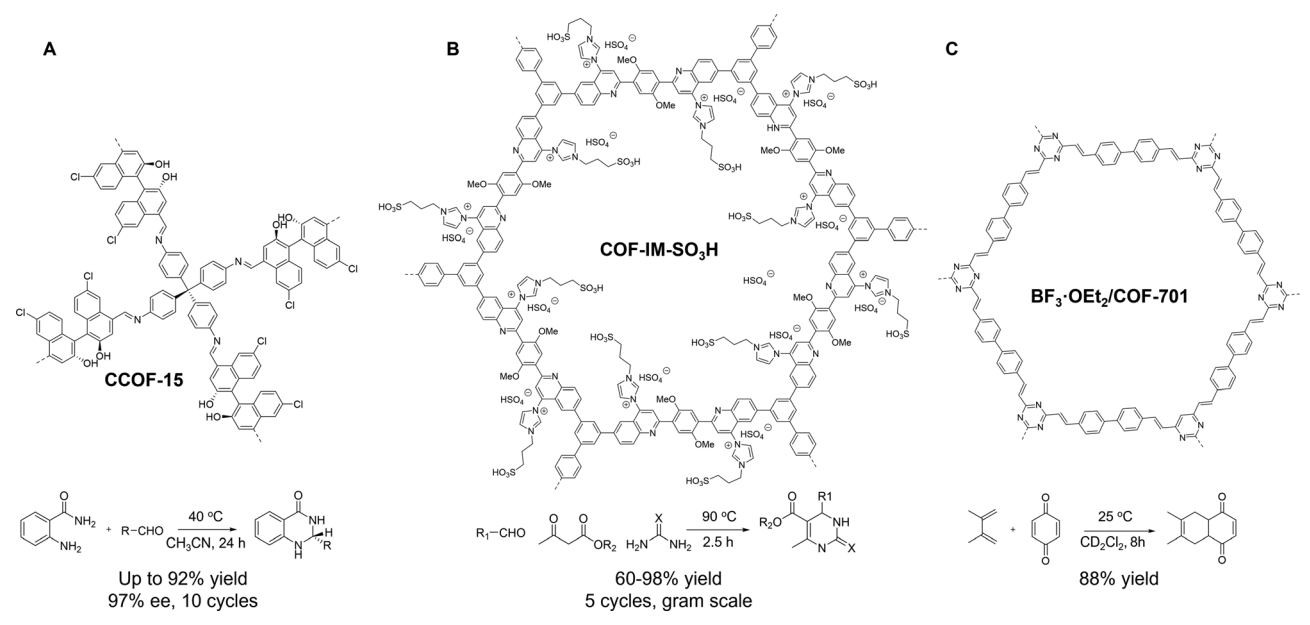


Fig. 2 Schematics of (A) 3D CCOF-15 with chiral acidic linkers, (B) COF-IM-SO $_3$ H made via PSM, (C) BF $_3$ ·OEt $_2$ /COF-701 as solid acids for thermocatalysis.

 $\alpha$ -benzylation of aldehydes with alkyl halides via photothermal conversion, outperforming the homogeneous Cu(II)-TAPP and (R)-BINOLPA-DA catalysts. A leaching test and recycling experiment confirmed the heterogeneity nature of (R)-CuTAPBP-COF, as the COF catalyst retained high activity and structural integrity after 5 catalytic cycles. Furthermore, (R)-CuTAPBP-COF was capable of catalyzing gram-scale enantioselective a-benzylation of propanal in high yield (93%) and enantioselectivity (93%), revealing its immense potential in practical catalysis. Notably, switching the chirality of the COF catalyst to (S)-CuTAPBP-COF led to a drastic change in the chirality of the product, suggesting that the COF catalyst can provide exquisite control over the catalytic outcomes in heterogeneous asymmetric catalysis.

Compared to 2D COFs, 3D acidic COFs are of great interest but have been less studied. In 2021, Cui and co-workers developed a pair of chiral 3D COFs, CCOF-15, and CCOF-16 (Fig. 2A), which contain acidic BINOL sites. These COFs were prepared by Schiff-base condensation of tetra(p-aminophenyl) methane and two BINOL-based chiral linkers with different lengths. The resulting isoreticular chiral COFs were highly crystalline with 9-fold and 11-fold interpenetrated diamondoid frameworks. The periodic arrangement of BINOL Brønsted acid sites within the 3D COFs engendered much stronger Brønsted acidity than those of homogenous acidic monomers, as confirmed by the Hammett indicator method. CCOF-15 with smaller pores was highly effective in the asymmetric acetalization of aldehydes and anthranilamides, with yields of up to 91% and 97% ee after 24 hours at 40  $^{\circ}\text{C}.$  In contrast, CCOF-16 with larger channels manifested much lower enantioselectivity. Furthermore, free homogeneous BINOL monomers exhibited no enantioselectivity and/or low activity, highlighting the superiority of chiral COFs over homogeneous counterparts in

asymmetric catalysis. To account for the catalytic difference, DFT calculations indicated that 3D COFs catalysts provide preferential secondary interactions between the substrate and framework, leading to enantioselectivities that are otherwise not accessible in homogeneous systems. Despite the remarkable progress made, the *de novo* synthesis of novel acidic COFs may still encounter challenges in crystallization. Moreover, the limited availability of acidic monomers could pose a significant barrier to the wide use of these materials.

Acidic COFs via PSM. To overcome the drawbacks mentioned above, the PSM strategy provides a facile way to incorporate acidic sites onto the backbone of pre-formed COFs. 63 Instead of attaching acid sites into the organic linkers, Dong and coworkers introduced an imidazole group in the linkage of a quinoline-linked COF via a one-pot multicomponent reaction, wherein imine was formed first, succeeded by Povarov reaction between the imine and 1-vinylimidazole.<sup>64</sup> The imidazole was then post-modified with 1,3-propane sultone to yield a sulfonic acid-decorated COF-IM-SO<sub>3</sub>H (Fig. 2B), which served as an efficient Brønsted acid catalyst for the Biginelli reaction under solventless conditions. COF-IM-SO<sub>3</sub>H achieved high yields, turnover frequency, recyclability (5 cycles), and wide substrate scope, placing it among the best catalysts for heterogeneous Biginelli reactions. The outstanding activity was attributed to the densely distributed sulfonic acid sites and the large surface area of COF-IM-SO<sub>3</sub>H. Importantly, a fixed-bed reactor based on the COF-IM-SO<sub>3</sub>H/chitosan aerogel was designed for a gramscale Biginelli reaction and achieved a 93% isolated yield of the target product (73.9 g) within 6 hours, demonstrating the tremendous potential of COFs in the practical catalysis. Grafting acidic sites directly onto COF linkages via multicomponent reaction not only reinforces the chemical stability but also

tailors the pore surface of COFs for targeted catalysis, 65 which merits more scientific attention in the future.

Acidic COFs via pore confinement. The design of solid acid catalysts can be achieved by encapsulating acidic species inside the pores of porous materials.<sup>66</sup> In a pioneering work (2019), Yaghi and co-workers demonstrated the immobilization of a strong Lewis acid, BF<sub>3</sub>·OEt<sub>2</sub>, into an unsubstituted sp<sup>2</sup> carbon-conjugated COF (sp<sup>2</sup>c-COF, COF-701, Fig. 2C), which was synthesized by the acid-catalyzed Aldol condensation between 2,4,6-trimethyl-1,3,5-triazine and 4,4'-biphenyldicarbaldehyde.<sup>67</sup> The sp<sup>2</sup> C=C linkages substantially improved the chemical stability of COF-701, enabling the non-covalent inclusion of BF<sub>3</sub>·OEt<sub>2</sub> inside the COF pore with the perseverance of crystallinity. BF3·OEt2/COF-701 retained 86% of the activity of free BF<sub>3</sub>·OEt<sub>2</sub> in a benchmark Diels-Alder reaction. However, this strategy remains relatively unexplored, as encapsulating acids may impair the structural integrity of COF hosts due to their dynamic linkages. To tackle this challenge, researchers can either use more chemically robust COFs as hosts or weaker acids. Further studies in this direction hold great promise for designing more efficient and stable solid acids.

4.2.2 COFs as solid bases. Solid base catalysts are central to numerous organic reactions, including alkylation, isomerization, alcohol dehydration, Michael addition, transesterification, and others, which are essential for the synthesis of fine chemicals. COF-derived solid base catalysts can be made by two main approaches: (i) de novo synthesis of COFs with intrinsic basic backbones and pendant groups, and (ii) the grafting of basic functionalities onto COFs via the PSM approach.

COFs with intrinsic basic backbones. COFs with intrinsic basicity can be conveniently designed de novo using Ncontaining building blocks. The inbuilt N-rich linkages (e.g.,

imine and amine) and aromatic skeleton (e.g., pyridine and porphyrin) can act as basic sites for thermocatalysis. 68,69 For example, in 2021, Beyzavi and co-workers used H<sub>3</sub>PO<sub>3</sub> as a bifunctional catalytic/reducing agent to prepare a 2D aminelinked porphyrin COF (COF-366-R, Fig. 3A) by the tandem condensation-reduction reaction between 5,10,15,20-tetra(4aminophenyl)porphyrin and terephthalaldehyde. 70 Thanks to the improved chemical stability and Lewis basicity endowed by amine linkage, COF-366-R catalyzed Knoevenagel condensation between benzaldehyde and malononitrile with good yields (62-97%), wide substrate scope, and superb recyclability, outperforming its imine COF analog, which structurally degraded under identical condition. Apart from using the Schiff-base linkage as a basic site, the N-doped aromatic skeleton can offer a viable option. In 2022, Zhang and co-workers constructed two pyridine-containing sp<sup>2</sup>c-COFs by a quaternization-promoted Knoevenagel condensation of 2,4,6-trimethylpyridine (TMP) and aryl aldehydes in the presence of acylating reagents, which converted TMP into electron-withdrawing alkylated pyridinium for efficient polycondensation.<sup>71</sup> The resultant sp<sup>2</sup>c-COFs are highly crystalline and porous (1915 m<sup>2</sup> g<sup>-1</sup> and 1345 m<sup>2</sup> g<sup>-1</sup>). Importantly, the abundant pyridine sites within the backbone of sp<sup>2</sup>c-COFs enabled active esterification of salicylic acid and acetic anhydride with high yields, selectivity, and recyclability (5 cycles). Notably, sp<sup>2</sup>c-COFs afforded higher yields than those of the pyridine-based small molecule catalysts and amorphous polymer counterparts. Furthermore, the catalytic use of two sp<sup>2</sup>c-COFs can be extended to the esterification of essential pharmaceutical intermediates with high yields and recyclability.

COFs with intrinsic basic pendant groups. In addition to the intrinsic basicity arising from the COF backbone, pendant groups in organic linkers can also introduce basicity. This strategy has been widely used for the construction of chiral COFs as solid bases in asymmetric catalysis, which is of utter

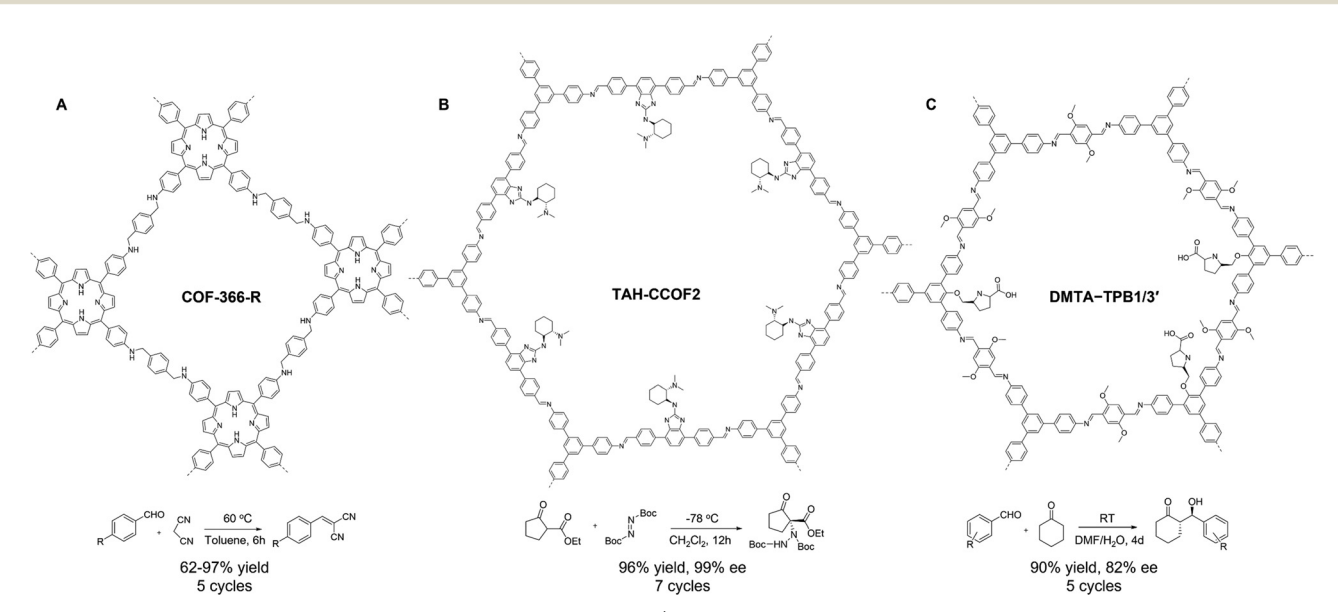


Fig. 3 Schematics of (A) COF-366-R, (B) TAH-CCOF2, (C) DMTA-TPB1/3' as solid bases for thermocatalysis.

interest to fundamental synthetic chemistry and the pharmaceutical industry. In 2019, Wang and co-workers disclosed a divergent strategy to construct a series of chiral 2D COFs with analogous structures but diverse functionalities.<sup>72</sup> The key to this strategy lies in the design of a highly modular platform molecule, 4,7-dibromo-2-chloro-1*H*-benzo[*d*]imidazole, which underwent various organic transformations to generate a library of ditopic aldehydes with diverse chiral functionalities. The covalent assembly of ditopic aldehyades and tritopic 1,3,5tris(4-aminophenyl)-benzene gave rise to nine chiral COFs bearing basic pendant groups, which were implemented as solid bases for asymmetric amination reaction. COFs with pendant tertiary-amine groups (TAH-CCOF2, Fig. 3B) and Hbonding sites manifested high yield (96%), exceptional enantioselectivity (99% ee), good recyclability (7 cycles), and broad substrate scope, outperforming the homogeneous controls. This superior catalytic performance was ascribed to the weakened intermolecular H-bonding facilitated by the COF catalyst. This approach significantly expands the structural diversity of chiral COFs and offers an auspicious platform to precisely correlate COF structure to asymmetric catalysis at the atomic level.

Basic COFs via PSM. The aforementioned de novo synthesis of COFs with monomers bearing bulky basic functionalities can be challenging, as these monomers may hinder the crystallization of COFs or be incompatible with COF synthesis. To circumvent this dilemma, basicity can be introduced into COFs through the PSM approach.73 In 2017, Cui and co-workers prepared a series of multivariate imine COFs by condensing bare triamine, tert-butyloxycarbonyl (Boc)-protected triamine, and dialdehyde. Upon the post-deprotection to remove the N-Boc and Me protecting groups in the triamines, a series of 2D chiral COFs bearing L-pyrrolidine and L-imidazolidines were derived.<sup>74</sup> In contrast, de novo synthesis using unprotected triamines failed to crystallize COFs. The resultant COF solid bases (Fig. 3C) were highly active and selective in three asymmetric reactions, including aminooxylation, Aldol condensation, and Diels-Alder reaction, surpassing their homogeneous analogs in terms of stereoselectivity and diastereoselectivity. Moreover, these COFs were highly recyclable, retaining their activity and enantioselectivity for up to 5 cycles.

4.2.3 Enzyme/COF biocatalysts. Enzyme catalysis has been the topic of active investigation recently, as it offers a sustainable means of chemical transformation with significantly accelerated reaction rates of over 1017-fold under mild conditions.<sup>75</sup> However, cell-free enzymes face limitations such as instability, low recyclability, and non-processability. To circumvent these challenges, COFs have emerged as potent supporting matrices for enzyme immobilization. In 2015, Banerjee and co-workers reported the first use of a hollow COF sphere to host trypsin for biocatalysis.<sup>76</sup> Since then, a plethora of enzyme/COF biocomposites has been developed through physical adsorption and covalent immobilization, paving promising pathways for the design of customized biocatalysts for numerous reactions. These biocomposites have shown

remarkable enzymatic activity in various reactions such as starch hydrolysis, hydrolysis of methyl ester, transesterification, etc. (Scheme 3).77

Traditional immobilization of enzymes in COFs typically suffers from drawbacks such as insufficient conformational freedom, slow mass transfer, low loading, and high leaching. To this end, Chen and co-workers (2020) designed a series of customizable hollow COF capsules for enzyme immobilization.<sup>78</sup> They first encapsulated enzymes (BSA and catalase) within digestible MOF cores (ZIF-90), accompanied by the ambient growth of hydrazone COF shells (COF-42). The resulting COF capsules were further modified by chemically etching the MOF cores under an acidic phosphate buffer solution to unleash the enzymes within the hollow COF capsule. Importantly, the pore sizes, thickness, and dimensions of COF shells can be facilely tuned. In addition, the novel COF capsules provided commodious environments for the optimal and robust enzymatic activities of the encapsulated enzyme, exceeding that of benchmark porous materials such as SBA-15.

In 2022, the same group devised a facile strategy to fabricate robust immobilized biocatalysts via in situ assemblies of lipase with COFs under ambient conditions.<sup>79</sup> They added the enzyme solution to an aqueous solution containing COF precusors and then introduced an acetic acid catalyst, which resulted in the rapid synthesis of enzyme@COF composites at room temperature. Impressively, this method was eco-friendly (aqueous medium), expeditious (10-30 minutes), scalable (~2.3 g per reaction), and highly amenable to plentiful enzyme/COF systems. More importantly, the obtained lipase/COF biocatalysts displayed salient reactivity and reusability (15 cycles) towards the hydrolysis of Aspirin methyl ester, superior to free enzymes or traditional lipase/MOF systems. This strategy shows tremendous potential for industrial enzyme applications.

4.2.4 Ionic liquids/COFs. Ionic liquids (ILs) are a unique class of nonmolecular solvents with remarkable physicochemical properties, such as high heat conductivity, high polarity, negligible vapor pressure, and superb thermal and electrochemical stability. Since the first attempt in 2016,80 composites of ILs with COFs (ILs/COFs) have garnered prominence for heterogenous catalysis, such as CO2 fixation, sorbitol dehydration, and Biginelli reaction (Scheme 3). The synthesis of ILs/COFs hybrid catalysts typically involves (i) covalent immobilization of ILs on the pore walls of COFs via PSM, (ii) de novo synthesis using IL-decorated monomers, (iii) post-impregnated confinement, and (iv) one-pot synthesis.81 These approaches have enabled the development of ILs/COFs catalysts with remarkable catalytic properties and improved stability.

In 2020, Cai and co-workers grafted an IL, 1-alkyl-3methylimidazolium bromide onto the pore walls of 2D porphyrin COF via a post-nucleophilic substitution reaction between phenolic hydroxyl-decorated COF and 1-alkyl-3methylimidazolium.82 1H NMR spectroscopy indicated that  $\sim$  16 mol% 1-methylimidazole was grafted onto the COF. The resulting imidazolium-salt-functionalized COFs were highly active (91-95% conversion) and selective in the cyclization reaction of CO2 and various substituted epoxides at 120 °C,

1.0 MPa CO<sub>2</sub>, which outperformed the non-functionalized COF and blank sample. Moreover, the COF catalyst can be reused for 5 consecutive cycles with retained porosity. Aside from CO<sub>2</sub> epoxidation, ILs/COFs composites were also effective in biomass upgrading. In 2021, Zhang and co-workers developed a series of ILs/COFs composites (PIL-COFs) via the postmodification of vinyl-decorated multivariate COFs with 4-vinyl benzyl chloride, followed by quaternization with tertiary amines.83 The resultant PIL-COFs with tunable amounts of basic ILs retained crystallinity and porosity. When used to catalyze the dehydration of sorbitol into isosorbide at 140 °C, PIL-COF-0.33 outperformed individual components and previously reported mesoporous PIL counterparts in terms of yields and catalytic efficiency, presumably due to uniform pore sizes and flexible linear catalytic chains. In addition, the robust PIL-COF-0.33 can be facilely recovered and reused for 10 cycles without significant loss of reactivity. Despite these advances, the use of ILs/COFs composites in heterogeneous catalysis is still in its infancy. As a result, expanding the ILs/COFs portfolio and catalytic scope will be crucial in unlocking their enormous potential in heterogenous catalysis.

#### 4.3 Metalated COFs for thermocatalysis

Homogeneous metal complexes are indisputably essential catalysts but are plagued by difficulty to reuse and rapid intermolecular deactivation. To overcome these limitations, the immobilization of homogeneous complex catalysts into porous materials has been a theme of extensive research. COFs, which possess open pore spaces and periodically arranged metal chelating sites, such as nitrogen, thiol, hydroxyl, Nheterocyclic-carbene, and alkynl, have emerged as promising scaffolds for encapsulating metal species, leading to numerous metalated COFs as heterogenous catalysts for thermocatalysis (Scheme 3). Depending on the precious nature of encapsulated

metals, we have categorized metalated COFs into two main types, i.e., non-noble metal/COF and noble metal/COF.

4.3.1 Non-noble metal/COFs. Non-noble metal catalysts are highly sought after due to their cost-effectiveness, high abundance, ease of scalability, and high space-time yields. Nonnoble metal/COF systems combine the merits of each component and represent a promising class of heterogeneous catalysts. Since 2014, a variety of earth-abundant metal species such as Mo, Ni, Fe, Mn, Co, V, Cu, and CdS have been immobilized within COFs, functioning as promising heterogeneous catalysts for ample reactions including the oxidation of olefin, Chan-Lam, Suzuki-Miyaura, Ullmann coupling, alcoholysis of epoxides, Prins reaction, nitro reduction, Mannich reaction, and more (Scheme 3 and Table 1).84,85

In 2020, McGrier and co-workers synthesized a 2D azinelinked COF with triangular macrocycle dehydrobenzoannulene (DBA) units, which acted as the solitary binding site to complex with Ni(0) through a simple solution impregnation method (Fig. 4).86 The resulting Ni-DBA-COF contained up to 8.56 wt% of Ni while retaining its crystallinity and porosity. Notably, Ni-DBA-COF reductively cleaved the C-S bond of several aryl thioethers at 140 °C, exhibiting yields of 22-87%, broad functional group tolerance, and high recyclability up to 5 cycles. Importantly, these activities were better or comparable to homogeneous catalyst Ni-DBA and previously reported Nibased homogeneous catalysts. However, the laborious synthesis of DBA limits its wide application. To facilely encapsulate metal species in COFs, Tang and co-workers prepared a defective 2D imine COF (COF-LZU1) by introducing a monodentate monomer, protocatechualdehyde, into the skeleton of COF through a facile one-pot condensation.87 The resulting defective COF-LZU1-OH contained abundant free hydroxy groups that can chelate with active Fe(III). The metaled COF-OFe was used to catalyze the alcoholysis of epoxides, showing a high

Table 1 Summary of the recent representative metal/COFs for thermocatalysis

| COFs                 | Linkage          | Metal          | Reaction                         | Condition                                | Yield                      | Recyclability      | Year | Ref. |
|----------------------|------------------|----------------|----------------------------------|--|----------------------------|--------------------|------|------|
| CCOF 19              | Imine            | Ir             | Asymmetric hydrogenation of      | RT, toluene                              | 72 h, up to 98%, up to 98% | 10 Cycles          | 2023 | 89   |
|                      |                  |                | quinolines                       | 1 bar H <sub>2</sub>                     | ee                         |                    |      |      |
| CCOF 20              |                  | Ru             | Asymmetric hydrogenation of      | 80 °C, EtOH, 2 bar                       | 5 d, up to 98%, up to      |                    |      |      |
|                      |                  |                | β-keto ester                     | $H_2$                                    | 99.9% ee                   |                    |      |      |
| Bth-Tp-COF           | Hydrazone        | Pd(II)         | Suzuki-Miyaura coupling          | 100 °C, dioxane/<br>H <sub>2</sub> O     | 20 min, 95–99%             | 5 Cycles           | 2023 | 90   |
| IISERP-COF15         | Imine            | Cu NPs         | Ullmann coupling                 | 135 °C, DMF                              | 24 h, 80-100%              | 3 Cycles           | 2022 | 85   |
| TTA-DFB              | Imine            | Pd(II)         | Suzuki-Miyaura coupling          | 150 °C, <i>p</i> -xylene                 | 2 h, 97%                   | 3 Cycles           | 2022 | 91   |
| (S)-NHC-Au-SA-       | Imine            | Au(ı)          | Oxidation-Aldol asymmetric relay | RT, air, toluene                         | 36 h, 69-90%, 91-95% ee    | 5 Cycles           | 2022 | 92   |
| COF                  |                  |                | reaction                         |  |                            |                    |      |      |
| Py-COF               | Imine            | Pd NPs         | Hydrogenation                    | 40 °C, EtOH, 10 bar                      | 0.75-10 h, 52-99%          | 4 Cycles           | 2022 | 100  |
| •                    |                  |                | -                                | $H_2$                                    |                            |                    |      |      |
| ТрВру                | Keto-            | Ag NPs         | Carboxylation of phenylacetylene | 60 °C, CO <sub>2</sub> , DMSO            | 6 h, 93%                   | 5 Cycles           | 2021 | 96   |
|                      | enamine          |                | with CO <sub>2</sub>             |  |                            |                    |      |      |
| NHC-COF              | Imine            | Au(ı)          | Carboxylation of phenylacetylene | 60 °C, H <sub>2</sub> O                  | 20 h, 99%                  | 5 Cycles           | 2020 | 93   |
|                      |                  |                | with CO <sub>2</sub>             |  |                            |                    |      |      |
| COF-DB               | Hydrazone        | Pd(II)         | Suzuki–Miyaura coupling          | 80 °C, EtOH-H <sub>2</sub> O             | 0.5 h, 95-99%              | 4 Cycles           | 2020 | 94   |
| Phos-COF-1           | Imine            | Au NPs         | Nitrophenol reduction            | RT, NaBH <sub>4</sub> , H <sub>2</sub> O | 2 h, 99%                   | 5 Cycles           | 2020 | 97   |
| TpBD-Me <sub>2</sub> | Keto-<br>enamine | $RuO_2$<br>NPs | Formic acid dehydrogenation      | 125–200 °C                               | 50%                        | 120 °C for 25<br>h | 2020 | 98   |
| COF-QA               | Hydrazone        | Pd NPs         | Suzuki-Miyaura coupling          | 50 °C, air H <sub>2</sub> O              | 6 h, >99%                  | 10 Cycles          | 2020 | 99   |
| DBA-COF-5            | Azine            | Ni(0)          | Aryl C–S bond cleavage           | 130 °C, toluene                          | 14 h, 2-87%                | 5 Cycles           | 2020 | 86   |
| LZU-COF              | Imine            | Fe(III)        | Alcoholysis of epoxides          | RT, CH <sub>3</sub> OH                   | 15 min, > 99%              | 5 Cycles           | 2020 | 87   |

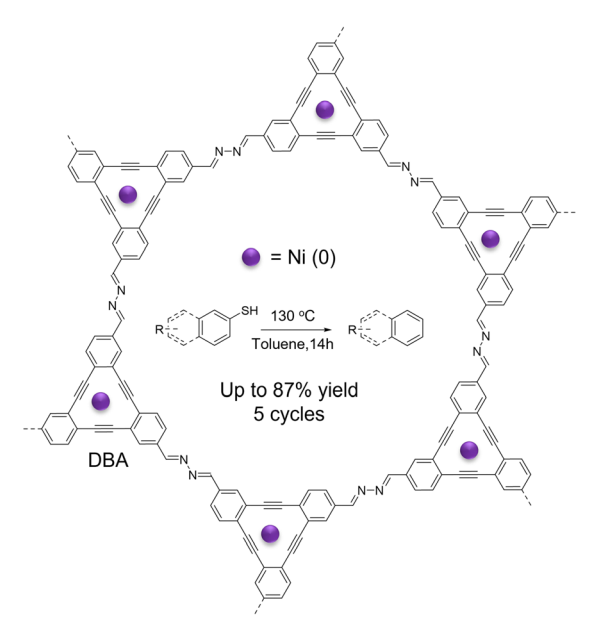


Fig. 4 Schematic of a Ni-doped dehydrobenzoannulene (DBA)containing COF for the reductive cleavage of aryl C-S bonds.

yield of >99% in just 15 minutes at room temperature and a remarkable TOF of 154 h<sup>-1</sup>. The strategy paves a facile route to incorporating desired chelating sites into COFs to immobilize metal complexes for heterogeneous catalysis.

4.3.2 Noble metal/COFs. The first use of 2D and 3D COFsupported noble metal for heterogeneous catalysis was reported in 2011 and 2016, respectively. A 2D imine COF (COF-LZU1)<sup>6</sup> and 3D imine COF (COF-300)<sup>88</sup> were employed as scaffolds to host palladium acetate for the Suzuki-Miyaura coupling reaction, with the imine linkages serving as anchoring sites for the immobilization of Pd(II) species. The adjustable skeletons and open pores of COFs facilitate the incorporation of various noble metal complexes, such as Ir,89 Ru, Pd,90,91 and Au, 92,93 which demonstrate efficient and recyclable catalytic performance in several reactions including hydrogenation, oxidation, Suzuki-Miyaura cross-coupling, carboxylation, etc. (Table 1). In 2020, Zhao and co-workers prepared two 2D hydrazone COFs with multiple supramolecular interactions, including inter-, intramolecular H-bonding, and electrostatic interactions,94 which exerted a profound influence on the physicochemical properties of COFs. Moreover, the hydrazone COF could chelate up to seven divalent transition metal ions, exhibiting enhanced crystallinity and stability over the pristine COF. Notably, the dynamic coordination bonding nature of the COF enabled the targeted installation of Pd(II) ions via a postsynthetic exchange at ambient conditions. The resulting Pd(II)/COF displayed high catalytic reactivity (95-99% yields) and recyclability (4 cycles) for the Suzuki-Miyaura crosscoupling reaction between various aryl bromides and phenylboronic acid, outperforming the Pd(II)/amorphous counterpart.

Apart from metal complexes, metal nanoparticles (NPs) are of paramount fundamental and applied interest in heterogeneous catalysis. The use of COFs as support for metal NPs has

gained increasing interest due to the precise control of the size, dispersion, and surrounding environment of NPs for efficient and synergistic catalysis.95 Various noble metal NPs including Au, Ag, Pd, Pd, Rh, Ru, and Ir NPs have been immobilized within COFs for a wide range of catalytic reactions, such as formic acid dehydrogenation, nitrophenol reduction, carboxylation, conjugate addition, Suzuki, Sonogashira, and Heck coupling reactions (Scheme 3 and Table 1). 96-98 In the pursuit of more active noble metal NPs/COF catalysts, Dong and coworkers encapsulated small Pd NPs (~2.4 nm) into paraffinchain quaternary ammonium salt-decorated hydrazone COF (Pd/COF-QA, Fig. 5) via an in situ reduction approach, in which the free-end formamide groups on COF served as reducing agent.99 Pd NPs/COF-QA functioned as a highly active phase transfer catalyst for the aqueous Suzuki-Miyaura coupling reaction at 50 °C for 6 hours, outperforming Pd NPs supported by quaternary ammonium-free COF and COF with a shorter quaternary ammonium chain. The heterogeneity of Pd NPs/ COF-QA was confirmed by the leaching and recycling tests (10 cycles). Remarkably, Pd/COF-QA represents a rare heterogeneous catalyst that displayed high activity (99%) for the challenging chlorobenzene-based Suzuki-Miyaura coupling reaction at mild conditions. Of particular interest, Pd NPs/ COF-QA/chitosan aerogel monolith retained high activity (88%) and cyclic stability (3 cycles) in a continuous gram-scale coupling reaction between chlorobenzene and phenylboronic acid, revealing its great potential for practical catalysis.

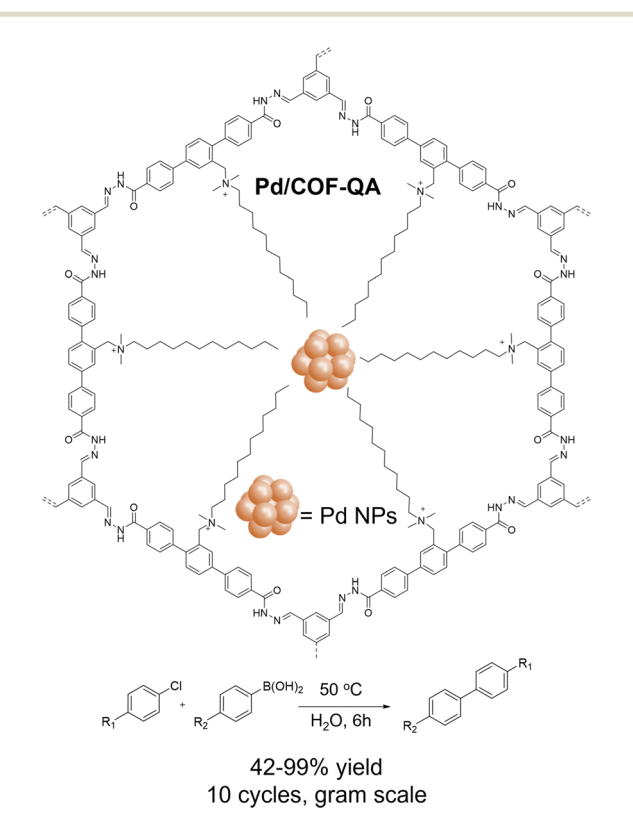


Fig. 5 Schematic of paraffin-chain quaternary ammonium salt-decorated COF supported Pd NPs for challenging chlorobenzene-based Suzuki-Miyaura coupling reaction.

COF hosts not only confine the size of encapsulated metal NPs but also considerably influence their catalytic efficiency through non-covalent interactions. In 2022, Yang and coworkers immobilized high loading (24-26%) ultrafine Pd NPs  $(\sim 1.7 \text{ nm})$  into three 2D imine COFs with different conjugated skeletons. 100 In situ FT-IR spectra of CO adsorption studies and XPS analysis revealed similar surface electronic/geometric structures of Pd NPs in the three COFs. Despite the similarities, Pd NPs supported by a pyrene-based 2D COF (Pd/Py-COF) showed a 3-10-fold enhanced activity in the hydrogenation of acetophenone compared to Pd NPs in COFs with no pyrene structs. Combined experimental results and DFT calculation disclosed that the strong  $\pi$ - $\pi$  interaction of acetophenone and pyrene motifs could drastically reduce the activation barrier in the rate-determining step and thus boost catalysis. Such promotion effect of  $\pi$ - $\pi$  interactions empowered Pd/Py-COF with high activity and cyclability (3 cycles) in the hydrogenation of aromatic compounds bearing various polar groups (C=O, NO<sub>2</sub>, C=N). This work underlines the pivotal role of non-covalent interaction between metal NPs and COF hosts in promoting activity in heterogenous catalysis.

## Photocatalysis in COFs

#### 5.1. Advantages of COFs in photocatalysis

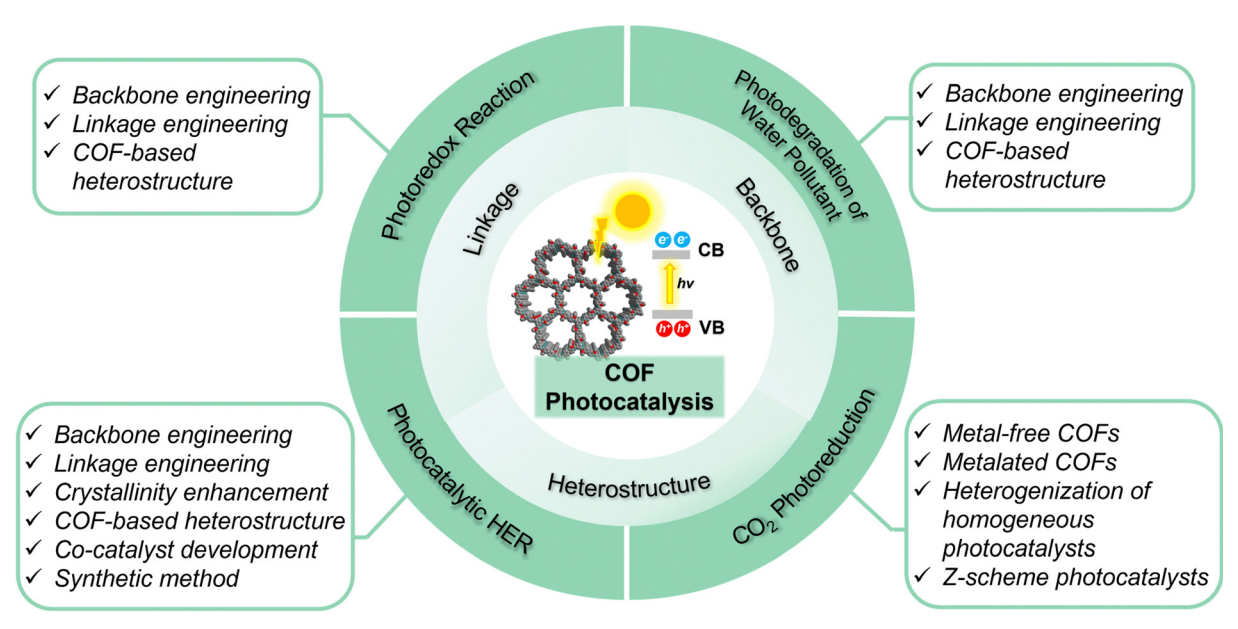
Photocatalysis enables the conversion of inexhaustible solar energy into clean fuel and/or fine chemicals, representing a promising solution to alleviating severe environmental pollution and the energy crisis nowadays. Upon absorption of light with higher energy than that of the band gap, photocatalysts generate electron-hole (e<sup>-</sup>-h<sup>+</sup>) pairs, which migrate to the catalyst surface and catalyze reduction and oxidation reactions, respectively. In comparison to other photocatalysts like inorganic semiconductors, MOFs, and  $\pi$ -conjugated polymers,

COFs are advantageous due to intriguing structural merits in several aspects:101,102 (i) The structure and optical band gap of COF photocatalysts can be precisely adjusted to maximize light harvesting, promote charge separation, migration, and transport, and enhance photocatalytic efficiency; (ii) the high porosity of COFs promotes the diffusion of substrates, sensitizers, and sacrificial agents; (iii) the long-range order of COFs facilitates charge transport, suppresses recombination of charge carriers, and minimizes charge trapping at defect sites; (iv) the synergistic hybridization of COFs with co-catalysts, photosensitizers, inorganic semiconductors, and MOFs leads to unique heterostructures with improved photocatalytic efficiency; (v) the enormous linkage diversity bestows COF with superb photochemical stability, which is the premise to the design of durable photocatalyst. (vi) The unequivocal structurephotocatalysis correlation in COFs shed light on the fundamental mechanism behind photocatalytic processes.

In this section, we will scrutinize the leading design strategies of COF photocatalysts through the engineering of linkage, backbone, and heterostructures (Scheme 4). Moreover, we will survey the up-to-date advances in four prevalent photocatalytic processes: photoredox reaction, photocatalytic hydrogen evolution, CO2 reduction, and photodegradation of water pollutants.

#### 5.2. COFs for photoredox catalysis

Visible-light photoredox catalysis has emerged as a frontier in organic synthesis, offering an eco-benign, sustainable, and effective means of producing valuable molecules. 103 The photoinduced electrons and holes generated in photoredox catalysis are harnessed as reactive species, such as superoxide radical anion  $O_2^{\bullet -}$  and single oxygen  $^1O_2$ , which function as potent oxidants for light-driven oxidation reactions. The first report of using COFs for photoredox catalysis dates back to 2016, when a 2D hydrazone COF was utilized in a visible-light mediated



Scheme 4 Leading design strategies of COF photocatalysts for diversified photocatalysis.

Table 2 Summary of the recent representative COFs for photoredox catalysis

| NiCN (Pyrene-based) Olefin 370 nm Boylation and trifluoromethylation (H <sub>3</sub> CN 18 h 2)   Hex-Azar-COF-3 Phenazine White LED Oxidative [3+2] cycloaddition (H <sub>3</sub> CN 18 h 2)   FTBC-Por COF Imine 400-780 nm Oxidation of sulfides (H <sub>3</sub> CN 40 h 1 h 2)   LZU-191 Oxazole 440 nm Oxidation of methylphenylsulfide (H <sub>3</sub> CN 40 h 1 h 2)   Applies (H <sub>3</sub> CN 50 h 2)   RT 83-95 h 1 h 1 h 2 LZU-191 Oxazole 440 nm Oxidation of methylphenylsulfide (H <sub>3</sub> CN 60 h 2) h 2 LZU-191 Oxazole 440 nm Oxidation of benzylamine (H <sub>4</sub> CN 2 h 2) h 2 Py-Bde-COF Olefin White LED Oxidation of benzylamine (H <sub>4</sub> CN 2 h 2) h 2 Py-Bde-COF (H <sub>3</sub> CN 2 h 3) h 2 h 2 RT, air 8-99% 1 h 1 h 2 RT, air 8-99% 1 h 1 h 2 RT 81-60 h 1 h 1 h 1 h 1 h 1 h 1 h 1 h 1 h 1 h  | otocatalyst              | Linkage        | Light irradiation          | Catalysis   | Condition                           | Activity | Year | Ref. |
|--|--------------------------|----------------|----------------------------|---|-------------------------------------|----------|------|------|
| NicN (Pyrene-based)         Olefin         370 nm         Borylation and trifluoromethylation         CH₂CN         18 h         2           Hex-Aza-COF-3         Phenazine         White LED         Oxidative [3+2] cycloaddition         CH₃CN         9 h         2           PTBC-Por COF         Imine         400-780 nm         Oxidation of sulfides         CH₃CN-MeOH         1 h         2           LZU-191         Oxazole         440 nm         Oxidation of methylphenylsulfide         CH₃CN         2 h         2           TA-Por-sp2-COF         Olefin         White LED         Oxidation of benzylamine         CH₃CN         2 h         2           Py-Bde-COF         Buta-1,3-dien         White LED         Oxidation of benzylamine         CH₃CN         1 h         2           NQ-COF <sub>TrippyPh</sub> Quinoline         460-465 nm         Oxidation of benzylamines and aryl ketones         CH₃CN         12 h         2           Ni-Ir@TpBpy COF         Keto-enamine         427 nm         C-N cross-coupling         CH₃CN         2 h         2           Ti-COF-1 (3D)         Imine         \$\lambda = 420 nm         Meerwein addition         CH₃CN         1 h         2           2D-PN-1         Imine         463 nm         Oxidation of aryl alcohol <td< td=""><td>Azo</td><td>Keto-enamine</td><td>467 nm</td><td>C–H borylation</td><td>CH<sub>3</sub>CN-H<sub>2</sub>O</td><td>16 h</td><td>2023</td><td>105</td></td<>   | Azo                      | Keto-enamine   | 467 nm                     | C–H borylation                                    | CH <sub>3</sub> CN-H <sub>2</sub> O | 16 h     | 2023 | 105  |
| Hex-Aza-COF-3  |                          |                |                            |   | $N_2$ , RT                          | 18-96%   |      |      |
| Hex-Aza-COF-3         Phenazine         White LED         Oxidative [3+2] cycloaddition         CH <sub>3</sub> CN<br>RT<br>RT         9 h<br>83-95"         2           PTBC-Por COF         Imine         400-780 nm         Oxidation of sulfides         CH <sub>3</sub> CN-MeOH<br>O <sub>2</sub> , RT         1 h<br>90-780 m         2           LZU-191         Oxazole         440 nm         Oxidation of methylphenylsulfide         CH <sub>3</sub> CN         2 h<br>02, RT         2         2           TA-Por-sp2-COF         Olefin         White LED         Oxidation of benzylamine         CH <sub>3</sub> CN         2 h<br>02, RT         2 p         2           Py-Bde-COF         Buta-1,3-dien         White LED         Oxidation of benzylamine         CH <sub>3</sub> CN         12 h<br>RT, air         299%         1           NQ-COF TrippyPh         Quinoline         460-465 nm         Oxidation of benzylamines and aryl ketone         CH <sub>3</sub> CN         12 h<br>RT         2           NI-I'a@TDBpy COF         Keto-enamin         427 nm         C-N cross-coupling         CH <sub>3</sub> CN         24 h<br>RT         2           Ti-COF-1 (3D)         Imine $\lambda$ 2420 nm         Meerwein addition         CH <sub>3</sub> CN         12 h<br>RT         2           2D-PN-1         Imine $\lambda$ 40 nm         Radical ring-opening polymerization         THF         48 h <b< td=""><td>CN (Pyrene-based)</td><td>Olefin</td><td>370 nm</td><td>Borylation and trifluoromethylation</td><td><math>CH_3CN</math></td><td></td><td>2023</td><td>106</td></b<>  | CN (Pyrene-based)        | Olefin         | 370 nm                     | Borylation and trifluoromethylation               | $CH_3CN$                            |          | 2023 | 106  |
| PTBC-Por COF         Imine         400-780 nm         Oxidation of sulfides         RT         83-95%           LZU-191         Oxazole         440 nm         Oxidation of methylphenylsulfide         CH <sub>3</sub> OM         2 h         91-98%           TA-Por-sp2-COF         Olefin         White LED         Oxidation of benzylamine         CH <sub>5</sub> ON         2 h <td></td> <td></td> <td></td> <td></td> <td>RT</td> <td>60-92%</td> <td></td> <td></td>  |                          |                |                            |   | RT                                  | 60-92%   |      |      |
| PTBC-Por COF         Imine         400-780 nm         Oxidation of sulfides         CH3CN-MeOM<br>$0_2$ , RT         1 h         2           LZU-191         Oxazole         440 nm         Oxidation of methylphenylsulfide         (H3CN)         2 h         2           TA-Por-sp2-COF         Olefin         White LED         Oxidation of benzylamine         (H3CN)         2 h         2           Py-Bde-COF         Buta-1,3-diene         White LED         Oxidation of benzylamine         CH3CN         12 h         2           NQ-COF ToppyPh         Quinoline         460-465 nm         Oxidation of benzylamines and arryl ketone         CH3CN         24 h         2           NQ-COF ToppyPh         Quinoline         460-465 nm         Oxidation of benzylamines and arryl ketone         CH3CN         44 h         2           NQ-COF ToppyPh         Quinoline         460-465 nm         Oxidation of benzylamines and arryl ketone         CH3CN         44 h         2           NQ-COF ToppyPh         Quinoline         460 -465 nm         Oxidation of benzylamines and arryl ketone         CH3CN         40 h         2         4         1         1         1         1         1         1         1         1         1         1         1         1         1         1   | x-Aza-COF-3              | Phenazine      | White LED                  | Oxidative [3+2] cycloaddition                     | CH <sub>3</sub> CN                  | 9 h      | 2023 | 113  |
|  |                          |                |                            |   | RT                                  | 83-95%   |      |      |
| LZU-191         Oxazole         440 nm         Oxidation of methylphenylsulfide         CH <sub>3</sub> OH         2 h         2           TA-Por-sp2-COF         Olefin         White LED         Oxidation of benzylamine         CH <sub>3</sub> CN         2 h         2           Py-Bde-COF         Buta-1,3-diene         White LED         Oxidation of benzylamine         CH <sub>3</sub> CN         12 h         9           NP-Bde-COF         Buta-1,3-diene         460-465 nm         Oxidation of benzylamines and aryl ketones         RT, air         82-99         RT, air         82-99         RT           NP-COF <sub>TrippyPh</sub> Quinoline         460-465 nm         Oxidation of benzylamines and aryl ketones         CH <sub>3</sub> ON         48 h         2           Ni-Ir@TpBpy COF         Keto-enamine         427 nm         C-N cross-coupling         CH <sub>3</sub> ON         48 h         2           Tp-AcrCOF-Ni         Keto-enamine         440 nm         C-N cross-coupling         DMAc         16-72 h         2           Ti-COF-1 (3D)         Imine $\lambda$ > 420 nm         Meerwein addition         CH <sub>3</sub> CN         RT         49-75w         1           2D-PN-1         Imine         440 nm         Radical ring-opening polymerization         THF         46,2N-H         1         42-98w         1  | BC-Por COF               | Imine          | 400-780 nm                 | Oxidation of sulfides                             | CH <sub>3</sub> CN-MeOH             | 1 h      | 2022 | 112  |
| TA-Por-sp2-COF Olefin White LED Oxidation of benzylamine (H <sub>3</sub> CN 2 h 2 y 99%) Py-Bde-COF Buta-1,3-diene White LED Oxidation of benzylamine (H <sub>3</sub> CN 2 h 82-99%) Py-Bde-COF Buta-1,3-diene White LED Oxidation of benzylamine (H <sub>3</sub> CN 12 h 82-99%) NQ-COF <sub>TIppyPh</sub> Quinoline 460-465 nm Oxidation of benzylamines and aryl ketones (H <sub>3</sub> CN 12 h 82-99%) NI-Ir@TpBpy COF Keto-enamine 427 nm C-N cross-coupling (H <sub>3</sub> CN 24 h 97-59%) Tp-AcrCOF-Ni Keto-enamine 440 nm C-N cross-coupling (H <sub>3</sub> CN 12 h 97-59%) Ti-COF-1 (3D) Imine λ > 420 nm Meerwein addition (H <sub>3</sub> CN 12 h 97-55%) D-PN-1 Imine 463 nm Oxidation of aryl alcohol (H <sub>3</sub> CN 14 h 97-55%) Te-Ax-COF Imine 463 nm Oxidation of aryl alcohol (H <sub>3</sub> CN 14 h 97-55%) To-BC-COF Imine 400-830 nm Oxidation of benzylamine (H <sub>3</sub> CN 70 min 24 h 97-55%) Ace-COF-Ni Imine 420-430 nm Oxidation of benzylamine (H <sub>3</sub> CN 70 min 24 h 97-55%) Ti-Ni@Phen-COF Imine 450 nm Oxidation of benzylamine (H <sub>3</sub> CN 24 h 97-55%) Ti-Ni@Phen-COF Imine 450 nm Oxidation of benzylamine (H <sub>3</sub> CN 24 h 97-55%) Ti-Ni@Phen-COF Imine 450 nm Oxidation of benzylamine (H <sub>3</sub> CN 24 h 97-55%) Ti-Ni@Phen-COF Imine 450 nm Oxidation of benzylamine (H <sub>3</sub> CN 24 h 97-55%) Ti-Ni@Phen-COF Imine 450 nm Oxidation of benzylamine (H <sub>3</sub> CN 24 h 97-55%) Ti-Ni@Phen-COF Imine 450 nm Oxidation of benzylamine (H <sub>3</sub> CN 34 h 97-55%) Ti-Ni@Phen-COF Imine 450 nm Oxidation of benzylamine (H <sub>3</sub> CN 34 h 97-55%) Ti-Ni@Phen-COF Imine 450 nm Oxidation of benzylamine (H <sub>3</sub> CN 34 h 97-55%) Ti-Ni@Phen-COF Imine 450 nm Oxidation of benzylamine (H <sub>3</sub> CN 34 h 97-55%) Ti-Ni@Phen-COF Imine 450 nm Oxidation of benzylamine (H <sub>3</sub> CN 34 h 97-55%) Ti-Ni@Phen-COF Imine 450 nm Oxidation of benzylamine (H <sub>3</sub> CN 35 h 97-55%) Ti-Ni@Phen-COF Imine 450 nm Oxidation of benzylamine (H <sub>3</sub> CN 34 h 97-55%) Ti-Ni@Phen-COF Imine 450 nm Oxidation of benzylamine (H <sub>3</sub> CN 34 h 97-55%) Ti-Ni@Phen-COF Imine 450 nm Oxidation of benzylamine (H <sub>3</sub> CN 34 h 97-55%) Ti-Ni@Phen-COF Imine 450 nm Oxidation of benzylamine (H <sub>3</sub> CN 34 h 97-55%) Ti-Ni@Phen-COF Imine 450 nm Oxidation of benzylamine (H <sub>3</sub> CN 34 h 97-55%) Ti |                          |                |                            |   | $O_2$ , RT                          | 91-98%   |      |      |
| $ \begin{array}{cccccccccccccccccccccccccccccccccccc$  | U-191                    | Oxazole        | 440 nm                     | Oxidation of methylphenylsulfide                  | $CH_3OH$                            | 2 h      | 2022 | 114  |
| Py-Bde-COF Buta-1,3-diene Py-Bde-COF Buta-1,3-diene Py-Bde-COF Buta-1,3-diene Py-Bde-COF Py-Bde-C   |                          |                |                            |   | $O_2$ , RT                          | 57-95%   |      |      |
| Py-Bde-COF         Buta-1,3-diene         White LED         Oxidation of benzylamine         CH <sub>3</sub> CN RT, air R2-99% RT S1-62% RT         2-99% RT S1-62% RT         2-99% RT S1-62% RT         2-99% RT S1-62% RT         2-99% RT         2-94% RT         2-948% RT <td>-Por-sp2-COF</td> <td>Olefin</td> <td>White LED</td> <td>Oxidation of benzylamine</td> <td><math>CH_3CN</math></td> <td>2 h</td> <td>2022</td> <td>115</td>   | -Por-sp2-COF             | Olefin         | White LED                  | Oxidation of benzylamine                          | $CH_3CN$                            | 2 h      | 2022 | 115  |
| $ \begin{array}{c ccccccccccccccccccccccccccccccccccc$   | -                        |                |                            | ·   | RT, air                             | >99%     |      |      |
| NQ-COF <sub>TippyPh</sub> Quinoline         460–465 nm         Oxidation of benzylamines and aryl ketones         CH <sub>3</sub> OH         48 h         2 mode           Ni-Ir@TpBpy COF         Keto-enamine         427 nm         C-N cross-coupling         CH <sub>3</sub> CN         24 h         2           Tp-AcrCOF-Ni         Keto-enamine         440 nm         C-N cross-coupling         DMAc         16-72 h         2           Ti-COF-1 (3D)         Imine         λ > 420 nm         Meerwein addition         CH <sub>3</sub> CN         12 h         2           2D-PN-1         Imine         440 nm         Radical ring-opening polymerization         THF         48 h         2           3D-PN-1         Imine         463 nm         Oxidation of aryl alcohol         CH <sub>3</sub> CN-H <sub>2</sub> O         17 h         2           FEAx-COF         Imine         400-830 nm         Oxidation of benzylamine         CH <sub>3</sub> CN-H <sub>2</sub> O         44 h         2           POr-BC-COF-Ni         Imine         420-430 nm         S-C cross-coupling         CH <sub>3</sub> CN         70 min         2           Ir,Ni@Phen-COF         Imine         450 nm         Csp³-Csp² cross-coupling         Acetone-MeOH         24 h         2           COF-UARK-49-Pt(II)         Imine         Blue LED         Decarboxylative dehalogenation         <  | -Bde-COF                 | Buta-1,3-diene | White LED                  | Oxidation of benzylamine                          | CH <sub>3</sub> CN                  | 12 h     | 2022 | 118  |
| $ \begin{array}{c ccccccccccccccccccccccccccccccccccc$   |                          |                |                            | ·   | RT, air                             | 82-99%   |      |      |
| Ni-Ir@TpBpy COF Keto-enamine 427 nm C-N cross-coupling CH $_3$ CN 24 h 2   Tp-AcrCOF-Ni Keto-enamine 440 nm C-N cross-coupling DMAc $_2$ COF-1 (3D)   Ti-COF-1 (3D) Imine $_2$ A 240 nm Meerwein addition   Ti-COF-1 (3D) Imine $_2$ A 240 nm Reductive dehalogenation   Ti-COF-1 (3D) Imine A 40 nm Reductive dehalogenation   Ti-COF-1 (3D) RT   Ace-COF-Ni Imine A 400-830 nm Reductive dehalogenation   Ti-COF-1 (3D) RT   Ace-COF-VIARK-49-Pt(II) Imine Reductive dehalogenation RT   Ti-COF-1 (3D) RT   Ace-COF-NI Imine RT   Ti-COF-1 (3D) RT   Ace-COF-NI Imine RT   Ti-COF-1 (3D) RT   Ti-COF-1 (3D) RT   Ace-COF-VIARK-49-Pt(II) Imine REDUCT   Ti-COF-1 (3D) RT   Ti-COF-1 (3D) R  | Q-COF <sub>TfppvPh</sub> | Quinoline      | 460-465 nm                 | Oxidation of benzylamines and aryl ketones        | CH <sub>3</sub> OH                  | 48 h     | 2022 | 119  |
| Tp-AcrCOF-Ni   |                          | -              |                            | •   | RT                                  | 51-62%   |      |      |
| $ \begin{array}{c ccccccccccccccccccccccccccccccccccc$   | -Ir@TpBpy COF            | Keto-enamine   | 427 nm                     | C-N cross-coupling                                | CH <sub>3</sub> CN                  | 24 h     | 2022 | 121  |
| Ti-COF-1 (3D)   Imine   $\lambda > 420$ nm   Meerwein addition   CH <sub>3</sub> CN   12 h   20   | C 1 17                   |                |                            | 1 8   |                                     | 75-94%   |      |      |
| Ti-COF-1 (3D)   Imine   $\lambda > 420$ nm   Meerwein addition   CH <sub>3</sub> CN   12 h   20   | -AcrCOF-Ni               | Keto-enamine   | 440 nm                     | C-N cross-coupling                                | DMAc                                | 16-72 h  | 2022 | 122  |
| Por-BC-COF   Imine   440 nm   Addition of aryl alcohol   CH3CN   70 min   20 mine   450 nm   CH3CN   20 mine   450 nm   COF-UARK-49-Pt(II)   Imine   Blue LED   Decarboxylative difluoroalkylation   CH3CN   47 mine   40 mine   Addition   CH3CN   Addition   CH  |                          |                |                            | 1 8   | RT                                  |          |      |      |
| 2D-PN-1   Imine   440 nm   Radical ring-opening polymerization   THF   48 h   2 m   3D-PN-1   10 °C   42-98%   10 °C   44%   10 °C   42-98%   10 °C   44%   1  | ·COF-1 (3D)              | Imine          | $\lambda > 420 \text{ nm}$ | Meerwein addition                                 | CH <sub>3</sub> CN                  | 12 h     | 2021 | 21   |
| $ \begin{array}{c ccccccccccccccccccccccccccccccccccc$   | ( )                      |                |                            |   |                                     |          |      |      |
| 3D-PN-1     10 °C   42-98%   FEAx-COF     Imine   463 nm   Oxidation of aryl alcohol   CH <sub>3</sub> CN-H <sub>2</sub> O   17 h   20   17 c   2  | )-PN-1                   | Imine          | 440 nm                     | Radical ring-opening polymerization               |                                     |          | 2021 | 107  |
| FEAx-COF         Imine         463 nm         Oxidation of aryl alcohol $CH_3CN-H_2O$ 17 h         2           Por-BC-COF         Imine $400-830$ nm         Oxidation of benzylamine $CH_3CN$ $70$ min $20$ min $2$   |                          |                |                            |   |                                     |          |      |      |
| $ \begin{array}{c ccccccccccccccccccccccccccccccccccc$   |                          | Imine          | 463 nm                     | Oxidation of aryl alcohol                         |                                     |          | 2021 | 108  |
| Por-BC-COF Imine $400-830 \text{ nm}$ Oxidation of benzylamine $CH_3CN$ $70 \text{ min}$ $20 \text{ Air}$ , $RT$ $97\%$ Ace-COF-Ni Imine $420-430 \text{ nm}$ S-C cross-coupling $CH_3CN$ $24 \text{ h}$ $25 \text{ Ar}$ , $RT$ $67-96\%$ Ir,Ni@Phen-COF Imine $450 \text{ nm}$ $Csp^3$ -Csp $^2$ cross-coupling Acetone-MeOH $24 \text{ h}$ $25 \text{ Ar}$ , $RT$ $34-99\%$ COF-UARK-49-Pt(II) Imine Blue LED Decarboxylative difluoroalkylation $RT$ $RT$ $RT$ $RT$ $RT$ $RT$ $RT$ $RT$   |                          |                |                            |   |                                     |          |      |      |
| $ \begin{array}{c ccccccccccccccccccccccccccccccccccc$   | r-BC-COF                 | Imine          | 400-830 nm                 | Oxidation of benzylamine                          |                                     |          | 2021 | 109  |
| $ \begin{array}{cccccccccccccccccccccccccccccccccccc$  | 1 20 001                 |                | 100 000 11111              | omadion of bondy annine                           |                                     |          | 2021 | 203  |
| $ \begin{array}{cccccccccccccccccccccccccccccccccccc$  | e-COF-Ni                 | Imine          | 420-430 nm                 | S-C cross-coupling                                |                                     |          | 2021 | 120  |
| $ \begin{array}{cccccccccccccccccccccccccccccccccccc$  | 0 001 111                |                | 120 100 11111              | s c cross coupling                                |                                     |          | 2021 |      |
| COF-UARK-49-Pt(II) Imine Blue LED Decarboxylative difluoroalkylation $\begin{array}{c} Ar, RT \\ CH_3CN \\ RT \\ CH-3FN \\ CH-3F$  | Ni@Phen-COF              | Imine          | 450 nm                     | Csp <sup>3</sup> -Csp <sup>2</sup> cross-coupling | ,                                   |          | 2021 | 123  |
| COF-UARK-49-Pt(II) Imine Blue LED Decarboxylative difluoroalkylation $C\dot{H}_3CN$ 3.5 h 2. RT 64-87% OH-TFP-TTA Imine 530 nm Reductive dehalogenation $CH_3CN$ 18 h 2. RT 90%  | mar nen cor              | mine           | 100 11111                  | csp csp cross coupling                            |                                     |          | 2021 | 120  |
| OH-TFP-TTA Imine 530 nm Reductive dehalogenation RT 64-87% $\rm CH_3CN$ 18 h $\rm 200$ RT 90%  | )F-11ΔRK-49-Pt(π)        | Imine          | Blue LED                   | Decarboxylative difluoroalkylation                | ,                                   |          | 2021 | 124  |
| OH-TFP-TTA Imine 530 nm Reductive dehalogenation CH $_3$ CN 18 h 2 RT 90%  | 71 Office 15 Te(II)      | IIIIIIC        | DIGC ELD                   | Decarboxylative unitabloantylation                |                                     |          | 2021 | 121  |
| RT 90%   | -I-TFP-TTA               | Imine          | 530 nm                     | Reductive dehalogenation                          |                                     |          | 2020 | 110  |
|  | 1 111 1 111              | IIIIIIC        | 330 1111                   | neductive defiatogenation                         |                                     |          | 2020 | 110  |
|  | naTph-Zn                 | Imine          | $\lambda > 420 \text{ nm}$ | Oxidation of α-terpinene                          | CH <sub>3</sub> CN                  | 4 h      | 2020 | 125  |
| O <sub>2</sub> , RT 99%  | mipii Zii                | mme            | ~ ~ <del>120</del> IIII    | omation of a terpinene                            |                                     |          | 2020 | 123  |
|  | J -MII -125@TADD         | DDA-3 Imine    | 1 > 420 nm                 | Ovidation of henzyl alcohol                       |                                     |          | 2020 | 120  |
| $\lambda > 420$ min Oxidation of belizyr accords $O_2$ , RT 94.7%  | 12-1411L-123@1APD-       | י אין וווווור  | / / 440 IIIII              | Oxidation of Delizyr alcohol                      |                                     |          | 2020 | 120  |

aerobic cross-dehydrogenative-coupling reaction. 104 Since then, considerable progress has been made in the design of COF photoredox catalysts through the backbone, linkage, and heterostructure engineering (Table 2 and Scheme 4). 105-107

Backbone engineering. To promote photocatalytic efficiency, the COF structure can be tailored by subtle modulations in the backbone to maximize light harvesting and charge separation. 108-110 One promising approach is to integrate alternating donor-acceptor (D-A) units into the COF backbone to facilitate charge transfer between donors and acceptors. 111 In 2022, Qin and co-workers prepared a series of 2D porphyrinbased D-A COFs by condensing 5,10,15,20-tetrakis(4aminophenyl)porphyrin with three electron-rich macro-ringbased aldehyde monomers (Fig. 6A). 112 These porphyrinbased D-A COFs demonstrated high crystallinity, exceptional surface areas ( $>2000 \text{ m}^2 \text{ g}^{-1}$ ), suitable optical band gaps, and superb photocurrent response, resulting in a remarkable catalytic performance for the selective oxidation of sulfides and reductive dehalogenation of 2-bromoacetophenone under visible light irradiation. Notably, the three isoreticular COFs displayed distinct reactivity and selectivity due to their different

photoelectric properties, indicating that subtle modulations to the D-A COF backbone can profoundly affect the emergent photoredox catalysis.

Linkage engineering. Photoredox catalysis using COFs has traditionally relied on imine-, hydrazone- or azine-linked 2D COFs, which possess inferior chemical stability and  $\pi$ conjugation. To overcome these drawbacks, significant research efforts have been devoted to developing COFs with novel linkages such as triazine, phenazine, 113 benzoxazole, 114 olefin, 115 and buta-1,3-diene for photoredox catalysis. Among these, sp<sup>2</sup>c-COFs bearing olefin linkages have emerged as promising photocatalysts because of their enhanced πconjugation and chemical robustness. 116 Since 2019, sp<sup>2</sup>c-COFs have been widely employed in various photoredox reactions, including photocatalytic NADH regeneration, selective oxidation of amines into imines, aerobic oxidation of sulfides into sulfoxides, oxidative thioamide cyclization, etc. 117 In 2022, Gu and co-workers constructed a unique buta-1,3-diene-linked 2D COF (Py-Bde-COF) via a multicomponent synthesis, 118 in which 4,4',4",4"'-(pyrene-1,3,6,8-tetrayl)tetrabenzaldehyde reacted with acetaldehyde and 2,2'-(1,4-phenylene)-diacetonitrile via a

Fig. 6 Schematics of (A) D-A por-COFs. (B) buta-1.3-diene-linked Pv-Bde-COF, and (C) NQ-COF for visible-light-driven photoredox catalysis.

consecutive Claisen-Schmidt and Knoevenagel condensation process (Fig. 6B). The resulting COF exhibited high crystallinity, porosity (902 m<sup>2</sup> g<sup>-1</sup>), and chemical stability towards 6 M NaOH and 6 M HCl, Importantly, D-A architectures in the ordered skeleton endowed the Py-Bde-COF with high photoactivity. In addition, Py-Bde-COF was utilized as a metal-free photocatalyst for the visible-light-driven oxidation of benzylamine derivatives and sulfides at room temperature. The buta-1,3-diene COF showed high activity and broad substrate scope in both reactions, exceeding many previously reported COF photocatalysts. This multicomponent polymerization strategy offers a promising avenue to expand the structural complexity of COFs, which warrants more efforts in the development of novel COF photocatalysts in future.

In addition to the multicomponent de novo synthesis, intriguing COF linkages can be obtained via PSM of labile imine linkages. In 2022, Xiang and co-workers demonstrated that unsubstituted quinoline-linked COFs (NQ-COFs) could be obtained via a postsynthetic Rhodium-catalyzed annulation of imine COFs (Fig. 6C). 119 This imine linkage conversion retained the crystallinity and porosity of NQ-COFs while significantly boosting the chemical stability. Moreover, the enhanced  $\pi$ conjugation empowered NQ-COFs with improved light absorption and charge carrier transfer efficiency, making them highly active, generalizable, and durable heterogeneous catalysts for the photocatalytic synthesis of 2,4,6-triphenylpyridines, benzimidazole, and sulfoxide derivatives at room temperature. Notably, NO-COFs displayed higher activity than their imine- and substituted quinoline-linked COF counterparts, underscoring the pivotal role of COF linkages in photoredox catalysis. These remarkable findings highlight the need for continued efforts towards the development of new linkages in COF catalysts, which not only advance the field of reticular chemistry but also engender unprecedented photocatalytic functions.

Heterostructure engineering. COFs have been hybridized with a wide range of functional materials, including single

metal sites, TiO<sub>2</sub>, CdS, Mxene, perovskite, g-C<sub>3</sub>N<sub>4</sub>, enzyme, and MOFs, to create synergistic heterojunctions and enhance photoredox catalysis. In 2021, Van Der Voort and co-workers reported the first immobilization of single nickel sites into a photosensitive triazine-based COF (Ace-COF), which was synthesized by condensing 4,4'4"-(1,3,5-triazine-2,4,6triyl)trianiline and acenaphthenequinone (Ace). 120 The uniform distribution of single Ni sites within the COF matrix was confirmed by high-resolution transmission electron microscopy. The resultant Ace-COF-Ni was highly effective in the photocatalytic S-C cross-coupling reaction between aryl iodides and thiols, with high yields (79-96%), wide functional group tolerance (25 substrates), and good recyclability (5 cycles). Notably, neither Ace-COF nor the model Ni compound alone showed photocatalytic activity, underscoring the synergistic effect of the two catalysts. Based on the photophysical and electrochemical analyses, they proposed a plausible mechanism for the dual-catalytic S-C cross-coupling reaction, in which the COF and Ni cycles are interconnected by electron and radical transfers. This pioneering work has sparked further efforts to incorporate single metal sites into photosensitive COFs for synthetic photocatalysis. In recent years, several transition metal/COFs have been developed for photocatalytic C-N, 121,122 Csp3-Csp2 cross-couplings 123 and decarboxylative difluoroalkylation, 124 revealing the enormous potential for visible-light-driven photoredox catalysis. 21,125

In addition to transition metal/COF photocatalysts, MOF/ COF heterostructures have been extensively utilized for photocatalysis since 2017, 126 due to their inherited structural merits from the parent reticular materials and improved charge separation efficiency. 127 For instance, in 2020, a core-shell (Ti)-NH<sub>2</sub>-MIL-125/TAPB-PDA COF heterostructure was prepared through a seed growth approach, 128 in which the imine TAPB-PDA COF nucleated and grew on the MOF seeds. Remarkably, the band gap and photocurrent density of COF/MOF heterostructures can be facilely regulated by varying the content of

COFs. With an optimal thickness of the COF shell, this composite was employed for the photocatalytic oxidation of aromatic alcohols at ambient temperature, showing excellent activity, high selectivity, wide substrate scope, and recyclability (5 cycles), far superior to those of the parent (Ti)-NH<sub>2</sub>-MIL-125, TAPB-PDA COF, and physically blended MOF/COF. The remarkable photocatalytic performance was attributed to the enhanced visible-light absorption and suppressed recombination of charge carriers endowed by the unique COF/MOF heterostructure. Aside from aryl alcohol oxidation, a Pddoped core-shell Pd/TiATA MOF/COF-LZU-1 heterostructure was developed and effectively catalyzed the olefin hydrogenation and dehydrogenation of ammonia borane under visiblelight irradiation. 129

#### 5.3. COFs for photocatalytic hydrogen evolution reaction (HER)

Hydrogen (H<sub>2</sub>) production using photocatalysis is a promising alternative to fossil fuels and can achieve near-zero emissions from energy consumption while fostering environmental sustainability. Efficient artificial photocatalysts are crucial to improve the efficiency of photocatalytic water splitting, which is an "uphill" chemical reaction. 130 In this process, a photocatalyst absorbs light to engender electron-hole pairs, which are then separated and migrate to the catalyst surface. Photogenerated electrons reduce the protons from H2O to yield H2, while the holes oxidize water to generate O2. Owing to the abovementioned structural uniqueness, COFs have aroused enormous research attention as organic photocatalysts for the hydrogen evolution reaction (HER). As illustrated in Fig. 7, there has been a remarkable increase in H2 evolution activity recently, from the initial 1.97 mmol g<sup>-1</sup> h<sup>-1</sup> in 2014 to benchmark 134.2 mmol g<sup>-1</sup> h<sup>-1</sup>. 131 Photocatalytic HER is arguably among the most studied reactions in COF photocatalysis and has been extensively explored in recent years (Table 3).

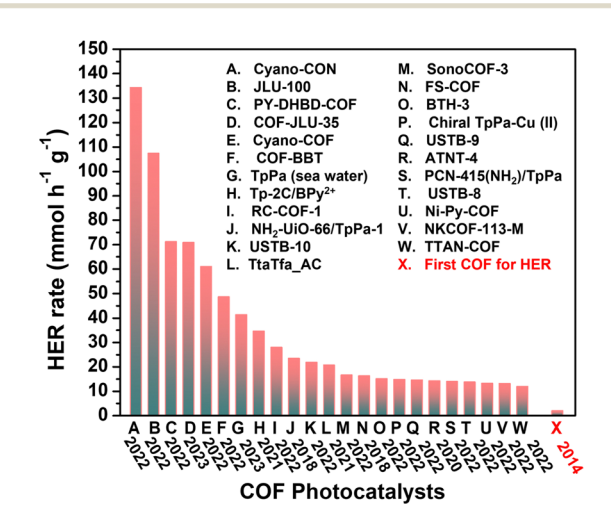


Fig. 7 Representative COF photocatalysts with exceptional H<sub>2</sub> evolution rates (>11 mmol g<sup>-1</sup> h<sup>-1</sup>) using Pt or Cu(II) as co-catalyst under visible-light irradiation. Corresponding references are summarised in Table 3.

To develop COF photocatalysts that meet the requirements of low cost, good durability, and high solar-to-H2 conversion efficiency, it is essential to maximize photon absorption, decrease the optical band gap, and improve charge carrier separation. To accomplish this, various strategies have been employed through the precise engineering of COF structures concerning the linkage, crystallinity, backbone, heterostructure, co-catalyst, and synthetic methods.

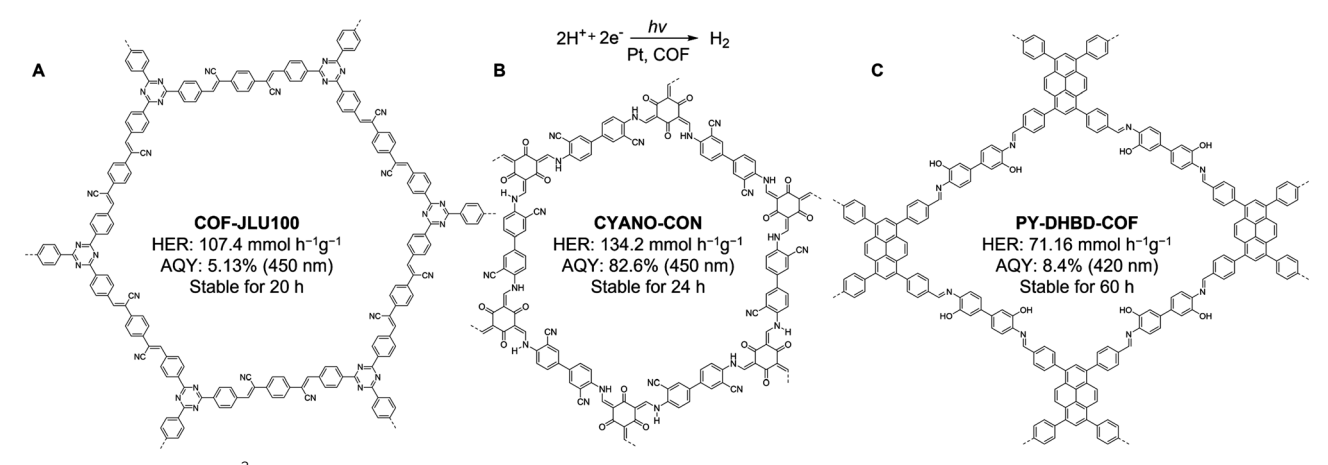
Linkage engineering. The efficiency of COF photocatalysts in HER is profoundly influenced by the type of COF linkage, as it governs the photostability and transport of charge carriers in COFs. In the first example of using COFs for visible-light-driven HER in 2014, a 2D hydrazone COF was utilized as support for Pt NPs and triethanolamine (TEOA) as the sacrificial agent, achieving an H<sub>2</sub> evolution rate of 1.97 mmol g<sup>-1</sup> h<sup>-1</sup>. 132 However, the dynamic polarized hydrazone linkage has incompetent stability and  $\pi$ -conjugation, which in turn limits the photocatalytic activity. To this end, researchers have actively pursued strategies to engineer the COF linkage for more efficient photocatalysts. 133-136 Among them, the olefin linkage offers uninterrupted  $\pi$ -conjugation and strong photostability, making sp<sup>2</sup>-COFs highly appealing for photocatalysis. Since the first attempt in 2018, the exploration of sp<sup>2</sup>c-COFs for photocatalytic HER has been flourishing. Recently (2022), Liu and coworkers synthesized a cyano-substituted sp<sup>2</sup>c-COF (COF-JLU100, a.k.a, TP-COF, 137 Fig. 8A) using a unique gradient heating strategy, whereby the Knoevenagel condensation 1,3,5-tris-(4-formylphenyl) triazine between phenylenediacetonitrile was conducted over 3 d using a temperature gradient ranging from 40 to 120 °C. 138 The obtained COF-JLU100 exhibited improved crystallinity and 5-fold higher porosity than the conventionally synthesized COF. When using TEOA or ascorbic acid as the sacrificial agent, the Pt-doped COF-JLU100 presented an astonishing HER activity of >100 mmol g<sup>-1</sup> h<sup>-1</sup>, rendering it among the best-performing COF photocatalysts for HER thus far. In addition, COF-JLU100 showed superior photocatalytic performance, enhanced electrical conductivity, and charge carrier transport efficiency compared to the imine-linked triazine-based N<sub>3</sub>-COF, highlighting the importance of linkage in photocatalytic HER. The extraordinary photocatalytic HER activity was due to the synergistic contribution of extended  $\pi$ -delocalization, improved charge transfer/separation, and excellent dispersion in water, which originated from the inbuilt cyano-vinylene linkages in COF-JLU100.

Crystallinity enhancement. The degree of crystallinity in COF photocatalysts is essential for their catalytic performance, as the long-range ordered periodic structure facilitates the transport of photogenerated charge carriers and reduces charge trapping at defect sites, ultimately promoting photocatalysis. In 2022, Cooper and co-workers reported that highly crystalline βketoenamine-linked COFs could be obtained by reconstructing labile urea-linked COFs via a framework reconstruction strategy, whereby monomers were pre-organized using a dynamic urea linkage, accompanied by thermal hydrolysis to remove urea tethers. 139 DFT calculations suggested the non-covalent

Table 3 Summary of the recent representative COFs for photocatalytic HER under visible-light irradiation (>420 nm)<sup>a</sup>

| Photocatalyst                               | Linkage          | Band gap (eV) | SED         | Co-catalyst         | HER (mmol h <sup>-1</sup> g <sup>-1</sup> ) | AQY (%)            | Year       | Ref. |
|---|------------------|---------------|-------------|---------------------|---|--------------------|------------|------|
| COF-JLU35                                   | Olefin           | 1.85          | AA          | 1%Pt                | 70.8  | 3.21 (500 nm)      | 2023       | 135  |
| ZnP-Pz-PEO-COF                              | Imine            | 1.45          | Lactic acid | $[Mo_3S_{13}]^{2-}$ | 10.7  | 5.3 (500 nm)       | 2023       | 154  |
| TpPa  | Keto-enamine     | 2.04          | AA          | 0.5%Pt              | 41.3  | 0.54 (TpPa 450 nm) | $2023^{b}$ | 163  |
| TpBd  |                  | 2.21          |             |                     | 21.7  | , ,                |            |      |
| ТрТРу                                       |                  | 2.32          |             |                     | 14.9  |                    |            |      |
| CYANO-CON                                   | Keto-enamine     | 2.17          | AA          | 1%Pt                | 134.2                                       | 82.6 (450 nm)      | 2022       | 152  |
| CYANO-COF                                   |                  |               |             |                     | 60.9  |                    |            |      |
| COF-JLU100                                  | Olefin           | 1.95          | TEOA        | 12%Pt               | 107.4                                       | 5.13 (450 nm)      | 2022       | 138  |
| PY-DHBD-COF                                 | Imine            | 2.28          | AA          | 3%Pt                | 71.2  | 8.4 (420 nm)       | 2022       | 153  |
| COF-BBT                                     | Keto-enamine     | 2.0           | AA          | 2.4%Pt              | 48.7  | 6.8 (420 nm)       | 2022       | 143  |
| RC-COF-1                                    | Keto-enamine     | 1.87          | AA          | 3%Pt                | 27.98                                       | 6.39 (420 nm)      | 2022       | 139  |
| USTB-8                                      | Imine            | 2.60          | AA          | 3%Pt                | 13.7  | 0.68 (420 nm)      | 2022       | 144  |
| USTB-9                                      |                  | 2.20          |             |                     | 14.6  |                    |            |      |
| USTB-10                                     |                  | 2.17          |             |                     | 21.8  |                    |            |      |
| SonoCOF-3                                   | Imine            | 2.46          | AA          | 8%Pt                | 16.6  | 3.71 (420 nm)      | 2022       | 162  |
| BTH-3                                       | Olefin           | 1.42          | AA          | 8%Pt                | 15.1  | 0.792 (420 nm)     | 2022       | 151  |
| ТрРа-Cu(п)                                  | Keto-enamine     | 1.72          | L-cysteine  | 10.51%Cu(п)         | 14.72                                       | 0.78 (600 nm)      | 2022       | 157  |
| PdTCPP-PCN-415(NH <sub>2</sub> )/TpPa       | Keto-enamine     | 1.72          | AA          | 1.2%Pt              | 13.98                                       | 5.7 (450 nm)       | 2022       | 161  |
| Ni-Py-COF                                   | Imine            | 1.82          | AA          | 14%Pt               | 13.2  | 4.28 (420 nm)      | 2022       | 145  |
| NKCOF-113-M                                 | Olefin           | 2.3           | TEOA        | 5%Pt                | 13.1  | 52.6 (475 nm)      | 2022       | 146  |
| TTAN-COF                                    | Olefin           | 2.66          | AA          | 1.6%Pt              | 11.94                                       | /                  | 2022       | 136  |
| $BT-Py_{BuOH}$ COF                          | Imine            | 2.36          | AA          | 2%Pt                | 11.28                                       | 4.88 (420 nm)      | 2022       | 140  |
| TtaTfa_AC                                   | Protonated Imine | 1.90          | AA          | 8%Pt                | 20.7  | 1.43 (450 nm)      | 2021       | 133  |
| CTF film                                    | Triazine         | /             | TEOA        | 2%Pt                | 10.2  | 0.11 (420 nm)      | 2021       | 134  |
| Tp-2C/BPy <sup>2+</sup> -COF                | Keto-enamine     | < 2.2         | AA          | 3%Pt                | 34.6  | 6.93 (420 nm)      | 2021       | 147  |
| NKCOF-108                                   | Imine            | 1.82          | AA          | 5%Pt                | 11.6  | 2.96 (520 nm)      | 2021       | 148  |
| $Tp(BT_{0.05} TP_{0.95})$ -COF              | Keto-enamine     | 2.18          | AA          | 5%Pt                | 9.84  | 2.34 (420 nm)      | 2021       | 149  |
| Py-ClTP-BT-COF                              | Imine            | 1.78          | AA          | 5%Pt                | 8.87  | 8.45 (420 nm)      | 2020       | 150  |
| NTU-BDA-THTA/NH $_2$ -Ti $_3$ C $_2$ T $_x$ |                  | 2.09          | AA          | 3%Pt                | 14.2  | 9.75 (500 nm)      | 2020       | 158  |
| $TiO_2$ -TpPa-1-COF (1:3)                   | Keto-enamine     | 2.15          | SA          | 3%Pt                | 11.2  | 7.6 (420 nm)       | 2020       | 159  |

<sup>&</sup>lt;sup>a</sup> SED: sacrificial electron donor; AQY: apparent quantum yield; TEA: triethylamine; AA: ascorbic acid; SA: sodium ascorbate; TEOA: triethanolamine. <sup>b</sup> The photocatalysis was performed in seawater.



Schematics of (A) sp<sup>2</sup>c-COF-JLU100, (B) CYANO-CON, and (C) in situ Pt-PY-DHBD-COF for visible-light-driven HER.

interactions during urea hydrolysis induced nanoconfinement effects that are essential for crystallinity retention. The reconstructed COF (RC-COF-1) displayed high crystallinity, improved surface area (1712 m<sup>2</sup> g<sup>-1</sup>), and significantly enhanced the charge carrier transport, exhibiting an H2 production activity of 27.98 mmol  $h^{-1}$   $g^{-1}$ , which was four times higher than the less crystalline COF analog made by direct polymerization. In the same year, Chou and co-workers showcased the significant influence of crystallinity on the HER

activity of benzothiadiazole-based COFs (BT-Py), which were constructed by condensing diphenyl benzothiadiazole dialdehyde and pyrene tetraamines. They found that the crystallinity of BT-Py was dramatically improved by increasing the solvent polarity during solvothermal synthesis. 140 Specifically, BT-Py synthesized using o-dichlorobenzene/ethanol and odichlorobenzene/n-butanol exhibited higher crystallinity than that obtained using mesitylene/dioxane. Despite having similar bandgap and chemical structures, the crystalline BT-Py COF

exhibited high H<sub>2</sub> production activity of 11.28 mmol h<sup>-1</sup> g<sup>-1</sup> with apparent quantum yields of 4.88% at 420 nm, corresponding to a 3.66-fold enhancement in the activity compared to its amorphous counterpart. These promising research calls for more endeavours to improve the crystallinity of COF photocatalysts through established strategies, 141 such as the optimization of synthetic reactions and improvement of the intra/ intermolecular interactions.

Backbone engineering. The bespoke COF backbone enables fine-tuning of the optoelectronic properties at the atomic level to achieve optimal photocatalytic properties. 142-150 Integrating D-A motifs into the ordered backbone of COFs is a viable strategy to enhance photocatalytic HER. In 2022, Zhao and co-workers tailored the backbone of three benzothiazolefunctionalized sp<sup>2</sup>c-COFs (BTH-1-3) by Knoevenagel condensation between benzothiazole-based monomer bearing two cyano units and three  $C_3$ -symmetric aryl aldehydes under a versatile condition, allowing for precise modulation of emergent photocatalytic properties. 151 Using ascorbic acid as a sacrificial electron donor, the D-A sp<sup>2</sup>c-COF (BTH-3) consisting of electron-rich benzotrithiophene and electron-deficient benzobisthiazole motifs demonstrated a remarkable HER rate of 15.1 mmol h<sup>-1</sup> g<sup>-1</sup> with Pt as a co-catalyst, far superior to the triazine-based BTH-1 (10.5 mmol h<sup>-1</sup> g<sup>-1</sup>) and the benzenebased BTH-2 (1.2 mmol h<sup>-1</sup> g<sup>-1</sup>). The superior photocatalytic performance was attributed to the enhanced charge separation and transport endowed by the D-A architecture. Likewise, a Ptdoped β-ketoenamine-linked 2D COF with inherent D-A (β-ketene-cyano) backbone (CYANO-COF, Fig. 8B) showed an outstanding photocatalytic activity, with an HER rate of 60.8 mmol  $h^{-1}$   $g^{-1}$ , equivalent to a 30-fold improvement over the cyano-free COF counterpart. 152 Astonishingly, the H<sub>2</sub> evolution rate was further accelerated to a record high 134.2 mmol h<sup>-1</sup> g<sup>-1</sup> with an ultrahigh quantum efficiency of 82.6% when exfoliated COF nanosheets (4-5 nm thickness, CYANO-CON) were used as photocatalysts. Further, CYANO-CON displayed exceptional long-term stability for over 24 hours. Charge carrier kinetic analysis and femtosecond transient absorption spectroscopy demonstrated the extraordinary photoactivity of CYANO-COF was attributed to intrinsically lower exciton binding energies and longer-lived charge carriers induced by cyano groups.

Co-catalyst development. Co-catalysts, such as Pt, are crucial in promoting efficient photocatalytic HER by lowering the overpotential of H2 evolution and strengthening photoexcited electron accumulation. The uniform morphologies and locations of Pt co-catalyst in COFs are essential for achieving high HER activity. In 2022, well-dispersed Pt clusters with precisely controlled sizes were achieved via in situ photodeposition in a 2D pyrene-based imine COF (PY-DHBD-COF, Fig. 8C), 153 in which the abundant hydroxyl groups and adjacent imine linkage anchored the Pt precursors. At 1 wt% Pt loading, the Ptdoped COF manifested an impressive HER activity of up to 71.16 mmol  $g^{-1} h^{-1}$  and steady  $H_2$  generation for over 60 hours. DFT calculations not only confirmed the essential role of -OH in stabilizing the adsorbed Pt precursors but also shed light on

the electron transfer from PY-DHBD-COF to the Pt cocatalyst, which was further corroborated by steady-state and timeresolved fluorescence spectroscopy. Moreover, the Pt-doped COF showed suppressed e<sup>-</sup>-h<sup>+</sup> recombination, as evident by the lower fluorescence lifetimes than that of pristine COF.

Until now, noble Pt has been the dominant co-catalysts in COF-based photocatalytic HER, so there is a dire necessity to develop low-cost co-catalysts for sustainable and economical photocatalysis. 154 While some progress has been made with the use of noble metal-free co-catalysts, such as chloro(pyridine)cobaloxime (2017)<sup>155</sup> and nickel-thiolate hexameric cluster (2019), 156 their photocatalytic HER activity is far from satisfactory, with rates of only 0.782 mmol g<sup>-1</sup> h<sup>-1</sup> and 0.941 mmol g<sup>-1</sup> h<sup>-1</sup>, respectively. A breakthrough was made in 2022, when Guo and co-workers showed that a well-known chiral 2D β-ketoenamine-linked COF (TpPa-1) in combination with a single atom Cu(II) as an electron transfer mediator and L-/D-cysteine as a sacrificial donor led to a record-high photocatalytic HER activity of 14.72 mmol h<sup>-1</sup> g<sup>-1</sup>, significantly outperforming all previous non-noble metal/COF photocatalytic systems. This unique photocatalytic system involved a cascade process, in which Cu(II) is reduced to Cu(I) in a dark reaction by L-cysteine, followed by a photochemical process for hole extraction using Cu(1). Moreover, DFT calculations revealed the electron transfer from the Tp-Cu(I) complex to the Tp moiety. The remarkable photocatalytic efficiency was attributed to the improved hole extraction kinetics, effective accumulation, and transfer of photoexcited electrons, and reduced energy barriers of H2 evolution due to the wellaligned COF layers. These studies on earth-abundant cocatalyst development uncover the vast potential of low-cost COF catalytic systems for solar-to-H2 conversion.

COF-based heterostructures. The hybridization of photoactive COFs with functional materials represents a promising approach to enhancing the efficiency of photocatalysis. 158,159 MOF/COF heterostructures have shown tremendous potential in photocatalytic HER since 2018, when Lan and co-workers pioneered the assembly of (Zr)-UiO-66-NH<sub>2</sub>/TpPa-1-COF coreshell hybrid by growing TpPa-1 COF on (Zr)-UiO-66-NH2 seeds. 160 More recently, in 2022, Ma and co-workers constructed a series of multivariate PdTCPP-PCN-415-NH<sub>2</sub>/TpPa-COF-1 heterostructures with different amounts of MOFs using a covalent integration strategy, wherein the -NH2 groups in Ti-MOF was covalently attached to the -CHO groups of COF. 161 Thanks to the broad visible-light harvesting, suitable band gaps, excellent optical response, and high surface area, the resulting MOF/COF composite gave a high H2 evolution rate of 13.98 mmol  $g^{-1} h^{-1}$  using the *in situ* formed Pt as co-catalyst and ascorbic acid as a sacrificial agent, which far surpassed that of individual MOF and TpPa-COF-1. Furthermore, the MOF/COF composite showed exceptional photocatalytic stability in a long-term 120 h test. The steady-state photoluminescence measurement indicated the enhanced e<sup>-</sup>-h<sup>+</sup> separation of PdTCPP-PCN-415-NH2/TpPa-COF-1. Moreover, DFT calculations demonstrated the photoexcited electrons from metal clusters to TpPa through the covalently connecting junction.

These fascinating photocatalytic properties rendered by MOF/ COF heterostructures will surely invoke more scientific attention. Expanding the structural complexity, manipulating the morphology, developing general synthetic strategies, in-depth theoretical insight of interface, and exquisite characterizations of MOF/COF heterostructures are worthy of more scientific efforts.

Synthetic method innovation. Most COF photocatalysts are made via conventional solvothermal synthesis, which suffers from several drawbacks, such as long reaction times, vacuum conditions, closed reaction vessels, and hazardous organic solvents. To address these issues, Cooper and co-workers recently (2022) demonstrated the first use of sonochemistry for the facile synthesis of 2D imine COFs in 6 M aqueous acetic acid within 1 hour. 162 Impressively, the nine COFs synthesized using sonochemistry exhibited equivalent or better crystallinity and porosity than their solvothermal counterparts. When used in visible-light-driven HER with Pt as a co-catalyst, sonoCOF-3 composed of 4,4',4"-(1,3,5-triazine-2,4,6-triyl) trianiline and tris(4-formylphenyl) amine showed a higher H<sub>2</sub> evolution rate of 16.6 mmol h<sup>-1</sup> g<sup>-1</sup> and a more stable long-term activity than that of its solvothermal analog, which is likely due to high crystallinity, good water dispersibility, and improved dispersion of Pt. This study paves a new avenue for the rapid synthesis of high-quality COF photocatalysts that outperform their solvothermal analogs. Despite this remarkable progress, the synthesis of COF photocatalysts using other promising synthetic methods, such as hydrothermal, microwave, 163 and mechanochemical approaches, remains largely unexplored. Further scientific efforts are warranted to explore these synthetic methods and expand the scope of COF photocatalyst synthesis.

#### 5.4. COFs for CO<sub>2</sub> photoreduction

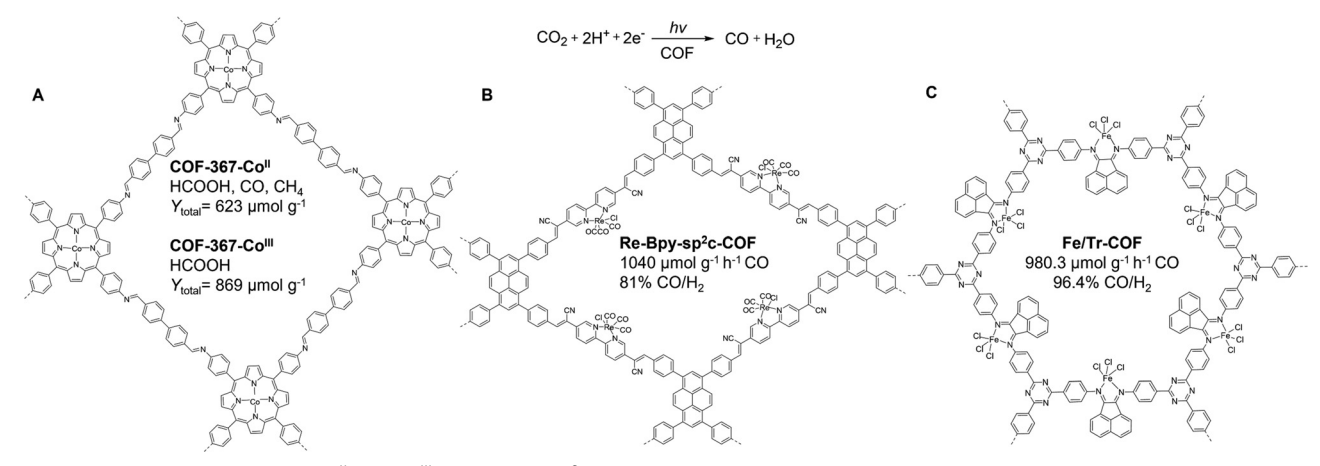
Artificially reducing excessive CO2 into hydrocarbon fuels using ubiquitous solar light represents an emerging approach to simultaneously address the worsening global warming and the energy crisis. In a typical CO2 photoreduction process, CO<sub>2</sub> molecules are firstly adsorbed onto the photocatalyst, which generates electron-hole pairs upon excitation of suitable light. The photoexcited electrons migrate to catalytic sites and reduce the adsorbed CO<sub>2</sub> to value-added carbon-based products such as CO, HCOOH, CH<sub>3</sub>OH, CH<sub>4</sub>, etc., Meanwhile, the holes oxidize H<sub>2</sub>O to generate O<sub>2</sub>. To facilitate the photoreduction of CO2 which has a high dissociation energy, it is essential to enhance CO<sub>2</sub> adsorption, lower the band gap of photocatalysts, and promote the migration of photoexcited electrons. Since 2018, COFs have been demonstrated to be promising electrocatalysts for CO2 photoreduction, with CO as the dominant carbonaceous product. In comparison to metal-free COFs, metalated COFs typically exhibit superior activity in CO<sub>2</sub> photoreduction.

Metal-free heteroatom-containing COFs. In 2021, Fu and coworkers first investigated the effect of functional groups in COFs on their CO<sub>2</sub> photoreduction efficiency. To achieve this goal, they synthesized a series of isoreticular β-ketoenaminelinked 2D COFs with different electron-withdrawing groups,

namely TpBD-H<sub>2</sub>, TpBD-(CH<sub>3</sub>)<sub>2</sub>, TpBD-(OCH<sub>3</sub>)<sub>2</sub> and TpBD-(NO<sub>2</sub>)<sub>2</sub>. The subtle structural variations of COFs resulted in distinct light absorption, thereby affecting their photocatalytic activity in CO<sub>2</sub> reduction. TpBD-(OCH<sub>3</sub>)<sub>2</sub> containing electrondonating groups displayed the highest activity with an HCOOH generation rate of 108.3  $\mu$ mol g<sup>-1</sup> h<sup>-1</sup>, exceeding that of TpBD- $H_2$  (45.7  $g^{-1} h^{-1}$ ), TpBD-(CH<sub>3</sub>)<sub>2</sub> (86.3  $g^{-1} h^{-1}$ ), and TpBD-(NO<sub>2</sub>)<sub>2</sub> (22.2 g<sup>-1</sup> h<sup>-1</sup>). Electrochemical impedance spectroscopy indicated that the introduction of electron-donating groups decreased the interfacial charge-transfer resistance of TpBD, while electron-withdrawing groups increased it. Photoluminescence spectroscopy showed that TpBD-(OCH3)2 efficiently suppressed e<sup>-</sup>-h<sup>+</sup> recombination, which might account for its high performance in CO<sub>2</sub> photoreduction.

Not surprisingly, the utilization of 3D COFs for CO<sub>2</sub> photoreduction remains elusive. In a recent study in 2022, a 3D imine COF (TAPP-HFPB-COF) adopting an unprecedented she net was synthesized by the condensation of  $D_{4h}$ -symmetric 5,10,15,20tetra(4-aminophenyl)porphyrin and D<sub>3d</sub>-symmetric hexa(4formylphenyl)benzene.165 The resulting TAPP-HFPB-COF displayed high crystallinity, large surface area (1060 m<sup>2</sup> g<sup>-1</sup>), superb chemical stability, more accessible porphyrin sites than 2D COFs, broad light absorption ranging from 300 to 700 nm, and well-aligned energy levels, making it an attractive photocatalyst for CO2 reduction. The metal-free TAPP-HFPB-COF acted as a photocatalyst for CO2 reduction, producing CO and CH<sub>4</sub> at rates of 128  $\mu$ mol g<sup>-1</sup> h<sup>-1</sup> and 5  $\mu$ mol g<sup>-1</sup> h<sup>-1</sup>, respectively. Additionally, it showed a high CO/CH<sub>4</sub> selectivity of 96%, outperforming the control porphyrin molecular analog and 2D porphyrin COF. The isotopic test using 13CO2 as the reactant produced <sup>13</sup>CO, indicating the CO is indeed from the reduction of CO<sub>2</sub>. Albeit the preliminary promise, the inferior activity of metal-free COFs substantially hinders their widespread use.

Metalated COFs with intrinsic metal sites. Active metal sites for CO<sub>2</sub> photoreduction can be introduced into the skeleton of COFs by using metalated monomer units like metalloporphyrin. In 2020, Jiang and co-workers demonstrated that the spin state of the central cobalt in the porphyrin of COF-367-Co can considerably influence its catalytic performance in CO2 photoreduction using CH<sub>3</sub>CN as solvent and triethylamine as the sacrificial agent. The oxidation state of Co can be simply controlled using N2 or air atmosphere (Fig. 9A). 166 The combined use of Fourier transform extended X-ray absorption fine structure (FT-EXAFS) spectra and DFT calculations showed that COF-367 contains both CoII and CoIII, with spin ground states of S = 1/2 and 0, respectively. Intriguingly, COF-367-Co<sup>III</sup> exhibited increased photocatalytic activity and selectivity towards HCOOH, while COF-367-Co<sup>II</sup> showed inferior activity and selectivity towards CO and CH4. Homogenous control catalysts, Co<sup>II</sup>-TAP and Co<sup>III</sup>-TAP did not produce any CO<sub>2</sub> reduction products under identical conditions. Photoelectrochemical measurements confirmed the superior charge separaof COF-367-Co<sup>III</sup> efficiency over COF-367-Co<sup>II</sup>. Furthermore, DFT calculations demonstrated that the presence of CoIII in COF-367-Co benefits the formation of HCOOH, but is



Schematics of (A) COF-367-Co<sup>II</sup> and Co<sup>III</sup>, (B) Re-Bpy-sp<sup>2</sup>c-COF, and (C) Fe/Tr-COF for CO<sub>2</sub> photoreduction under visible-light irradiation.

unfavorable for its subsequent conversion, which explained the discriminative photocatalytic behaviors of COF-367-CoII and COF-367-Co<sup>III</sup> as well as the impact of spin-state transition on CO<sub>2</sub> photoreduction.

Very recently in 2023, Fang, Jiang, and co-workers extended this strategy to 3D porphyrin COFs (JUC-640-M, M = Co, Ni, or H), which were prepared by condensing the 6-connected 2,3,6,7,14,15-hexa(4'-formylphenyl) triptycene with 5,10,15,20tetrakis(4-aminophenyl)porphyrin bearing different metal sites. 167 The resulting JUC-640-M has a non-interpenetrated stp net, a record-low density of 0.106 g cm<sup>-3</sup>, ultra-large interconnected pore size of 4.6 nm, a large surface area of 2204 m<sup>2</sup> g<sup>-1</sup>, and abundant exposed porphyrin sites of 0.845 mmol g<sup>-1</sup>, which endowed JUC-640-M with vast potential in CO<sub>2</sub> photoreduction. Using 1,3-dimethyl-2-phenyl-2,3dihydro-1H-benzo[d]imidazole as the sacrificial agent and Ru(bpy)<sub>3</sub>Cl<sub>2</sub>·6H<sub>2</sub>O as the photosensitizer, JUC-640-Co exhibited a record-high CO production rate (15.1 mmol  $g^{-1} h^{-1}$ ) and selectivity (94.4%), rendering it the most active photocatalyst among reported COF-based materials for CO2 photoreduction. Moreover, JUC-640-Co displayed high photocatalytic stability after 5 cycles. The Gibbs free-energy diagram from DFT calculations revealed that the high photocatalytic activity of JUC-640-Co could be attributed to the much lower free-energy barriers of Co-porphyrin compared to its Ni-counterparts. Despite the great promise of metalloporphyrin COFs for CO<sub>2</sub> photoreduction, 168 the arduous synthesis of metalloporphyrin monomers necessitates the development of cost-effective COF catalysts for CO<sub>2</sub> photoreduction.

Heterogenization of homogeneous photocatalysts in COFs. Encapsulating molecular homogenous photocatalysts into COFs can mitigate biomolecular deactivation and engender enhanced photocatalytic activity. The first attempt was made in 2018 when a well-known homogenous photocatalyst, Re(bpy)(CO)<sub>3</sub>Cl, was incorporated into a triazine-based 2D imine COF through a postsynthetic complexation method. 169 In 2020, Cooper and co-workers constructed a bipyridine-based sp<sup>2</sup>c-COF by Knoevenagel condensation of 1,3,6,8-tetrakis(4formylphenyl)pyrene and 5,5'-bis(cyanomethyl)-2,2'-bipyridine,

followed by facile solution impregnation to immobilize [Re(bpy)(CO)<sub>3</sub>Cl] complex into the COF (Fig. 9B). The resultant Re-Bpy-sp<sup>2</sup>c-COF possessed superb chemical stability, broad light absorption, and high CO<sub>2</sub> affinity. When illuminated with visible light (>420 nm) and TEOA was used as the sacrificial electron donor, Re-Bpy-sp<sup>2</sup>c-COF exhibited a high CO production rate of 1040 μmol g<sup>-1</sup> h<sup>-1</sup> and 81% CO/H<sub>2</sub> selectivity, exceeding that of its homogenous counterpart under identical conditions. 170 Additionally, dye-sensitization of Re-Bpy-sp<sup>2</sup>c-COF increased CO production up to 1400 μmol g<sup>-1</sup> h<sup>-1</sup>. Time-correlated single-photon counting measurements and transient absorption spectroscopic studies indicated that the Re center in the COF generated a longlived charge-separated state. DFT calculations further supported the electron transfer from COF to the Re center upon electronic excitation.

In addition to expensive noble metal complexes, earthabundant metal catalysts are of great interest for their economic and environmental advantages in CO<sub>2</sub> photoreduction. In 2022, Hou and co-workers reported a universal synthetic strategy to anchor multiple single-atom metal sites (e.g., Fe, Co, Ni, Zn, Cu, and Mn) onto the backbone of a triazine-based 2D COF (Tr-COF), which was prepared by condensing 4,4'4"-(1,3,5triazine-2,4,6-triyl)trianiline and ace-naphthenequinone monomers (Fig. 9C). 171 The facile solution impregnation method enabled the integration of various metal ions into the Tr-COF with the retention of porosity and crystallinity. X-Ray absorption near-edge structure (XANES) analysis confirmed the atomically dispersed Fe sites in Tr-COF. Steady-state photoluminescence spectra together with ultra-fast femtosecond timeresolved transient absorption spectroscopy indicated the suppressed e<sup>-</sup>-h<sup>+</sup> recombination in Fe/Tr-COF compared to Tr-COF. Notably, the Fe/Tr-COF afforded a high CO generation rate of 980.3  $\mu$ mol g<sup>-1</sup> h<sup>-1</sup> and 96.4% CO/H<sub>2</sub> selectivity for CO<sub>2</sub> photoreduction, which outperformed the bare Tr-COF significantly. This exceptional catalytic performance was primarily due to the synergy between single-atom metal sites and the COF host, which reduced the energy barriers of COOH\* intermediates formation and improved CO2 adsorption, activation, and CO desorption.

COF-based Z-scheme photocatalysts. Z-scheme photocatalysts, which imitate natural photosynthesis by incorporating two or more semiconductors, offer numerous advantages over conventional single-component photocatalysts, such as enhanced light absorption, spatially separated charge carriers, and strong redox ability. 172,173 In 2020, Lan and co-workers reported the first Z-scheme COF photocatalytic system, which was synthesized by covalently connecting ether-linked COF-316/318 with hydroxylfunctionalized inorganic semiconductors. 174 This system leveraged the high reduction potential of COF and the strong oxidation capability of TiO2. COF-318/TiO2 Z-scheme catalyst photoreduced  $CO_2$  to CO with a high production rate of 69.67  $\mu$ mol g<sup>-1</sup> h<sup>-1</sup> and impressive 100% CO/H<sub>2</sub> selectivity, without the need for a photosensitizer and electron sacrificial agent. Both experiments and DFT calculations validated the efficient electron transfer from TiO<sub>2</sub> to COF, resulting in electron accumulation in the cyano/ pyridine functionalities of COF for CO2 photoreduction and holes in the TiO2 for H2O oxidation. Later in 2022, COF-318 was replaced with a Cu(II) porphyrin-based imine COF to create a new Z-scheme CuTAPP/TiO2 photocatalyst with a CO evolution rate of 50.5  $\mu$ mol g<sup>-1</sup> h<sup>-1</sup>. Given the great promise of Z-scheme photocatalysts, more research endeavors should be dedicated to expanding the portfolio and leveraging the structural merits of COF-based Z-scheme photocatalysts.

#### 5.5. COFs for photodegradation of water contaminants

Photocatalysis has been long recognized as a promising tool for sustainable environmental remediation. 130 In recent years, COFs have emerged as potential catalysts for the photocatalytic degradation of aqueous pollutants, providing a feasible solution to mitigate severe water pollution. Upon photoexcitation, photoactive and hydrolytically stable COFs generate highly oxidative holes to degrade organic contaminants including dyes, pesticides, pharmaceuticals, and agrochemicals in sewage. Additionally, the photoexcited electrons can reduce noxious high-valence metal ions such as Cr(v1). Since the earliest report in 2017, 176 a broad array of COF photocatalysts has been developed for water depollution using bare COFs and COFbased heterostructures.

Bare COFs. Bare COFs have been widely utilized in the photodegradation of pollutants, and several proven strategies such as backbone and linkage engineering have been adopted to augment the photoactivity. 177 Besides common imine COFs, other water-stable COFs bearing robust linkages such as βketonenamine and olefin have emerged as promising photocatalysts for aqueous pollutant degradation, such as organic dyes<sup>178</sup> and Cr(v<sub>1</sub>).<sup>179</sup> In 2023, Zhang and co-workers developed a pyrylium cation containing sp<sup>2</sup>c-COF (v-2D-COF-O1) through melt-polymerization of 2,4,6-tris(4-formylphenyl)-1,3,5-triazine and 2,4,6-trimethylpyrylium tetrafluoroborate in the presence of benzoic anhydride. The resultant v-2D-COF-O1 showed high crystallinity, moderate BET surface area (448 m<sup>2</sup> g<sup>-1</sup>), exceptional chemical stability, and wide-range light absorption up to ~920 nm. Importantly, electron paramagnetic resonance showed that v-2D-COF-O1 can readily activate molecular O2 to produce highly reactive oxygen species including superoxide

(\*O<sub>2</sub><sup>-</sup>) and hydroxyl radicals (\*OH) upon simulated sunlight irradiation, which endowed COF with high activity in the photodegradation of organic pollutants. 95% of the methyl orange was decomposed after 100 minutes of irradiation, outperforming the benchmark P25 TiO2 under identical conditions. Moreover, v-2D-COF-O1 exhibited high photocatalytic disinfection ability in killing bacterial in water. Two bacterial S. aureus and E. coli were efficiently killed under aerobic conditions with light. The high bactericidal activity and high reusability demonstrate the vast potential of COF in practical water treatment.

COF-based heterostructures. Beyond the bare COF photocatalysts, COF-based heterostructures, such as COF/MOF, COF/ g-C<sub>3</sub>N<sub>4</sub>, COF/Fe<sub>3</sub>O<sub>4</sub>, COF/TiO<sub>2</sub>, and COF/metal sites, have garnered enormous attention since the inherent heterojunction can effectively foster the transport and separation of photogenerated charge carriers, which intensifies the photodegradation efficiency of pollutants. <sup>126</sup> In 2020, Lu and co-workers immobilized ultrasmall Au clusters into a thiol-decorated imine COF, which was prepared by a post-synthetic thiol-ene reaction between 1,2-ethanedithiol and a divinyl-tagged COF. 180 Due to the strong Au-SH interaction that stabilized Au NPs, Au clusters were in situ formed within the COF, exhibiting ultrasmall size and monodispersity. Importantly, the resultant Z-scheme photocatalysts presented a 2-fold higher activity than that of the bare COF in the photodegradation of organic pollutants including RhB and bisphenol A, which is due to the promoted charge separation originating from the COF-Au Z-scheme photocatalytic system.

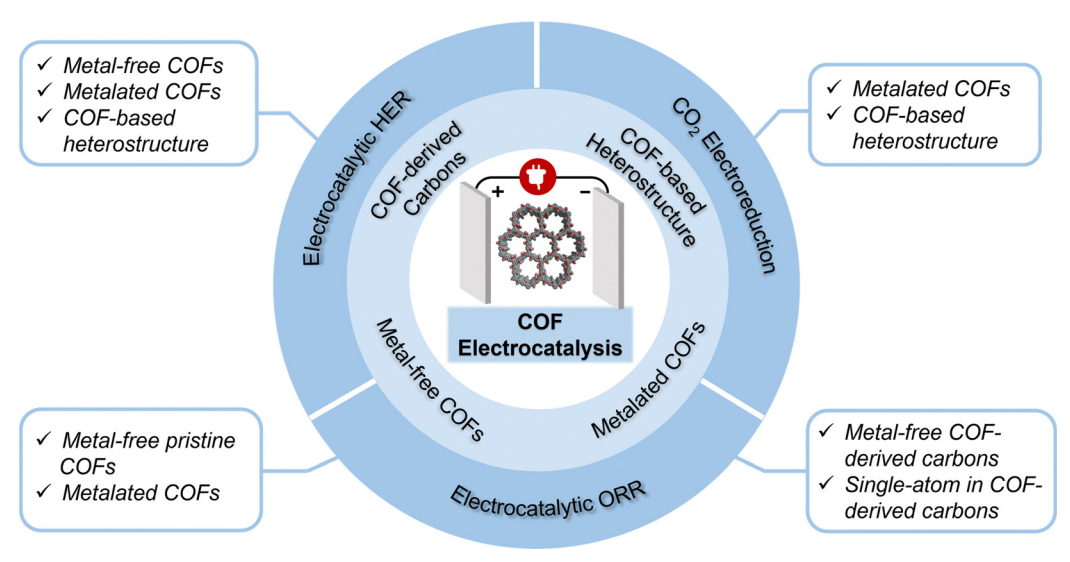
## 6. Electrocatalysis in COFs

#### 6.1. Advantages of COFs in electrocatalysis

The urgent goal of achieving carbon neutrality by mid-century in response to global warming and energy shortage demands advanced energy conversion and storage, making electrocatalysis a potent option for this goal. To fabricate highperformance electrocatalysts, high intrinsic electrical conductivity, large surface area, exposed catalytic sites, and profound stabilities are imperative. Like the advantages of using COFs for thermocatalysis and photocatalysis, the ordered  $\pi$ -skeletons, large surface area, tunable pore metrics, precise pore environment, and homogeneous dispersion of active sites endow COFs with high catalytic efficiency in various electrocatalytic reactions in acidic/alkaline media. 181 COF-based electrocatalysts are categorized as follows: metal-free heteroatom-doped COFs, metalated COFs, COF-based heterostructures, and COF-derived carbons (Scheme 5). In this section, we will elaborate on the leading design principles of COF electrocatalysts and highlight their most recent progress in electrocatalytic HER, oxygen reduction reaction, and CO2 reduction.

#### 6.2 COFs for electrocatalytic HER

Electrocatalytic HER can convert electricity into clean H2 on a large scale and is of immense significance for addressing the



Scheme 5 Main design strategies of COF electrocatalysts for diversified electrocatalysis.

pressing energy crisis. However, HER requires a large driving overpotential to overcome the energy barrier of water splitting, which can be lowered with the aid of state-of-the-art Pt catalysts. Nevertheless, the scarcity of Pt hinders its extensive application. Consequently, pursuing alternate electrocatalysts combing both low cost and high efficiency has been the subject of extensive research. Since 2017, COFs have gained increasing popularity for electrocatalytic HER and COF catalysts can be designed by using bare heteroatom-doped COFs, metalated COFs, and COF-based heterostructures.

Bare metal-free heteroatom-doped COFs. Heteroatoms (e.g., N, S, P) arranged in the ordered skeleton of COFs have been shown as electroactive centers for HER. The first heteroatomdoped COF electrocatalyst for HER was described by Pradhinan and co-workers in 2017. 182 Since then, a few 2D imine COFs have been reported as metal-free electrocatalysts for HER. 183 In 2022, Fang and co-workers developed two thiophene-triazinebased imine COFs (JLNU-301 and 302, Fig. 10A).<sup>184</sup> The resultant COFs exhibited low overpotentials of 136 and 91 at 10 mA cm<sup>-2</sup>, as well as small Tafel slopes in alkaline solution. This high HER activity was attributed to the abundant thiophene-S units, which imparted enhanced conductivity,

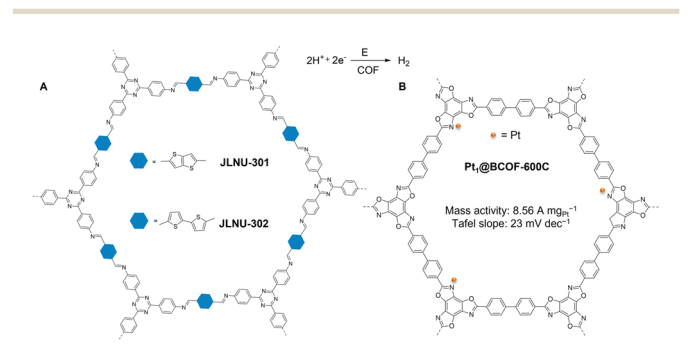


Fig. 10 Schematics of (A) JLNU-301 and -302; (B) single-atom Pt<sub>1</sub>@BCOF-600C for electrocatalytic HER in acidic media.

charge mobility, and synergistic effects with the 1D nanochannels of COFs. Furthermore, these experimental results are corroborated by DFT calculations. Despite these promising findings, the electrocatalytic activity of metal-free COFs in HER is far from satisfactory.

Metalated COFs. To promote the electrocatalytic HER activity of metal-free bare COFs, incorporating catalytically active metal sites into chemically robust COFs like sp<sup>2</sup>c-COFs has been actively explored. For instance, an active HER electrocatalyst, Ru/COF-1, was reported in 2022 by encapsulating ruthenium(III) chloride in a triazine-cored sp<sup>2</sup>c-COF (COF-1) composted of 2,4,6-trimethyl-1,3,5-triazine and terephthaldehyde via a solution impregnation method. Ru/COF-1 retained its high crystallinity and porosity. Importantly, the protonation of triazine cores under acidic conditions significantly improved the conductivity of Ru/COF-1, resulting in a low overpotential of 200 mV at 10 mA cm<sup>-2</sup>. In contrast, the metal-free COF-1 was almost inactive, indicating the essential role of Ru as the active site in electrocatalytic HER. Moreover, the sp<sup>2</sup>c linkage endowed Ru/COF-1 with salient durability in a 0.5 M H<sub>2</sub>SO<sub>4</sub> solution after 1000 consecutive voltammetry cycles. DFT calculations suggested that tetracoordinated Ru-N<sub>2</sub>Cl<sub>2</sub> moieties are the major active sites for superb HER performance. Analogously, Pd(II) chloride was immobilized in a pyrene-based 2D sp<sup>2</sup>c-COF and the resultant Pd/COF functioned as an active HER electrocatalyst with an overpotential of 128 mV at 10 mA cm $^{-2}$ , <sup>186</sup> exceeding the electrocatalytic activity of bare COF and free PdCl<sub>2</sub>. These studies have shown the great promise of metalated sp<sup>2</sup>c-COF electrocatalysts towards HER, calling for more scientific efforts in this field.

COF-based heterostructures. Bare COF electrocatalysts often have low electrical conductivity, which limits their electrocatalytic activity. To alleviate this shortcoming, Baek and coworkers recently (2022) applied a thermal treatment (600 °C, 1 hour in N<sub>2</sub>) to an ultrastable 2D benzoxazole-linked COF (BCOF) composed of 1,3,5-triamino-2,4,6-benzenetriol

and 4,4'-biphenyldicarboxaldehyde (Fig. 10B), 187 giving rise to a conductive benzoxazole COF/carbon hybrid (BCOF-600C) with high porosity (1820 m<sup>2</sup> g<sup>-1</sup>), retained crystallinity, and exceptional chemical stability under harsh chemical conditions. In addition, single-atom Pt was incorporated into the nanochannels of BCOF-600C (Pt<sub>1</sub>@BCOF-600C) via a facile solution impregnation approach. The atomically dispersed Pt atoms anchored in the COF were confirmed by high-angle annular dark-field scanning transmission electron microscopy coupled with EXAFS analysis. Pt<sub>1</sub>@BCOF-600C showed a high mass activity of 8.56 A mg<sub>Pt</sub><sup>-1</sup> at 30 mV and the smallest Tafel slope of 23 mV dec<sup>-1</sup> towards HER in acidic media, making it the best-performing COF-based HER electrocatalyst to date. Moreover, Pt<sub>1</sub>@BCOF-600C displayed high electrochemical durability, as evidenced by a long-term chronoamperometry test. This work showcases a new strategy for the design of metal/COF heterostructures as efficient electrocatalysts.

#### 6.3 COFs for electrocatalytic oxygen reduction reaction (ORR)

Electrocatalytic ORR is of prime importance for electrochemical energy conversion and storage, as it is ubiquitous in proton exchange membrane fuel cells and metal-air batteries. To accelerate the kinetics of ORR, a wide range of electrocatalysts have been developed, including noble metals, transition metal chalcogenides, single-atom catalysts, conjugated porous polymers, carbonaceous materials, and MOFs. Since 2015, COFs and their derivatives have drawn extensive attention in electrocatalytic ORR, 188 which can be rationally designed by using metal-free COFs, metalated COFs, metal-free COF-derived carbons, and single-atom metal in COF-derived carbons.

Metal-free heteroatom-doped COFs. Heteroatom-doped carbons are highly effective ORR electrocatalysts, but the pyrolysis synthesis makes it extremely challenging to clarify the real active sites. To develop ORR catalysts with atomically precise active centers, Fang and co-workers reported the first pyrolysisfree bulk COFs (JUC-527 and JUC-528, Fig. 11A) as ORR electrocatalysts in 2020.189 These COFs were synthesized by Schiffbase condensation of 2,4,6-tris(4-aminophenyl) benzene and thiophene-containing building blocks. JUC COFs demonstrated a higher ORR activity than that of the thiophene-free COF in a 0.1 M KOH electrolyte, indicating that thiophene-sulfur motifs acted as electroactive centers. JUC-528 with more thiophene-S

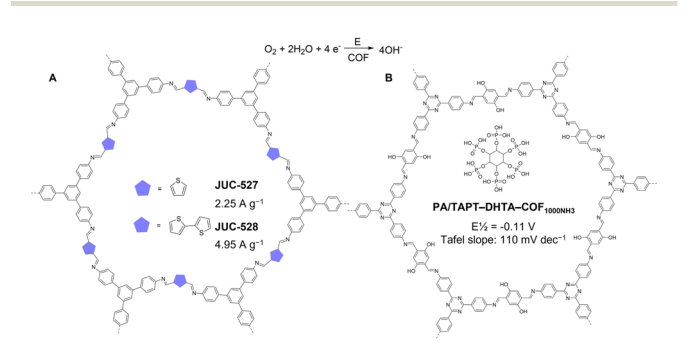


Fig. 11 Schematics of (A) JUC-527 and JUC-528, (B) PA/TAPT-DHTA- $\mathsf{COF}_{\mathsf{1000\,NH}_3}$  electrocatalytic ORR in alkaline media.

structures showed a more positive half-wave potential, a smaller Tafel slope, and higher mass activity than those of JUC-527. DFT calculations further disclosed the adjacent pentacyclic thiophene-S units mainly contributed to the ORR activity. Despite the initial success of metal-free COFs for electrocatalytic ORR, 190 their intrinsically low conductivity usually results in inferior catalytic performances.

Metalated COFs. Metalloporphyrin and metallophthalocyanine-based COFs are commonly used as ORR electrocatalysts. 191-193 However, the clear structure-activity relationships in COF-based electrocatalytic ORR are not yet fully understood. In 2021, Tang and co-workers investigated the effect of metal sites in metalloporphyrin COFs on their corresponding ORR activity. 194 Four novel isoreticular porphyrin COFs (M-TP-COF, M = H2, Co, Ni, and Mn) were rationally designed by condensing different 5,10,15,20-tetrakis(paraaminophenyl) porphyrins (M-TAPP,  $M = H_2$ , Co, Ni, and Mn) and 1,1,2,2-tetrakis(4-formyl-(1,10biphenyl))ethane, which were utilized as ORR catalysts in a 0.1 M KOH electrolyte. Despite similar structures and metal coordination environment, Co-porphyrin-COF displayed higher catalytic performance, with a half-wave potential of 0.73 V, an onset potential of 0.81 V, and a current density of 4.8 mA cm<sup>2</sup> compared to those of Mn-, Ni-, H-porphyrin-COFs and commercial Pt/C. DFT calculations revealed that the ORR activity difference was consistent with the Gibbs free energy diagram based on O<sub>2</sub>-O<sub>2</sub>\*-OOH\*-O\*-OH\*-OH<sup>-</sup> route. This work demonstrates an effective strategy for adjusting ORR catalytic performance by subtly tunning the COF skeleton, ultimately resulting in the rational design and improvement of COF electrocatalysts.

Metal-free COF-derived carbons. Heteroatom-doped carbons have emerged as promising non-noble catalysts for ORR, due to their exceptional combination of conductivity, durability, and cost-effectiveness. Since 2016, researchers have explored COFs as sacrificial precursors for the synthesis of heteroatom-doped carbons. 195,196 To preserve the 2D features of pyrolyzed COFs, Jiang and co-workers introduced phytic acid (PA) as a template to guide the pyrolysis of a 2D imine COF (TAPT-DHTA-COF, Fig. 11B) at 1000 °C under N<sub>2</sub>. 197 The produced 2D graphitic carbons (PA/TAPT-DHTA-COF<sub>1000</sub>) exhibited high electrical conductivity, hierarchical porosity, and abundant N- and P-doped catalytic edges, superior to that obtained from the direct template-free thermolysis. Further pyrolysis of the 2D graphitic carbons under an ammonia atmosphere at 900 °C increased the active site and improved the pore volume of the emergent PA/ TAPT-DHTA-COF<sub>1000NH</sub>, which showed a much higher ORR activity than commercial Pt/C under alkaline conditions. Intrigued by this finding, there has been growing interest in developing heteroatom-doped COF-derived carbons for ORR. A few COF precursors have been pyrolyzed, including LZU-COF-1, 198 β-ketonenamine-linked BDF COF, 199 etc.

Single-atom metal in COF-derived carbons. Single-atom catalysts (SACs) are at the forefront of catalysis due to their maximum atom utilization efficiency and extraordinary catalytic performance. Recently, COF-derived carbons have emerged as promising support for SACs as ORR catalysts.200 In 2020, Li and co-workers first prepared atomically dispersed Fe atoms in

COF-derived carbons (Fe-ISAS/CN) via an absorption-pyrolysis strategy, <sup>201</sup> wherein Fe(III) ions were first immobilized in a 2D imine COF made by ambient condensation of 1,3,5-tris(4aminophenyl) benzene and benzene-1,3,5-tricarboxaldehyde, succeeded by pyrolysis in an inert atmosphere at 900 °C. Single-atom Fe sites were uniformly embedded in the COFderived N-doped carbon nanospheres (Fe-ISAS/CN), which was unambiguously confirmed by XANES and EXAFS analyses. Fe-ISAS/CN served as an excellent ORR electrocatalyst in a 0.1 M KOH electrolyte, exhibiting a half-wave potential of 0.861 V and a current density of 5.47 mA cm<sup>2</sup>, which exceeded those of Pt/C, metal-free COF-derived carbons, and Fe NPs/COF-derived carbons. Furthermore, Fe-ISAS/CN showed good stability even after 5000 cycles and methanol tolerance. Following this strategy, various SACs embedded in COF-derived carbons have been reported, such as single-atom Pt/3D imine COF-derived carbons, 202 single-atom Fe/sp2c-COF-derived carbons, 203 exhibiting higher ORR activity than commercial Pt/C.

#### 6.4 COFs for CO<sub>2</sub> electroreduction

The conversion of CO<sub>2</sub> into value-added carbonaceous products via electroreduction under mild operating conditions has been recognized as a sustainable strategy to achieve carbon neutrality. However, a significant obstacle to the broad use of CO2 electroreduction is the competitive HER in aqueous electrolytes, which leads to low energy efficiency and poor selectivity for CO2 electroreduction. To address this issue, massive efforts have been focused on enhancing CO<sub>2</sub> reduction while simultaneously inhibiting competitive HER, leading to the development of a wide range of active, selective, and durable electrocatalysts, such as metal NPs, metal dichalcogenide, molecular catalysts, and MOFs. Since the first attempt in 2015, COFs have attracted enormous attention for CO2 electroreduction recently (Table 4). COF-based electrocatalysts can be

synthesized by incorporating active metal sites like metalloporphyrin and metallophthalocyanines into the skeletons of COFs and hybridizing COFs with conductive carbon materials. As of now, most COF-based electrocatalysts produce CO as the primary product via a two-electron transfer pathway, with few deeply reduced multi-carbon (C2+) products observed. 204

Metalated COFs. COFs containing metalated secondary structural units such as metalloporphyrins and metallophthalocyanine have demonstrated significant in heterogeneous CO<sub>2</sub> electroreduction. The precise integration of metalated macrocyclic units into the periodic networks of COFs not only overcomes the limitations of molecular catalysts but also enables the reticular electronic tuning of metalated sites to achieve optimized catalytic performance.205 The first exploration of COFs for CO2 electroreduction was pioneered by Yaghi and co-workers in 2015. 206 Two Co(II)-porphyrin imine-linked COFs were deposited on porous conductive carbon fabric for the electroreduction of CO<sub>2</sub> to CO. To enhance the stability of the COF electrocatalyst, Jiang and co-workers reported two polyimide-linked Co(II)-phthalocyanine-based COFs (CoPc-PI-COF-1 and CoPc-PI-COF-2, Fig. 12A), which were prepared by condensing tetraanhydrides of 2,3,9,10,16,17,23,24-octacarboxyphthalocyaninato cobalt(II) with 1,4-phenylenediamine and 4,4'-biphenyldiamine, respectively. 207 Thanks to the abundant Co(II) electroactive sites, exceptional chemical resistance (12 M HCl for 20 d), permanent porosity, and strong CO<sub>2</sub> adsorption, CoPc-PI-COFs/carbon black cathodes displayed high CO faradaic efficiency (87-97%) at various potentials of -0.60 to -0.90 V (vs. RHE) in 0.5 M KHCO<sub>3</sub> solution, outperforming the homogeneous control CoPc/carbon black electrode. Notably, CoPc-PI-COF-1 provided a larger current density and higher electrical conductivity than those of expanded CoPc-PI-COF-2. In addition, CoPc-PI-COFs displayed excellent longterm durability with high faradaic efficiency (>91%) of CO

Table 4 Summary of the recent representative COFs for CO<sub>2</sub> electroreduction<sup>a</sup>

| Photocatalyst             | Linkage      | Electrolyte             | Potential<br>(V vs. RHE) | FEco<br>(%)     | TOF                                    | $J_{\rm CO} \  m (mA\ m^{-2})$ | Tafel slope<br>(mV dec <sup>-1</sup> ) | Year       | Ref. |
|---------------------------|--------------|-------------------------|--------------------------|-----------------|--|--------------------------------|--|------------|------|
| 3D-Por(Co/H)-COF          | Imine        | 0.5 M KHCO <sub>3</sub> | -0.6                     | 92.4            | 4610 h <sup>-1</sup> (-1.1 V)          | -15.5 (-1.1 V)                 | _                                      | 2022       | 208  |
| CoPc-PI-COF-3 (3D)        | Imide        | 0.5 M KHCO <sub>3</sub> | -0.9                     | 96              | $0.6 \text{ s}^{-1}$                   | -31.7                          | 117                                    | 2022       | 209  |
| MWCNT-Por-COF-Co          | Imine        | 0.5 M KHCO <sub>3</sub> | -0.6                     | 99.3            | $70.6 \text{ s}^{-1} (-1.0 \text{ V})$ | -18.77                         | 319                                    | 2022       | 221  |
| MCH-3 (Cu-COF-366-OH@MOF) | Imine        | 1 M KOH                 | -1.0                     | $76.7^{b}$      | _                                      | -398.1                         | _                                      | 2022       | 222  |
| CoPc-PI-COF-1             | Imide        | 0.5 M KHCO <sub>3</sub> | -0.7                     | 93              | $2.2 \text{ s}^{-1}$                   | -9.4                           | 95                                     | 2021       | 207  |
| CoPc-PI-COF-2             |              |                         | -0.9                     | 95              | $4.9 \text{ s}^{-1}$                   | -21.2                          |  |            |      |
|                           |              |                         | -0.7                     | 95              | $1.9 \text{ s}^{-1}$                   | -6.2                           | 105                                    |            |      |
|                           |              |                         | -0.9                     | 92              | $5.0 \text{ s}^{-1}$                   | -16.6                          |  |            |      |
| Cu-Tph-COF-Dct            | Imine        | 1 M KOH                 | -0.9                     | $80^b$          | _                                      | -175.2                         | _                                      | 2021       | 210  |
| AAn-COF-Cu (NF)           | Keto-enamine | 1 M KOH                 | -0.9                     | 77 <sup>b</sup> | _                                      | -128.1                         | 379.7                                  | 2021       | 211  |
| OH-AAn-COF-Cu (HT)        |              |                         | -1.0                     | $61^b$          |  | -47.1                          | 311.2                                  |            |      |
| $COF_{bpyMn}$             | Imine        | 0.5 M KHCO <sub>3</sub> | -1.34                    | 55              | $805 \text{ h}^{-1}$                   | -15                            | _                                      | 2021       | 218  |
| TAPP(Co)-B18C6-COF        | Imine        | 0.5 M KHCO <sub>3</sub> | -0.7                     | 93.3            | $696 \text{ h}^{-1}$                   | -9.45                          | 173                                    | 2021       | 219  |
|                           |              |                         | -0.9                     | 84.4            | $1267 h^{-1}$                          |                                |  |            |      |
| NiPc-COF                  | Phenazine    | 0.5 M KHCO <sub>3</sub> | -0.9                     | 99.1            | $2155 h^{-1}$                          | -35 (-1.1 V)                   | 117                                    | 2020       | 212  |
| Co-TTCOF                  | Imine        | 0.5 M KHCO <sub>3</sub> | -0.7                     | 91.3            | $267 h^{-1}$                           | -1.84                          | 237                                    | 2020       | 213  |
| TT-Por(Co)-COF            | Imine        | 0.5 M KHCO <sub>3</sub> | -0.6                     | 91.4            | 481 h <sup>-1</sup> (-0.7 V)           | -7.28                          | _                                      | 2020       | 214  |
| CoPc-PDQ-COF              | Phenazine    | 0.5 M KHCO <sub>3</sub> | -0.66                    | 96              | $11412 \text{ h}^{-1}$                 | -49.4                          | 112                                    | 2020       | 215  |
| NiPc-TFPN COF             | Ether        | 0.5 M KHCO <sub>3</sub> | -0.9                     | 99.8            | $490 \text{ h}^{-1}$                   | -14.1                          | 209.9                                  | $2020^{c}$ | 216  |
| CoPc-TFPN COF             |              |                         | -0.9                     | 96.1            | 369 h <sup>-1</sup>                    | -10.6                          | 570                                    |            |      |

<sup>&</sup>lt;sup>a</sup> FE: faradaic efficiency; TOF: turnover of frequency. J: partial current density. <sup>b</sup> The main product is CH<sub>4</sub>. <sup>c</sup> Photo-coupled electrocatalysts.

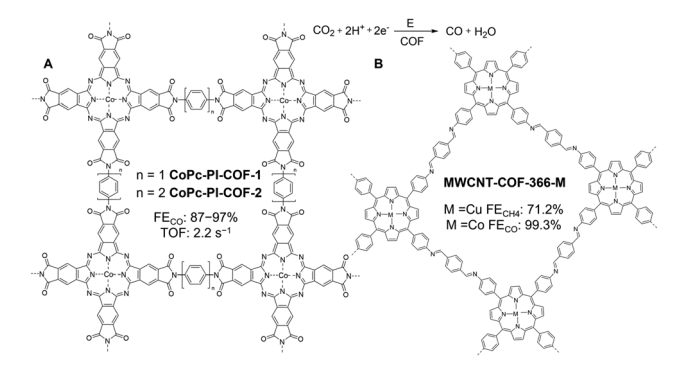


Fig. 12 Schematics of (A) CoPc-PI-COF-1 and CoPc-PI-COF-2; and (B) CNT@COF-366-R-M for CO<sub>2</sub> electroreduction in alkaline media.

even after 40 hours. DFT-calculated Gibbs free energy diagram accounts for the high and discriminative electrocatalytic activities of CoPc-PI-COFs. Later in 2021, the same group extended this strategy to 3D COFs, which has been largely unexplored in CO<sub>2</sub> electroreduction.<sup>208</sup> They synthesized two polyimidelinked phthalocyanine-based 3D COFs (MPc-PI-COF-3, M = Co and H<sub>2</sub>) through the condensation of 2,3,9,10,16,17,23,24octacarboxyphthalocyanine tetraanhydride, M(TAPc) and 1,3,5,7-tetra(4-aminophenyl)adamantine. The resultant 3D COFs adopted interpenetrated pts nets and exhibited high affinity towards CO2. Importantly, 3D COFs possessed high concentrations of exposed electrocatalytic sites, accounting for 32.7% of the total Co-Pc units. These unique structural attributes made them highly active in CO<sub>2</sub> electroreduction. The CoPc-PI-COF-3 exhibited a high CO faradaic efficiency (88-96%) at the voltage range of -0.60 to -1.00 V (vs. RHE), and a large current density of  $-31.7 \text{ mA cm}^{-2}$  at -0.90 V, far exceeding its 2D COF and metal-free 3D COF counterparts. Recently, exploring metalated COFs for CO2 electroreduction has been a theme of intense research, 210-214 resulting in a few notable electrocatalysts, such as phenazine-linked cobalt(II) phthalocyanine COFs, 215 dioxin-linked metallophthalocyanine COFs, 216 Agdoped 3D amine-linked COF (Ag/COF-300-RR), 217 single-atom Mn in bipyridine-based COFs, 218 crown-ether functionalized Co(TAPP)-COF, 219 zwitterionic cobalt tetraamino phthalocyanine-based squaraine-linked COF (COP-SA), 220 etc.

COF-based heterostructures. To improve the low electrical conductivity of bare COFs while retaining the atomically precise structure, COFs can be hybridized with electrically conducting carbon materials (e.g., graphene, and carbon nanotubes) to afford conductive COF/carbon heterostructures. Zhang and coworkers recently (2022) developed a series of COF/carbon nanotubes (CNT) heterostructures by covalently linking metalloporphyrin COF-366 (Co, Ni, Fe, Cu, Fig. 12B) with CNTs for CO2 electroreduction.221 The CNTs acted as both carriers to uniformly disperse COF-366 and as controllers to facilitate the electron transfer between porphyrin and metal active centers. Noteworthy, CNT/COF-366-Cu displayed high CH<sub>4</sub> faradaic efficiency of 71.2% in a 1.0 M KOH electrolyte, which was attributed to the in situ generated Cu nanoclusters during the electrocatalytic process. Altering the metal sites from Cu to Co

led to a remarkable CO faradaic efficiency of up to 99.3% at -0.60 V, much higher than those of bare Por-COF-Co and physically blended CNT/Por-COF-Co.

Apart from CNTs, a honeycomb-like MOF/COF heterostructure (MCH-1-4) was designed by growing COF-366-OH-Cu layers on the surface of (Zr)-UiO-66-NH<sub>2</sub> MOF in 2022.<sup>222</sup> The high porosity, structural regularity, unique honeycomb morphology of MOFs, and abundant Cu-N<sub>4</sub> catalytic centers in MCH-3 facilitated the CO2 adsorption, activation, and reduction into a rare CH<sub>4</sub> product, showing an outstanding current density (398.1 mA cm $^{-2}$ ) and a higher CH<sub>4</sub> faradaic efficiency (76.7%) than that of bare COF (37.5%), and MOF (15.9%), the physically blended mixture (38.0%), and COF/MOF with no honeycomb morphology (47.7%). DFT calculations corroborated the crucial role of (Zr)-UiO-66-NH2 in CO2 adsorption, activation, intermediate stabilization, and overcoming the energy barrier of the rate-determining step in CO2 electroreduction.

## 7. Summary and outlook

COFs are a rapidly developing class of porous materials that offer an advantageous catalytic platform over traditional porous solids. Their unique combination of crystallinity, porosity, structural tunability, functional diversity, and durability render them a game-changer in heterogeneous catalysis. In this review, we have shed light on the chemistry of COFs and highlighted the current research frontiers in structural evolution, linkage chemistry, and expeditious synthesis. We have surveyed the core design principles of COF catalysts (Scheme 2) and spotlighted the most recent advances (2020-2023) in COF-based heterogeneous catalysis. In thermocatalysis (Scheme 3), COF catalysts are designed by de novo synthesis using monomers with catalytically active sites, PSM strategy, encapsulating catalytic species within COFs, and creating COF-based heterostructures. These catalysts have revealed excellent activity, selectivity, and recyclability in diverse chemical reactions, including cross-coupling reactions, redox reactions, biomass conversion, addition reactions, etc. In photocatalysis (Scheme 4), COF photocatalysts are judiciously fabricated by using bare COFs with desired linkage and backbone, immobilizing homogeneous photocatalysts in COFs, and creating heterojunction in COFs. The emergent photocatalysts exhibit high yet controllable catalytic performance in photoredox catalysis, HER, CO<sub>2</sub> photoreduction, and aqueous pollutant degradation. Lastly, although in infancy, various COF electrocatalysts (Scheme 5), such as heteroatomdoped bare COFs, metalated COFs, COF-based heterostructures, and COF-derived carbons, have demonstrated enormous prospects in electrocatalytic applications including HER, ORR, and CO<sub>2</sub> reduction.

Despite a decade of research, COF catalysis is still in its nascent stage and calls for more scientific efforts to fully harness the potential of COF catalysts. Several unsettled challenges are yet to tackle and are listed below.

(i). The utilization of 2D COFs dominates the field of heterogeneous catalysis, while 3D COFs remain largely

underexplored, despite their intriguing properties that are apt for catalysis. Hence, exploring the potential of 3D COF catalysis is of vast scientific significance and highly desired.

- (ii). Developing COF catalysts that can maintain long-term stability under stringent conditions remains a grand challenge. Emerging robust COFs such as sp<sup>2</sup>c-COFs and aryl ether-linked COFs feature extraordinary chemical stabilities in drastic chemical environments and hold immense potential in practical catalysis.
- (iii). The predominant solvothermal synthesis of COFs is a major hurdle to their practical use due to the slow reaction times, cumbersome conditions, and deficient scalability. Therefore, it is of utmost interest to develop facile, rapid, green, economical, and scalable methods for synthesizing COF catalysts.
- (iv). The intrinsic micro- and mesopores in COFs can restrict the mass transport and diffusion of substrates during catalysis. Therefore, there is a growing interest in the development of COFs with hierarchical porosity, which are expected to improve catalytic efficiency and merit further exploration.
- (v). To meet industrial needs, shaping the brittle COF powders into processable solids, such as thin films, monoliths, pellets, gels, and foams may result in unique catalytic outcomes. However, this area of study remains scarcely explored thus far.
- (vi). The catalytic reaction scope of COF catalysts is rather limited when compared to MOFs. The potential of COFs in highly sought-after catalytic processes such as gas-phase reaction, continuous flow catalysis, biomass valorization, cascade catalysis, C-H activation, selective methane oxidation, and nitrogen fixation remains largely unexplored. Therefore, it is crucial to invest significant efforts in expanding the application of COF catalysts in these cutting-edge catalytic reactions.
- (vii). An in-depth understanding of catalytic mechanisms is imperative for the rational design and improvement of COF catalysts. Therefore, a synergistic combination of computational, in situ spectroscopic methods (e.g., IR, Raman, X-ray absorption spectroscopy, etc.) and sophisticated characterization techniques can collectively unravel underlying catalytic mechanisms by dint of monitoring the progression of the reaction, uncovering real active sites, clarifying reaction intermediates, and deconvoluting the reaction pathway.

Addressing the challenges outlined above will not only unleash the immense potential of COFs in heterogeneous catalysis, but also exert profound impacts on other niche applications. Looking forward, future research should prioritize addressing these knowledge gaps by developing COF catalysts with an unrivaled combination of high reactivity, superb selectivity, pronounced stability, broad scope, facile synthesis, and clarified mechanism. Despite tremendous challenges ahead, we foresee that COFs will continue to trigger everincreasing research efforts in heterogeneous catalysis, ultimately contributing to the global efforts to combat the energy and ecological crisis.

#### Conflicts of interest

The authors declare no conflict of interest.

## Acknowledgements

The authors acknowledge the support from the U.S. Department of Energy Early Career Award (DE-SC0022000), the National Science Foundation HBCU-UP-RIA program (2100360), and the PREM program (DMR-2122147). Z. A. acknowledges the support from Qassim University. Finally, X. L. is grateful for his daughter, Aria Li's birth during the preparation of this review.

#### Notes and references

- 1 F. Zaera, The New Materials Science of Catalysis: Toward Controlling Selectivity by Designing the Structure of the Active Site, J. Phys. Chem. Lett., 2010, 1, 621-627.
- 2 F. Wang, J. D. Harindintwali, Z. Yuan, M. Wang, F. Wang, S. Li, Z. Yin, L. Huang, Y. Fu and L. Li, Technologies and perspectives for achieving carbon neutrality, Innovation, 2021, 2, 100180.
- 3 R. Schlögl, Heterogeneous catalysis, Angew. Chem., Int. Ed., 2015, 54, 3465-3520.
- 4 C. S. Diercks and O. M. Yaghi, The atom, the molecule, and covalent organic framework, Science, 2017, 355, eaal1585.
- 5 K. Geng, T. He, R. Liu, S. Dalapati, K. T. Tan, Z. Li, S. Tao, Y. Gong, Q. Jiang and D. Jiang, Covalent organic frameworks: design, synthesis, and functions, Chem. Rev., 2020, **120**, 8814-8933.
- 6 S.-Y. Ding, J. Gao, Q. Wang, Y. Zhang, W.-G. Song, C.-Y. Su and W. Wang, Construction of covalent organic framework for catalysis: Pd/COF-LZU1 in Suzuki-Miyaura coupling reaction, J. Am. Chem. Soc., 2011, 133, 19816-19822.
- 7 R. K. Sharma, P. Yadav, M. Yadav, R. Gupta, P. Rana, A. Srivastava, R. Zbořil, R. S. Varma, M. Antonietti and M. B. Gawande, Recent development of covalent organic frameworks (COFs): synthesis and catalytic (organicelectro-photo) applications, Mater. Horiz., 2020, 7, 411-454.
- 8 J. Guo and D. Jiang, Covalent organic frameworks for heterogeneous catalysis: principle, current status, and challenges, ACS Cent. Sci., 2020, 6, 869-879.
- 9 Y. Yusran, H. Li, X. Guan, Q. Fang and S. Qiu, Covalent organic frameworks for catalysis, EnergyChem, 2020, 2, 100035.
- 10 Y. Zhi, Z. Wang, H. L. Zhang and Q. Zhang, Recent progress in metal-free covalent organic frameworks as heterogeneous catalysts, Small, 2020, 16, 2001070.
- 11 A. P. Cote, A. I. Benin, N. W. Ockwig, M. O'Keeffe, A. J. Matzger and O. M. Yaghi, Porous, crystalline, covalent organic frameworks, Science, 2005, 310, 1166-1170.
- 12 Y. Zhao, S. Das, T. Sekine, H. Mabuchi, T. Irie, J. Sakai, D. Wen, W. Zhu, T. Ben and Y. Negishi, Record Ultralarge-Pores, Low Density Three-Dimensional Covalent Organic Framework for Controlled Drug Delivery, Angew. Chem., Int. Ed., 2023, 135, e202300172.
- 13 L. A. Baldwin, J. W. Crowe, D. A. Pyles and P. L. McGrier, Metalation of a Mesoporous Three-Dimensional Covalent

- Organic Framework, J. Am. Chem. Soc., 2016, 138, 15134-15137.
- 14 Z. Mu, Y. Zhu, B. Li, A. Dong, B. Wang and X. Feng, Covalent Organic Frameworks with Record Pore Apertures, J. Am. Chem. Soc., 2022, 144, 5145-5154.
- 15 Y. Yue, H. Li, H. Chen and N. Huang, Piperazine-Linked Covalent Organic Frameworks with High Electrical Conductivity, J. Am. Chem. Soc., 2022, 144, 2873-2878.
- 16 R.-R. Liang and X. Zhao, Heteropore covalent organic frameworks: a new class of porous organic polymers with well-ordered hierarchical porosities, Org. Chem. Front., 2018, 5, 3341-3356.
- 17 N. Huang, L. Zhai, D. E. Coupry, M. A. Addicoat, K. Okushita, K. Nishimura, T. Heine and D. Jiang, Multiple-component covalent organic frameworks, Nat. Commun., 2016, 7, 12325.
- 18 S. J. Lyle, P. J. Waller and O. M. Yaghi, Covalent organic frameworks: organic chemistry extended into two and three dimensions, Trends Chem., 2019, 1, 172-184.
- 19 Q. Zhu, X. Wang, R. Clowes, P. Cui, L. Chen, M. A. Little and A. I. Cooper, 3D Cage COFs: A Dynamic Three-Dimensional Covalent Organic Framework with High-Connectivity Organic Cage Nodes, J. Am. Chem. Soc., 2020, 142, 16842-16848.
- 20 C. Yu, H. Li, Y. Wang, J. Suo, X. Guan, R. Wang, V. Valtchev, Y. Yan, S. Qiu and Q. Fang, Three-Dimensional Triptycene-Functionalized Covalent Organic Frameworks with hea Net for Hydrogen Adsorption, Angew. Chem., Int. Ed., 2022, 61, e202117101.
- 21 H.-S. Lu, W.-K. Han, X. Yan, C.-J. Chen, T. Niu and Z.-G. Gu, A 3D Anionic Metal Covalent Organic Framework with soc Topology Built from an Octahedral TiIV Complex for Photocatalytic Reactions, Angew. Chem., Int. Ed., 2021, 60, 17881-17886.
- 22 C. Gropp, T. Ma, N. Hanikel and O. M. Yaghi, Design of higher valency in covalent organic frameworks, Science, 2020, 370, eabd6406.
- 23 N. Huang, P. Wang and D. Jiang, Covalent organic frameworks: a materials platform for structural and functional designs, Nat. Rev. Mater., 2016, 1, 1-19.
- 24 D. Jiang, Covalent organic frameworks: an amazing chemistry platform for designing polymers, Chem, 2020, 6, 2461-2483.
- 25 R. Liu, K. T. Tan, Y. Gong, Y. Chen, Z. Li, S. Xie, T. He, Z. Lu, H. Yang and D. Jiang, Covalent organic frameworks: an ideal platform for designing ordered materials and advanced applications, Chem. Soc. Rev., 2021, 50, 120-242.
- 26 J. Hu, S. K. Gupta, J. Ozdemir and H. Beyzavi, Applications of dynamic covalent chemistry concept toward tailored covalent organic framework nanomaterials: A review, ACS Appl. Nano Mater., 2020, 3, 6239-6269.
- 27 B. J. Smith, A. C. Overholts, N. Hwang and W. R. Dichtel, Insight into the crystallization of amorphous imine-linked polymer networks to 2D covalent organic frameworks, Chem. Commun., 2016, 52, 3690-3693.
- 28 Z. Xiong, B. Sun, H. Zou, R. Wang, Q. Fang, Z. Zhang and S. Qiu, Amorphous-to-Crystalline Transformation: General

- Synthesis of Hollow Structured Covalent Organic Frameworks with High Crystallinity, J. Am. Chem. Soc., 2022, 144, 6583-6593.
- 29 C. Feriante, A. M. Evans, S. Jhulki, I. Castano, M. J. Strauss, S. Barlow, W. R. Dichtel and S. R. Marder, New mechanistic insights into the formation of imine-linked twodimensional covalent organic frameworks, J. Am. Chem. Soc., 2020, 142, 18637-18644.
- 30 C. Kang, K. Yang, Z. Zhang, A. K. Usadi, D. C. Calabro, L. S. Baugh, Y. Wang, J. Jiang, X. Zou and Z. Huang, Growing single crystals of two-dimensional covalent organic frameworks enabled by intermediate tracing study, Nat. Commun., 2022, 13, 1370.
- 31 X. Guan, F. Chen, Q. Fang and S. Qiu, Design and applications of three dimensional covalent organic frameworks, Chem. Soc. Rev., 2020, 49, 1357-1384.
- 32 X. Guan, Q. Fang, Y. Yan and S. Qiu, Functional regulation and stability engineering of three-dimensional covalent organic frameworks, Acc. Chem. Res., 2022, 55, 1912-1927.
- 33 X. Guan, F. Chen, S. Qiu and Q. Fang, Three-Dimensional Covalent Organic Frameworks: From Synthesis to Applications, Angew. Chem., Int. Ed., 2023, 62, e202213203.
- 34 H. L. Nguyen, C. Gropp, Y. Ma, C. Zhu and O. M. Yaghi, 3D Covalent Organic Frameworks Selectively Crystallized through Conformational Design, J. Am. Chem. Soc., 2020, 142, 20335-20339.
- 35 X. Guan, Y. Ma, H. Li, Y. Yusran, M. Xue, Q. Fang, Y. Yan, V. Valtchev and S. Qiu, Fast, ambient temperature and pressure ionothermal synthesis of three-dimensional covalent organic frameworks, J. Am. Chem. Soc., 2018, 140, 4494-4498.
- 36 T. Ma, E. A. Kapustin, S. X. Yin, L. Liang, Z. Zhou, J. Niu, L.-H. Li, Y. Wang, J. Su, J. Li, X. Wang, W. D. Wang, W. Wang, J. Sun and O. M. Yaghi, Single-crystal X-ray diffraction structures of covalent organic frameworks, Science, 2018, 361, 48-52.
- 37 L. Peng, Q. Guo, C. Song, S. Ghosh, H. Xu, L. Wang, D. Hu, L. Shi, L. Zhao, Q. Li, T. Sakurai, H. Yan, S. Seki, Y. Liu and D. Wei, Ultra-fast single-crystal polymerization of largesized covalent organic frameworks, Nat. Commun., 2021, **12**, 5077.
- 38 B. Gui, H. Ding, Y. Cheng, A. Mal and C. Wang, Structural design and determination of 3D covalent organic frameworks, Trends Chem., 2022, 4, 437-450.
- 39 F. Haase and B. V. Lotsch, Solving the COF trilemma: towards crystalline, stable and functional covalent organic frameworks, Chem. Soc. Rev., 2020, 49, 8469-8500.
- 40 X. Li, S. Cai, B. Sun, C. Yang, J. Zhang and Y. Liu, Chemically robust covalent organic frameworks: progress and perspective, Matter, 2020, 3, 1507-1540.
- 41 Y. Jin, Y. Hu, M. Ortiz, S. Huang, Y. Ge and W. Zhang, Confined growth of ordered organic frameworks at an interface, Chem. Soc. Rev., 2020, 49, 4637-4666.
- 42 B. Zhang, M. Wei, H. Mao, X. Pei, S. A. Alshmimri, J. A. Reimer and O. M. Yaghi, Crystalline dioxin-linked

- covalent organic frameworks from irreversible reactions, *I. Am. Chem. Soc.*, 2018, **140**, 12715–12719.
- 43 X. Li, H. Wang, H. Chen, Q. Zheng, Q. Zhang, H. Mao, Y. Liu, S. Cai, B. Sun and C. Dun, Dynamic covalent synthesis of crystalline porous graphitic frameworks, *Chem*, 2020, **6**, 933–944.
- 44 S. Yang, C. Yang, C. Dun, H. Mao, R. S. H. Khoo, L. M. Klivansky, J. A. Reimer, J. J. Urban, J. Zhang and Y. Liu, Covalent Organic Frameworks with Irreversible Linkages *via* Reductive Cyclization of Imines, *J. Am. Chem.* Soc., 2022, 144, 9827–9835.
- 45 L. Cusin, H. Peng, A. Ciesielski and P. Samorì, Chemical conversion and locking of the imine linkage: enhancing the functionality of covalent organic frameworks, *Angew. Chem., Int. Ed.*, 2021, **133**, 14356–14370.
- 46 X. Li, C. Zhang, S. Cai, X. Lei, V. Altoe, F. Hong, J. J. Urban, J. Ciston, E. M. Chan and Y. Liu, Facile transformation of imine covalent organic frameworks into ultrastable crystalline porous aromatic frameworks, *Nat. Commun.*, 2018, 9, 2998.
- 47 S. T. Emmerling, L. S. Germann, P. A. Julien, I. Moudrakovski, M. Etter, T. Friščić, R. E. Dinnebier and B. V. Lotsch, In situ monitoring of mechanochemical covalent organic framework formation reveals templating effect of liquid additive, *Chem*, 2021, 7, 1639–1652.
- 48 W. Zhao, P. Yan, B. Li, M. Bahri, L. Liu, X. Zhou, R. Clowes, N. D. Browning, Y. Wu and J. W. Ward, Accelerated Synthesis and Discovery of Covalent Organic Framework Photocatalysts for Hydrogen Peroxide Production, *J. Am. Chem. Soc.*, 2022, 144, 9902–9909.
- 49 Z. Alsudairy, N. Brown, C. Yang, S. Cai, F. Akram, A. Ambus, C. Ingram and X. Li, Facile Microwave-Assisted Synthesis of 2D Imine-Linked Covalent Organic Frameworks for Exceptional Iodine Capture, *Precis. Chem.*, 2023, DOI: 10.1021/prechem.3c00006.
- 50 M. Zhang, J. Chen, S. Zhang, X. Zhou, L. He, M. V. Sheridan, M. Yuan, M. Zhang, L. Chen and X. Dai, Electron beam irradiation as a general approach for the rapid synthesis of covalent organic frameworks under ambient conditions, *J. Am. Chem. Soc.*, 2020, 142, 9169–9174.
- 51 M. Matsumoto, R. R. Dasari, W. Ji, C. H. Feriante, T. C. Parker, S. R. Marder and W. R. Dichtel, Rapid, low temperature formation of imine-linked covalent organic frameworks catalyzed by metal triflates, *J. Am. Chem. Soc.*, 2017, 139, 4999–5002.
- 52 T. Feng, B. Sun, Q. Hao, J. Li, Y. Xu, H. Shang and D. Wang, Ambient synthesis of metal–covalent organic frameworks with Fe-iminopyridine linkages, *Chem. Commun.*, 2022, **58**, 8830–8833.
- 53 L. Zhang, R. Liang, C. Hang, H. Wang, L. Sun, L. Xu, D. Liu, Z. Zhang, X. Zhang, F. Chang, S. Zhao and W. Huang, A facile solution-phase synthetic approach for constructing phenol-based porous organic cages and covalent organic frameworks, *Green Chem.*, 2020, 22, 2498–2504.
- 54 J. A. Martín-Illán, D. Rodríguez-San-Miguel, C. Franco, I. Imaz, D. Maspoch, J. Puigmartí-Luis and F. Zamora,

- Green synthesis of imine-based covalent organic frameworks in water, *Chem. Commun.*, 2020, **56**, 6704–6707.
- 55 F. Zhang, J. Zhang, B. Zhang, X. Tan, D. Shao, J. Shi, D. Tan, L. Liu, J. Feng, B. Han, G. Yang, L. Zheng and J. Zhang, Room-Temperature Synthesis of Covalent Organic Framework (COF-LZU1) Nanobars in CO<sub>2</sub>/Water Solvent, *ChemSusChem*, 2018, 11, 3576–3580.
- 56 J. Maschita, T. Banerjee, G. Savasci, F. Haase, C. Ochsenfeld and B. V. Lotsch, Ionothermal Synthesis of Imide-Linked Covalent Organic Frameworks, *Angew. Chem.*, Int. Ed., 2020, 59, 15750–15758.
- 57 X. Li, J. Qiao, S. W. Chee, H.-S. Xu, X. Zhao, H. S. Choi, W. Yu, S. Y. Quek, U. Mirsaidov and K. P. Loh, Rapid, Scalable Construction of Highly Crystalline Acylhydrazone Two-Dimensional Covalent Organic Frameworks via Dipole-Induced Antiparallel Stacking, J. Am. Chem. Soc., 2020, 142, 4932–4943.
- 58 C. H. Feriante, S. Jhulki, A. M. Evans, R. R. Dasari, K. Slicker, W. R. Dichtel and S. R. Marder, Rapid Synthesis of High Surface Area Imine-Linked 2D Covalent Organic Frameworks by Avoiding Pore Collapse During Isolation, *Adv. Mater.*, 2020, 32, 1905776.
- 59 X. Li, C. Yang, B. Sun, S. Cai, Z. Chen, Y. Lv, J. Zhang and Y. Liu, Expeditious synthesis of covalent organic frameworks: a review, J. Mater. Chem. A, 2020, 8, 16045–16060.
- 60 A. R. Bagheri and N. Aramesh, Towards the room-temperature synthesis of covalent organic frameworks: a mini-review, *J. Mater. Sci.*, 2021, **56**, 1116–1132.
- 61 Y. Peng, Z. Hu, Y. Gao, D. Yuan, Z. Kang, Y. Qian, N. Yan and D. Zhao, Synthesis of a sulfonated two-dimensional covalent organic framework as an efficient solid acid catalyst for biobased chemical conversion, *ChemSusChem*, 2015, **8**, 3208–3212.
- 62 H.-C. Ma, Y.-N. Sun, G.-J. Chen and Y.-B. Dong, A BINOL-phosphoric acid and metalloporphyrin derived chiral covalent organic framework for enantioselective α-benzylation of aldehydes, *Chem. Sci.*, 2022, **13**, 1906–1911.
- 63 J. L. Segura, S. Royuela and M. M. Ramos, Post-synthetic modification of covalent organic frameworks, *Chem. Soc. Rev.*, 2019, 48, 3903–3945.
- 64 B.-J. Yao, W.-X. Wu, L.-G. Ding and Y.-B. Dong, Sulfonic acid and ionic liquid functionalized covalent organic framework for efficient catalysis of the Biginelli reaction, *J. Org. Chem.*, 2021, 86, 3024–3032.
- 65 Q. Guan, L.-L. Zhou and Y.-B. Dong, Construction of Covalent Organic Frameworks *via* Multicomponent Reactions, *J. Am. Chem. Soc.*, 2023, 145, 1475–1496.
- 66 B. Zhang, X. Li, J. Chen, T. Liu, A. Cruz, Y. Pei, M. Chen, X. Wu and W. Huang, Tandem Synthesis of ε-Caprolactam from Cyclohexanone by an Acidified Metal-organic Framework, *ChemCatChem*, 2021, 13, 3084–3089.
- 67 H. Lyu, C. S. Diercks, C. Zhu and O. M. Yaghi, Porous crystalline olefin-linked covalent organic frameworks, *J. Am. Chem. Soc.*, 2019, **141**, 6848–6852.
- 68 Q. Fang, S. Gu, J. Zheng, Z. Zhuang, S. Qiu and Y. Yan, 3D microporous base-functionalized covalent organic

- frameworks for size-selective catalysis, Angew. Chem., Int. Ed., 2014, 126, 2922-2926.
- 69 D. B. Shinde, S. Kandambeth, P. Pachfule, R. R. Kumar and R. Banerjee, Bifunctional covalent organic frameworks with two dimensional organocatalytic micropores, Chem. Commun., 2015, 51, 310-313.
- 70 J. Hu, F. Zanca, G. J. McManus, I. A. Riha, H. G. T. Nguyen, W. Shirley, C. G. Borcik, B. J. Wylie, M. Benamara and R. D. Van Zee, Catalyst-Enabled In Situ Linkage Reduction in Imine Covalent Organic Frameworks, ACS Appl. Mater. Interfaces, 2021, 13, 21740-21747.
- 71 F. Meng, S. Bi, Z. Sun, D. Wu and F. Zhang, 2, 4, 6-Trimethylpyridine-Derived Vinylene-Linked Organic Frameworks for Confined Catalytic Esterification, Angew. Chem., Int. Ed., 2022, 61, e202210447.
- 72 L.-K. Wang, J.-J. Zhou, Y.-B. Lan, S.-Y. Ding, W. Yu and W. Wang, Divergent Synthesis of Chiral Covalent Organic Frameworks, Angew. Chem., Int. Ed., 2019, 58, 9443-9447.
- 73 H. Xu, X. Chen, J. Gao, J. Lin, M. Addicoat, S. Irle and D. Jiang, Catalytic covalent organic frameworks via pore surface engineering, Chem. Commun., 2014, 50, 1292-1294.
- 74 J. Zhang, X. Han, X. Wu, Y. Liu and Y. Cui, Multivariate Chiral Covalent Organic Frameworks with Controlled Crystallinity and Stability for Asymmetric Catalysis, J. Am. Chem. Soc., 2017, 139, 8277-8285.
- 75 J. P. Richard, Enzymatic Rate Enhancements: A Review and Perspective, Biochem, 2013, 52, 2009-2011.
- 76 S. Kandambeth, V. Venkatesh, D. B. Shinde, S. Kumari, A. Halder, S. Verma and R. Banerjee, Self-templated chemically stable hollow spherical covalent organic framework, Nat. Commun., 2015, 6, 6786.
- 77 F. L. Oliveira, A. S. de França, A. M. de Castro, R. O. Alves de Souza, P. M. Esteves and R. S. B. Gonçalves, Enzyme immobilization in covalent organic frameworks: Strategies and applications in biocatalysis, ChemPlusChem, 2020, 85, 2051-2066.
- 78 M. Li, S. Qiao, Y. Zheng, Y. H. Andaloussi, X. Li, Z. Zhang, A. Li, P. Cheng, S. Ma and Y. Chen, Fabricating covalent organic framework capsules with commodious microenvironment for enzymes, J. Am. Chem. Soc., 2020, 142, 6675-6681.
- 79 Y. Zheng, S. Zhang, J. Guo, R. Shi, J. Yu, K. Li, N. Li, Z. Zhang and Y. Chen, Green and Scalable Fabrication of High-Performance Biocatalysts Using Covalent Organic Frameworks as Enzyme Carriers, Angew. Chem., Int. Ed., 2022, **61**, e202208744.
- 80 B. Dong, L. Wang, S. Zhao, R. Ge, X. Song, Y. Wang and Y. Gao, Immobilization of ionic liquids to covalent organic frameworks for catalyzing the formylation of amines with CO<sub>2</sub> and phenylsilane, Chem. Commun., 2016, 52, 7082-7085.
- 81 Y. Zhang, M.-X. Wu, G. Zhou, X.-H. Wang and X. Liu, A Rising Star from Two Worlds: Collaboration of COFs and ILs, Adv. Funct. Mater., 2021, 31, 2104996.
- 82 J. Qiu, Y. Zhao, Z. Li, H. Wang, Y. Shi and J. Wang, Imidazolium-Salt-Functionalized Covalent Organic Frameworks

- for Highly Efficient Catalysis of CO2 Conversion, Chem-SusChem, 2019, 12, 2421-2427.
- 83 Y.-R. Du, B.-H. Xu, J.-S. Pan, Y.-W. Wu, X.-M. Peng, Y.-F. Wang and S.-J. Zhang, Confinement of Brønsted acidic ionic liquids into covalent organic frameworks as a catalyst for dehydrative formation of isosorbide from sorbitol, Green Chem., 2019, 21, 4792-4799.
- 84 D. Chakraborty, D. Mullangi, C. Chandran and R. Vaidhyanathan, Nanopores of a Covalent Organic Framework: A Customizable Vessel for Organocatalysis, ACS Omega, 2022, 7, 15275-15295.
- 85 C. Chandran, H. D. Singh, L. S. Leo, P. Shekhar, D. Rase, D. Chakraborty, C. P. Vinod and R. Vaidhyanathan, A covalent organic framework with electrodeposited copper nanoparticles - a desirable catalyst for the Ullmann coupling reaction, J. Mater. Chem. A, 2022, 10, 15647-15656.
- 86 W. K. Haug, E. R. Wolfson, B. T. Morman, C. M. Thomas and P. L. McGrier, A nickel-doped dehydrobenzoannulenebased two-dimensional covalent organic framework for the reductive cleavage of inert aryl C-S bonds, J. Am. Chem. Soc., 2020, 142, 5521-5525.
- 87 Y. Shi, X. Zhang, H. Liu, J. Han, Z. Yang, L. Gu and Z. Tang, Metalation of Catechol-Functionalized Defective Covalent Organic Frameworks for Lewis Acid Catalysis, Small, 2020, 16, 2001998.
- 88 R. S. B. Gonçalves, A. B. V. de Oliveira, H. C. Sindra, B. S. Archanjo, M. E. Mendoza, L. S. A. Carneiro, C. D. Buarque and P. M. Esteves, Heterogeneous Catalysis by Covalent Organic Frameworks (COF): Pd(OAc)2@ COF-300 in Cross-Coupling Reactions, ChemCatChem, 2016, 8, 743-750.
- 89 Z. Zheng, C. Yuan, M. Sun, J. Dong, Y. Liu and Y. Cui, Construction of Monophosphine-Metal Complexes in Privileged Diphosphine-Based Covalent Organic Frameworks for Catalytic Asymmetric Hydrogenation, J. Am. Chem. Soc., 2023, 145, 6100-6111.
- 90 Y. Nailwal, M. A. Addicoat, M. Gaurav and S. K. Pal, Role of Intralayer Hydrogen Bonding in the Fast Crystallization of the Hydrazone-Linked Nanoporous Covalent Organic Framework for Catalytic Suzuki-Miyaura Cross-Coupling Reactions, ACS Appl. Nano Mater., 2023, 6, 1714-1723.
- 91 C. Krishnaraj, H. S. Jena, K. S. Rawat, J. Schmidt, K. Leus, V. Van Speybroeck and P. Van Der Voort, Linker Engineering of 2D Imine Covalent Organic Frameworks for the Heterogeneous Palladium-Catalyzed Suzuki Coupling Reaction, ACS Appl. Mater. Interfaces, 2022, 14, 50923-50931.
- 92 Y. Li, J.-M. Wang, J.-L. Kan, F. Li, Y. Dong and Y.-B. Dong, Combination of a Metal-N-Heterocyclic-Carbene Catalyst and a Chiral Aminocatalyst within a Covalent Organic Framework: a Powerful Cooperative Approach for Relay Asymmetric Catalysis, *Inorg. Chem.*, 2022, **61**, 2455–2462.
- 93 Y. Li, Y. Dong, J.-L. Kan, X. Wu and Y.-B. Dong, Synthesis and catalytic properties of metal-N-heterocyclic-carbenedecorated covalent organic framework, Org. Lett., 2020, 22, 7363-7368.

- 94 C. Qian, W. Zhou, J. Qiao, D. Wang, X. Li, W. L. Teo, X. Shi, H. Wu, J. Di and H. Wang, Linkage engineering by harnessing supramolecular interactions to fabricate 2D hydrazone-linked covalent organic framework platforms toward advanced catalysis, *J. Am. Chem. Soc.*, 2020, 142, 18138–18149.
- 95 P. Pachfule, S. Kandambeth, D. Díaz Díaz and R. Banerjee, Highly stable covalent organic framework–Au nanoparticles hybrids for enhanced activity for nitrophenol reduction, *Chem. Commun.*, 2014, **50**, 3169–3172.
- 96 L. Zhang, R. Bu, X.-Y. Liu, P.-F. Mu and E.-Q. Gao, Schiff-base molecules and COFs as metal-free catalysts or silver supports for carboxylation of alkynes with CO2, *Green Chem.*, 2021, 23, 7620–7629.
- 97 R. Tao, X. Shen, Y. Hu, K. Kang, Y. Zheng, S. Luo, S. Yang, W. Li, S. Lu, Y. Jin, L. Qiu and W. Zhang, Phosphine-Based Covalent Organic Framework for the Controlled Synthesis of Broad-Scope Ultrafine Nanoparticles, *Small*, 2020, 16, 1906005.
- 98 L. P. L. Gonçalves, D. B. Christensen, M. Meledina, L. M. Salonen, D. Y. Petrovykh, E. Carbó-Argibay, J. P. S. Sousa, O. S. G. P. Soares, M. F. R. Pereira, S. Kegnæs and Y. V. Kolen'ko, Selective formic acid dehydrogenation at low temperature over a RuO<sub>2</sub>/COF pre-catalyst synthesized on the gram scale, *Catal. Sci. Technol.*, 2020, 10, 1991–1995.
- 99 J.-C. Wang, C.-X. Liu, X. Kan, X.-W. Wu, J.-L. Kan and Y.-B. Dong, Pd@COF-QA: a phase transfer composite catalyst for aqueous Suzuki–Miyaura coupling reaction, *Green Chem.*, 2020, 22, 1150–1155.
- 100 M. Guo, S. Jayakumar, M. Luo, X. Kong, C. Li, H. Li, J. Chen and Q. Yang, The promotion effect of  $\pi$ – $\pi$  interactions in Pd NPs catalysed selective hydrogenation, *Nat. Commun.*, 2022, **13**, 1770.
- 101 S. Liu, M. Wang, Y. He, Q. Cheng, T. Qian and C. Yan, Covalent organic frameworks towards photocatalytic applications: Design principles, achievements, and opportunities, *Coord. Chem. Rev.*, 2023, 475, 214882.
- 102 Y.-N. Gong, X. Guan and H.-L. Jiang, Covalent organic frameworks for photocatalysis: Synthesis, structural features, fundamentals and performance, *Coord. Chem. Rev.*, 2023, 475, 214889.
- 103 X. Kang, X. Wu, X. Han, C. Yuan, Y. Liu and Y. Cui, Rational synthesis of interpenetrated 3D covalent organic frameworks for asymmetric photocatalysis, *Chem. Sci.*, 2020, **11**, 1494–1502.
- 104 W. Liu, Q. Su, P. Ju, B. Guo, H. Zhou, G. Li and Q. Wu, A Hydrazone-Based Covalent Organic Framework as an Efficient and Reusable Photocatalyst for the Cross-Dehydrogenative Coupling Reaction of N-Aryltetrahydroisoquinolines, *Chem-SusChem*, 2017, 10, 664–669.
- 105 A. Basak, S. Karak and R. Banerjee, Covalent Organic Frameworks as Porous Pigments for Photocatalytic Metal-Free C–H Borylation, *J. Am. Chem. Soc.*, 2023, **145**, 7592–7599.
- 106 Y. Fan, D. W. Kang, S. Labalme, J. Li and W. Lin, Enhanced Energy Transfer in A  $\pi$ -Conjugated Covalent Organic

- Framework Facilitates Excited-State Nickel Catalysis, *Angew. Chem., Int. Ed.*, 2023, **135**, e202218908.
- 107 K. Wang, X. Kang, C. Yuan, X. Han, Y. Liu and Y. Cui, Porous 2D and 3D Covalent Organic Frameworks with Dimensionality-Dependent Photocatalytic Activity in Promoting Radical Ring-Opening Polymerization, *Angew. Chem., Int. Ed.*, 2021, 60, 19466–19476.
- 108 S. Trenker, L. Grunenberg, T. Banerjee, G. Savasci, L. M. Poller, K. I. Muggli, F. Haase, C. Ochsenfeld and B. V. Lotsch, A flavin-inspired covalent organic framework for photocatalytic alcohol oxidation, *Chem. Sci.*, 2021, 12, 15143–15150.
- 109 H. He, X. Fang, D. Zhai, W. Zhou, Y. Li, W. Zhao, C. Liu, Z. Li and W. Deng, A Porphyrin-Based Covalent Organic Framework for Metal-Free Photocatalytic Aerobic Oxidative Coupling of Amines, *Chem. Eur. J.*, 2021, 27, 14390–14395.
- 110 H. Liu, C. Li, H. Li, Y. Ren, J. Chen, J. Tang and Q. Yang, Structural engineering of two-dimensional covalent organic frameworks for visible-light-driven organic transformations, ACS Appl. Mater. Interfaces, 2020, 12, 20354–20365.
- 111 J. Zhao, J. Ren, G. Zhang, Z. Zhao, S. Liu, W. Zhang and L. Chen, Donor-Acceptor Type Covalent Organic Frameworks, *Eur. J. Chem.*, 2021, 27, 10781–10797.
- 112 H. Shan, D. Cai, X. Zhang, Q. Zhu, P. Qin and J. Baeyens, Donor-acceptor type two-dimensional porphyrin-based covalent organic framework for visible-light-driven heterogeneous photocatalysis, J. Chem. Eng., 2022, 432, 134288.
- 113 P. T. Parvatkar, S. Kandambeth, A. C. Shaikh, I. Nadinov, J. Yin, V. S. Kale, G. Healing, A. H. Emwas, O. Shekhah, H. N. Alshareef, O. F. Mohammed and M. Eddaoudi, A Tailored COF for Visible-Light Photosynthesis of 2,3-Dihydrobenzofurans, J. Am. Chem. Soc., 2023, 145, 5074–5082.
- 114 C.-J. Wu, X.-Y. Li, T.-R. Li, M.-Z. Shao, L.-J. Niu, X.-F. Lu, J.-L. Kan, Y. Geng and Y.-B. Dong, Natural Sunlight Photocatalytic Synthesis of Benzoxazole-Bridged Covalent Organic Framework for Photocatalysis, *J. Am. Chem. Soc.*, 2022, 144, 18750–18755.
- 115 X. Liu, R. Qi, S. Li, W. Liu, Y. Yu, J. Wang, S. Wu, K. Ding and Y. Yu, Triazine–Porphyrin-Based Hyperconjugated Covalent Organic Framework for High-Performance Photocatalysis, *J. Am. Chem. Soc.*, 2022, **144**, 23396–23404.
- 116 X. Li, sp2 carbon-conjugated covalent organic frameworks: synthesis, properties, and applications, *Mater. Chem. Front.*, 2021, 5, 2931–2949.
- 117 S. Xu, M. Richter and X. Feng, Vinylene-Linked Two-Dimensional Covalent Organic Frameworks: Synthesis and Functions, *Acc. Chem. Res.*, 2021, 2, 252–265.
- 118 Y. Su, B. Li, H. Xu, C. Lu, S. Wang, B. Chen, Z. Wang, W. Wang, K.-I. Otake, S. Kitagawa, L. Huang and C. Gu, Multi-Component Synthesis of a Buta-1,3-diene-Linked Covalent Organic Framework, *J. Am. Chem. Soc.*, 2022, 144, 18218–18222.
- 119 X. Zhao, H. Pang, D. Huang, G. Liu, J. Hu and Y. Xiang, Construction of Ultrastable Nonsubstituted Quinoline-Bridged Covalent Organic Frameworks *via* Rhodium-Catalyzed Dehydrogenative Annulation, *Angew. Chem., Int. Ed.*, 2022, **61**, e202208833.

- 120 H. Chen, W. Liu, A. Laemont, C. Krishnaraj, X. Feng, F. Rohman, M. Meledina, Q. Zhang, R. Van Deun, K. Leus and P. Van Der Voort, A Visible-Light-Harvesting Covalent Organic Framework Bearing Single Nickel Sites as a Highly Efficient Sulfur-Carbon Cross-Coupling Dual Catalyst, Angew. Chem., Int. Ed., 2021, 60, 10820-10827.
- 121 A. Jati, K. Dey, M. Nurhuda, M. A. Addicoat, R. Banerjee and B. Maji, Dual Metalation in a Two-Dimensional Covalent Organic Framework for Photocatalytic C-N Cross-Coupling Reactions, J. Am. Chem. Soc., 2022, 144, 7822-7833.
- 122 M. Traxler, S. Gisbertz, P. Pachfule, J. Schmidt, J. Roeser, S. Reischauer, J. Rabeah, B. Pieber and A. Thomas, Acridine-Functionalized Covalent Organic Frameworks (COFs) as Photocatalysts for Metallaphotocatalytic C-N Cross-Coupling, Angew. Chem., Int. Ed., 2022, 61, e202117738.
- 123 A. López-Magano, B. Ortín-Rubio, I. Imaz, D. Maspoch, J. Alemán and R. Mas-Ballesté, Photoredox Heterobimetallic Dual Catalysis Using Engineered Covalent Organic Frameworks, ACS Catal., 2021, 11, 12344-12354.
- 124 Z. Almansaf, J. Hu, F. Zanca, H. R. Shahsavari, B. Kampmeyer, M. Tsuji, K. Maity, V. Lomonte, Y. Ha, P. Mastrorilli, S. Todisco, M. Benamara, R. Oktavian, A. Mirjafari, P. Z. Moghadam, A. R. Khosropour and H. Beyzavi, Pt(II)-Decorated Covalent Organic Framework for Photocatalytic Difluoroalkylation and Oxidative Cyclization Reactions, ACS Appl. Mater. Interfaces, 2021, 13, 6349-6358.
- 125 Y. Qian, D. Li, Y. Han and H.-L. Jiang, Photocatalytic Molecular Oxygen Activation by Regulating Excitonic Effects in Covalent Organic Frameworks, J. Am. Chem. Soc., 2020, 142, 20763-20771.
- 126 Y. Peng, M. Zhao, B. Chen, Z. Zhang, Y. Huang, F. Dai, Z. Lai, X. Cui, C. Tan and H. Zhang, Hybridization of MOFs and COFs: A New Strategy for Construction of MOF@COF Core-Shell Hybrid Materials, Adv. Mater., 2018, 30, 1705454.
- 127 Z. Chen, X. Li, C. Yang, K. Cheng, T. Tan, Y. Lv and Y. Liu, Hybrid porous crystalline materials from metal organic frameworks and covalent organic frameworks, Adv. Sci., 2021, 8, 2101883.
- 128 G. Lu, X. Huang, Y. Li, G. Zhao, G. Pang and G. Wang, Covalently integrated core-shell MOF@COF hybrids as efficient visible-light-driven photocatalysts for selective oxidation of alcohols, J. Energy Chem., 2020, 43, 8-15.
- 129 D. Sun, S. Jang, S.-J. Yim, L. Ye and D.-P. Kim, Metal Doped Core-Shell Metal-Organic Frameworks@Covalent Organic Frameworks (MOFs@COFs) Hybrids as a Novel Photocatalytic Platform, Adv. Funct. Mater., 2018, 28, 1707110.
- 130 A. Sudhaik, P. Raizada, T. Ahamad, S. M. Alshehri, V.-H. Nguyen, Q. Van Le, S. Thakur, V. K. Thakur, R. Selvasembian and P. Singh, Recent advances in cellulose supported photocatalysis for pollutant mitigation: A review, Int. J. Biol. Macromol., 2023, 226, 1284-1308.
- 131 Y. Li, X. Song, G. Zhang, L. Wang, Y. Liu, W. Chen and L. Chen, 2D Covalent Organic Frameworks Toward

- Efficient Photocatalytic Hydrogen Evolution, Chem-SusChem, 2022, 15, e202200901.
- 132 L. Stegbauer, K. Schwinghammer and B. V. Lotsch, A hydrazone-based covalent organic framework for photocatalytic hydrogen production, Chem. Sci., 2014, 5, 2789-2793.
- 133 J. Yang, A. Acharjya, M.-Y. Ye, J. Rabeah, S. Li, Z. Kochovski, S. Youk, J. Roeser, J. Grüneberg, C. Penschke, M. Schwarze, T. Wang, Y. Lu, R. van de Krol, M. Oschatz, R. Schomäcker, P. Saalfrank and A. Thomas, Protonated Imine-Linked Covalent Organic Frameworks for Photocatalytic Hydrogen Evolution, Angew. Chem., Int. Ed., 2021, 60, 19797-19803.
- 134 X. Hu, Z. Zhan, J. Zhang, I. Hussain and B. Tan, Immobilized covalent triazine frameworks films as effective photocatalysts for hydrogen evolution reaction, Nat. Commun., 2021, 12, 6596.
- 135 Z. Li, T. Deng, S. Ma, Z. Zhang, G. Wu, J. Wang, Q. Li, H. Xia, S.-W. Yang and X. Liu, Three-Component Donor $-\pi$ -Acceptor Covalent-Organic Frameworks for Boosting Photocatalytic Hydrogen Evolution, J. Am. Chem. Soc., 2023, DOI: 10.1021/jacs.2c11893.
- 136 Y. Yang, N. Luo, S. Lin, H. Yao and Y. Cai, Cyano Substituent on the Olefin Linkage: Promoting Rather than Inhibiting the Performance of Covalent Organic Frameworks, ACS Catal., 2022, 12, 10718-10726.
- 137 Y. Zhao, H. Liu, C. Wu, Z. Zhang, Q. Pan, F. Hu, R. Wang, P. Li, X. Huang and Z. Li, Fully Conjugated Two-Dimensional sp2-Carbon Covalent Organic Frameworks as Artificial Photosystem I with High Efficiency, Angew. Chem., Int. Ed., 2019, 58, 5376-5381.
- 138 S. Ma, T. Deng, Z. Li, Z. Zhang, J. Jia, Q. Li, G. Wu, H. Xia, S.-W. Yang and X. Liu, Photocatalytic Hydrogen Production on a sp2-Carbon-Linked Covalent Organic Framework, Angew. Chem., Int. Ed., 2022, 61, e202208919.
- 139 W. Zhang, L. Chen, S. Dai, C. Zhao, C. Ma, L. Wei, M. Zhu, S. Y. Chong, H. Yang, L. Liu, Y. Bai, M. Yu, Y. Xu, X.-W. Zhu, Q. Zhu, S. An, R. S. Sprick, M. A. Little, X. Wu, S. Jiang, Y. Wu, Y.-B. Zhang, H. Tian, W.-H. Zhu and A. I. Cooper, Reconstructed covalent organic frameworks, Nature, 2022, 604, 72-79.
- 140 A. M. Elewa, A. F. M. El-Mahdy, A. E. Hassan, Z. Wen, J. Jayakumar, T.-L. Lee, L.-Y. Ting, I. M. A. Mekhemer, T.-F. Huang, M. H. Elsayed, C.-L. Chang, W.-C. Lin and H.-H. Chou, Solvent polarity tuning to enhance the crystallinity of 2D-covalent organic frameworks for visible-light-driven hydrogen generation, J. Mater. Chem. A, 2022, 10, 12378-12390.
- 141 J. Yang, F. Kang, X. Wang and Q. Zhang, Design strategies for improving the crystallinity of covalent organic frameworks and conjugated polymers: a review, Mater. Horiz., 2022, 9, 121-146.
- 142 R. Chen, Y. Wang, Y. Ma, A. Mal, X.-Y. Gao, L. Gao, L. Qiao, X.-B. Li, L.-Z. Wu and C. Wang, Rational design of isostructural 2D porphyrin-based covalent organic frameworks for tunable photocatalytic hydrogen evolution, Nat. Commun., 2021, 12, 1354.
- 143 W. Huang, Y. Hu, Z. Qin, Y. Ji, X. Zhao, Y. Wu, Q. He, Y. Li, C. Zhang, J. Lu and Y. Li, Highly crystalline and water-

- wettable benzobisthiazole-based covalent organic frameworks for enhanced photocatalytic hydrogen production, *Natl. Sci. Rev.*, 2022, 10.
- 144 W. Li, X. Ding, B. Yu, H. Wang, Z. Gao, X. Wang, X. Liu, K. Wang and J. Jiang, Tuning Molecular Chromophores of Isoreticular Covalent Organic Frameworks for Visible Light-Induced Hydrogen Generation, *Adv. Funct. Mater.*, 2022, 32, 2207394.
- 145 L. Sun, M. Lu, Z. Yang, Z. Yu, X. Su, Y.-Q. Lan and L. Chen, Nickel Glyoximate Based Metal–Covalent Organic Frameworks for Efficient Photocatalytic Hydrogen Evolution, *Angew. Chem., Int. Ed.*, 2022, 61, e202204326.
- 146 Z. Zhao, X. Chen, B. Li, S. Zhao, L. Niu, Z. Zhang and Y. Chen, Spatial Regulation of Acceptor Units in Olefin-Linked COFs toward Highly Efficient Photocatalytic H2 Evolution, Adv. Sci., 2022, 9, 2203832.
- 147 Z. Mi, T. Zhou, W. Weng, J. Unruangsri, K. Hu, W. Yang, C. Wang, K. A. I. Zhang and J. Guo, Covalent Organic Frameworks Enabling Site Isolation of Viologen-Derived Electron-Transfer Mediators for Stable Photocatalytic Hydrogen Evolution, *Angew. Chem., Int. Ed.*, 2021, 60, 9642–9649.
- 148 Z. Zhao, Y. Zheng, C. Wang, S. Zhang, J. Song, Y. Li, S. Ma, P. Cheng, Z. Zhang and Y. Chen, Fabrication of Robust Covalent Organic Frameworks for Enhanced Visible-Light-Driven H<sub>2</sub> Evolution, ACS Catal., 2021, 11, 2098–2107.
- 149 T. Zhou, X. Huang, Z. Mi, Y. Zhu, R. Wang, C. Wang and J. Guo, Multivariate covalent organic frameworks boosting photocatalytic hydrogen evolution, *Polym. Chem.*, 2021, 12, 3250–3256.
- 150 W. Chen, L. Wang, D. Mo, F. He, Z. Wen, X. Wu, H. Xu and L. Chen, Modulating benzothiadiazole-based covalent organic frameworks *via* halogenation for enhanced photocatalytic water splitting, *Angew. Chem., Int. Ed.*, 2020, 132, 17050–17057.
- 151 Y. Wang, W. Hao, H. Liu, R. Chen, Q. Pan, Z. Li and Y. Zhao, Facile construction of fully sp<sup>2</sup>-carbon conjugated two-dimensional covalent organic frameworks containing benzobisthiazole units, *Nat. Commun.*, 2022, **13**, 100.
- 152 C. Li, J. Liu, H. Li, K. Wu, J. Wang and Q. Yang, Covalent organic frameworks with high quantum efficiency in sacrificial photocatalytic hydrogen evolution, *Nat. Commun.*, 2022, **13**, 2357.
- 153 Y. Li, L. Yang, H. He, L. Sun, H. Wang, X. Fang, Y. Zhao, D. Zheng, Y. Qi, Z. Li and W. Deng, In situ photodeposition of platinum clusters on a covalent organic framework for photocatalytic hydrogen production, *Nat. Commun.*, 2022, 13, 1355.
- 154 T. He, W. Zhen, Y. Chen, Y. Guo, Z. Li, N. Huang, Z. Li, R. Liu, Y. Liu and X. Lian, Integrated interfacial design of covalent organic framework photocatalysts to promote hydrogen evolution from water, *Nat. Commun.*, 2023, 14, 329.
- 155 K. Gottschling, G. Savasci, H. Vignolo-González,
  S. Schmidt, P. Mauker, T. Banerjee, P. Rovó,
  C. Ochsenfeld and B. V. Lotsch, Rational Design of

- Covalent Cobaloxime-Covalent Organic Framework Hybrids for Enhanced Photocatalytic Hydrogen Evolution, *J. Am. Chem. Soc.*, 2020, 142, 12146–12156.
- 156 H. N. Kagalwala, E. Gottlieb, G. Li, T. Li, R. Jin and S. Bernhard, Photocatalytic Hydrogen Generation System Using a Nickel-Thiolate Hexameric Cluster, *Inorg. Chem.*, 2013, **52**, 9094–9101.
- 157 W. Weng and J. Guo, The effect of enantioselective chiral covalent organic frameworks and cysteine sacrificial donors on photocatalytic hydrogen evolution, *Nat. Commun.*, 2022, **13**, 5768.
- 158 H. Wang, C. Qian, J. Liu, Y. Zeng, D. Wang, W. Zhou, L. Gu, H. Wu, G. Liu and Y. Zhao, Integrating Suitable Linkage of Covalent Organic Frameworks into Covalently Bridged Inorganic/Organic Hybrids toward Efficient Photocatalysis, J. Am. Chem. Soc., 2020, 142, 4862–4871.
- 159 C.-C. Li, M.-Y. Gao, X.-J. Sun, H.-L. Tang, H. Dong and F.-M. Zhang, Rational combination of covalent-organic framework and nano  ${\rm TiO_2}$  by covalent bonds to realize dramatically enhanced photocatalytic activity, *Appl. Catal.*, *B*, 2020, **266**, 118586.
- 160 F.-M. Zhang, J.-L. Sheng, Z.-D. Yang, X.-J. Sun, H.-L. Tang, M. Lu, H. Dong, F.-C. Shen, J. Liu and Y.-Q. Lan, Rational Design of MOF/COF Hybrid Materials for Photocatalytic H2 Evolution in the Presence of Sacrificial Electron Donors, Angew. Chem., Int. Ed., 2018, 57, 12106–12110.
- 161 C.-X. Chen, Y.-Y. Xiong, X. Zhong, P. C. Lan, Z.-W. Wei, H. Pan, P.-Y. Su, Y. Song, Y.-F. Chen, A. Nafady, S. Sirajuddin and S. Ma, Enhancing Photocatalytic Hydrogen Production *via* the Construction of Robust Multivariate Ti-MOF/COF Composites, *Angew. Chem., Int. Ed.*, 2022, 61, e202114071.
- 162 W. Zhao, P. Yan, H. Yang, M. Bahri, A. M. James, H. Chen, L. Liu, B. Li, Z. Pang, R. Clowes, N. D. Browning, J. W. Ward, Y. Wu and A. I. Cooper, Using sound to synthesize covalent organic frameworks in water, *Nat. Syn.*, 2022, 1, 87–95.
- 163 Q. Yue, G. Li, P. Fu, B. Meng, F. Ma, Y. Zhou and J. Wang, In-situ polarization of covalent organic frameworks in seawater enables enhanced photocatalytic hydrogen evolution under visible-light irradiation, *Nano Res.*, 2023, 1–9.
- 164 L. Peng, S. Chang, Z. Liu, Y. Fu, R. Ma, X. Lu, F. Zhang, W. Zhu, L. Kong and M. Fan, Visible-light-driven photocatalytic CO<sub>2</sub> reduction over ketoenamine-based covalent organic frameworks: role of the host functional groups, *Catal. Sci. Technol.*, 2021, 11, 1717–1724.
- 165 X. Xu, P. Cai, H. Chen, H.-C. Zhou and N. Huang, Three-Dimensional Covalent Organic Frameworks with she Topology, *J. Am. Chem. Soc.*, 2022, **144**, 18511–18517.
- 166 Y.-N. Gong, W. Zhong, Y. Li, Y. Qiu, L. Zheng, J. Jiang and H.-L. Jiang, Regulating Photocatalysis by Spin-State Manipulation of Cobalt in Covalent Organic Frameworks, *J. Am. Chem. Soc.*, 2020, **142**, 16723–16731.
- 167 J. Ding, X. Guan, J. Lv, X. Chen, Y. Zhang, H. Li, D. Zhang, S. Qiu, H.-L. Jiang and Q. Fang, Three-Dimensional Covalent Organic Frameworks with Ultra-Large Pores for Highly

- Efficient Photocatalysis, J. Am. Chem. Soc., 2023, 145, 3248-3254.
- 168 M. Lu, J. Liu, Q. Li, M. Zhang, M. Liu, J.-L. Wang, D.-Q. Yuan and Y.-Q. Lan, Rational Design of Crystalline Covalent Organic Frameworks for Efficient CO2 Photoreduction with H2O, Angew. Chem., Int. Ed., 2019, 58, 12392-12397.
- 169 S. Yang, W. Hu, X. Zhang, P. He, B. Pattengale, C. Liu, M. Cendejas, I. Hermans, X. Zhang, J. Zhang and J. Huang, 2D Covalent Organic Frameworks as Intrinsic Photocatalysts for Visible Light-Driven CO2 Reduction, J. Am. Chem. Soc., 2018, 140, 14614-14618.
- 170 Z. Fu, X. Wang, A. M. Gardner, X. Wang, S. Y. Chong, G. Neri, A. J. Cowan, L. Liu, X. Li, A. Vogel, R. Clowes, M. Bilton, L. Chen, R. S. Sprick and A. I. Cooper, A stable covalent organic framework for photocatalytic carbon dioxide reduction, Chem. Sci., 2020, 11, 543-550.
- 171 L. Ran, Z. Li, B. Ran, J. Cao, Y. Zhao, T. Shao, Y. Song, M. K. H. Leung, L. Sun and J. Hou, Engineering Single-Atom Active Sites on Covalent Organic Frameworks for Boosting CO<sub>2</sub> Photoreduction, J. Am. Chem. Soc., 2022, 144, 17097-17109.
- 172 W. Zhang, A. R. Mohamed and W. J. Ong, Z-scheme photocatalytic systems for carbon dioxide reduction: where are we now?, Angew. Chem., Int. Ed., 2020, 59, 22894-22915.
- 173 A. Kumar, P. Raizada, P. Singh, R. V. Saini, A. K. Saini and A. Hosseini-Bandegharaei, Perspective and status of polymeric graphitic carbon nitride based Z-scheme photocatalytic systems for sustainable photocatalytic water purification, J. Chem. Eng., 2020, 391, 123496.
- 174 M. Zhang, M. Lu, Z.-L. Lang, J. Liu, M. Liu, J.-N. Chang, L.-Y. Li, L.-J. Shang, M. Wang, S.-L. Li and Y.-Q. Lan, Semiconductor/Covalent-Organic-Framework **Z-Scheme** Heterojunctions for Artificial Photosynthesis, Angew. Chem., Int. Ed., 2020, 59, 6500-6506.
- 175 L. Wang, G. Huang, L. Zhang, R. Lian, J. Huang, H. She, C. Liu and Q. Wang, Construction of TiO2-covalent organic framework Z-Scheme hybrid through coordination bond for photocatalytic CO2 conversion, J. Energy Chem., 2022, 64, 85-92.
- 176 S. He, Q. Rong, H. Niu and Y. Cai, Construction of a superior visible-light-driven photocatalyst based on a C3N4 active centre-photoelectron shift platform-electron withdrawing unit triadic structure covalent organic framework, Chem. Commun., 2017, 53, 9636-9639.
- 177 S. He, B. Yin, H. Niu and Y. Cai, Targeted synthesis of visible-light-driven covalent organic framework photocatalyst via molecular design and precise construction, Appl. Catal., B, 2018, 239, 147-153.
- 178 Y. Yang, H. Niu, L. Xu, H. Zhang and Y. Cai, Triazine functionalized fully conjugated covalent organic framework for efficient photocatalysis, Appl. Catal., B, 2020, 269, 118799.
- 179 W. Chen, Z. Yang, Z. Xie, Y. Li, X. Yu, F. Lu and L. Chen, Benzothiadiazole functionalized D-A type covalent organic frameworks for effective photocatalytic reduction of aqueous chromium(vi), J. Mater. Chem. A, 2019, 7, 998-1004.

- 180 Y. Deng, Z. Zhang, P. Du, X. Ning, Y. Wang, D. Zhang, J. Liu, S. Zhang and X. Lu, Embedding Ultrasmall Au Clusters into the Pores of a Covalent Organic Framework for Enhanced Photostability and Photocatalytic Performance, Angew. Chem., Int. Ed., 2020, 59, 6082-6089.
- 181 H. B. Aiyappa, J. Thote, D. B. Shinde, R. Banerjee and S. Kurungot, Cobalt-Modified Covalent Organic Framework as a Robust Water Oxidation Electrocatalyst, Chem. Mater., 2016, 28, 4375-4379.
- 182 S. Bhunia, S. K. Das, R. Jana, S. C. Peter, S. Bhattacharya, M. Addicoat, A. Bhaumik and A. Pradhan, Electrochemical Stimuli-Driven Facile Metal-Free Hydrogen Evolution from Pyrene-Porphyrin-Based Crystalline Covalent Organic Framework, ACS Appl. Mater. Interfaces, 2017, 9, 23843-23851.
- 183 S. Ruidas, B. Mohanty, P. Bhanja, E. S. Erakulan, R. Thapa, P. Das, A. Chowdhury, S. K. Mandal, B. K. Jena and A. Bhaumik, Metal-Free Triazine-Based 2D Covalent Organic Framework for Efficient H2 Evolution by Electrochemical Water Splitting, ChemSusChem, 2021, 14, 5057-5064.
- 184 Y. Ma, Y. Fu, W. Jiang, Y. Wu, C. Liu, G. Che and Q. Fang, Excellent electrocatalytic performance of metal-free thiophene-sulfur covalent organic frameworks for hydrogen evolution in alkaline medium, J. Mater. Chem. A, 2022, 10, 10092-10097.
- 185 Y. Zhao, Y. Liang, D. Wu, H. Tian, T. Xia, W. Wang, W. Xie, X.-M. Hu, X. Tian and Q. Chen, Ruthenium Complex of sp2 Carbon-Conjugated Covalent Organic Frameworks as an Efficient Electrocatalyst for Hydrogen Evolution, Small, 2022, 18, 2107750.
- 186 J.-Y. Yue, X.-L. Ding, L.-P. Song, Y.-T. Wang, P. Yang, Y. Ma and B. Tang, Pd(II) functionalized vinylene-linked covalent organic frameworks for acidic electrocatalytic hydrogen evolution reaction, Microporous Mesoporous Mater., 2022, 344, 112169.
- 187 J.-M. Seo, H.-J. Noh, J.-P. Jeon, H. Kim, G.-F. Han, S. K. Kwak, H. Y. Jeong, L. Wang, F. Li and J.-B. Baek, Conductive and Ultrastable Covalent Organic Framework/ Carbon Hybrid as an Ideal Electrocatalytic Platform, J. Am. Chem. Soc., 2022, 144, 19973-19980.
- 188 W. Ma, P. Yu, T. Ohsaka and L. Mao, An efficient electrocatalyst for oxygen reduction reaction derived from a Coporphyrin-based covalent organic framework, Electrochem. Commun., 2015, 52, 53-57.
- 189 D. Li, C. Li, L. Zhang, H. Li, L. Zhu, D. Yang, Q. Fang, S. Qiu and X. Yao, Metal-Free Thiophene-Sulfur Covalent Organic Frameworks: Precise and Controllable Synthesis of Catalytic Active Sites for Oxygen Reduction, J. Am. Chem. Soc., 2020, 142, 8104-8108.
- 190 S. Wu, M. Li, H. Phan, D. Wang, T. S. Herng, J. Ding, Z. Lu and J. Wu, Toward Two-Dimensional π-Conjugated Covalent Organic Radical Frameworks, Angew. Chem., Int. Ed., 2018, 57, 8007-8011.
- 191 Z. Liang, H.-Y. Wang, H. Zheng, W. Zhang and R. Cao, Porphyrin-based frameworks for oxygen electrocatalysis and catalytic reduction of carbon dioxide, Chem. Soc. Rev., 2021, 50, 2540-2581.

- 192 Z. Lei, F. W. Lucas, E. C. Moya, S. Huang, Y. Rong, A. Wesche, P. Li, L. Bodkin, Y. Jin and A. Holewinski, Highly stable dioxin-linked metallophthalocyanine covalent organic frameworks, *Chin. Chem. Lett.*, 2021, 32, 3799–3802.
- 193 P. Peng, L. Shi, F. Huo, S. Zhang, C. Mi, Y. Cheng and Z. Xiang, In Situ Charge Exfoliated Soluble Covalent Organic Framework Directly Used for Zn-Air Flow Battery, ACS Nano, 2019, 13, 878-884.
- 194 J.-Y. Yue, Y.-T. Wang, X. Wu, P. Yang, Y. Ma, X.-H. Liu and B. Tang, Two-dimensional porphyrin covalent organic frameworks with tunable catalytic active sites for the oxygen reduction reaction, *Chem. Commun.*, 2021, 57, 12619–12622.
- 195 Y.-B. Huang, P. Pachfule, J.-K. Sun and Q. Xu, From covalent-organic frameworks to hierarchically porous B-doped carbons: a molten-salt approach, *J. Mater. Chem. A*, 2016, 4, 4273–4279.
- 196 X. Zhuang, W. Zhao, F. Zhang, Y. Cao, F. Liu, S. Bi and X. Feng, A two-dimensional conjugated polymer framework with fully sp<sup>2</sup>-bonded carbon skeleton, *Polym. Chem.*, 2016, 7, 4176–4181.
- 197 Q. Xu, Y. Tang, X. Zhang, Y. Oshima, Q. Chen and D. Jiang, Template Conversion of Covalent Organic Frameworks into 2D Conducting Nanocarbons for Catalyzing Oxygen Reduction Reaction, *Adv. Mater.*, 2018, **30**, 1706330.
- 198 T. Jiang, W. Jiang, Y. Li, Y. Xu, M. Zhao, M. Deng and Y. Wang, Facile regulation of porous N-doped carbon-based catalysts from covalent organic frameworks nanospheres for highly-efficient oxygen reduction reaction, *Carbon*, 2021, **180**, 92–100.
- 199 J. Ning, Y. Gao, X. Cao, H. Wei, B. Wang and L. Hao, Substituent engineering of covalent organic frameworks modulates the crystallinity and electrochemical reactivity, *J. Energy Chem.*, 2022, **65**, 490–496.
- 200 V. Hasija, S. Patial, P. Raizada, A. Aslam Parwaz Khan, A. M. Asiri, Q. Van Le, V.-H. Nguyen and P. Singh, Covalent organic frameworks promoted single metal atom catalysis: Strategies and applications, *Coord. Chem. Rev.*, 2022, 452, 214298.
- 201 S. Wei, Y. Wang, W. Chen, Z. Li, W.-C. Cheong, Q. Zhang, Y. Gong, L. Gu, C. Chen, D. Wang, Q. Peng and Y. Li, Atomically dispersed Fe atoms anchored on COF-derived N-doped carbon nanospheres as efficient multi-functional catalysts, *Chem. Sci.*, 2020, 11, 786–790.
- 202 M. Zhou, M. Liu, Q. Miao, H. Shui and Q. Xu, Synergetic Pt Atoms and Nanoparticles Anchored in Standing Carbon-Derived from Covalent Organic Frameworks for Catalyzing ORR, Adv. Mater. Interfaces, 2022, 9, 2201263.
- 203 S. Yang, X. Li, T. Tan, J. Mao, Q. Xu, M. Liu, Q. Miao, B. Mei, P. Qiao, S. Gu, F. Sun, J. Ma, G. Zeng and Z. Jiang, A fully-conjugated covalent organic framework-derived carbon supporting ultra-close single atom sites for ORR, *Appl. Catal.*, B, 2022, 307, 121147.
- 204 Y. Fan, M. Chen, N. Xu, K. Wang, Q. Gao, J. Liang and Y. Liu, Recent progress on covalent organic framework

- materials as CO2 reduction electrocatalysts, *Front. Chem.*, 2022, **10**, 882.
- 205 C. S. Diercks, S. Lin, N. Kornienko, E. A. Kapustin, E. M. Nichols, C. Zhu, Y. Zhao, C. J. Chang and O. M. Yaghi, Reticular Electronic Tuning of Porphyrin Active Sites in Covalent Organic Frameworks for Electrocatalytic Carbon Dioxide Reduction, *J. Am. Chem. Soc.*, 2018, 140, 1116–1122.
- 206 S. Lin, C. S. Diercks, Y. B. Zhang, N. Kornienko, E. M. Nichols, Y. Zhao, A. R. Paris, D. Kim, P. Yang, O. M. Yaghi and C. J. Chang, Covalent organic frameworks comprising cobalt porphyrins for catalytic CO<sub>2</sub> reduction in water, *Science*, 2015, 349, 1208–1213.
- 207 B. Han, X. Ding, B. Yu, H. Wu, W. Zhou, W. Liu, C. Wei, B. Chen, D. Qi, H. Wang, K. Wang, Y. Chen, B. Chen and J. Jiang, Two-Dimensional Covalent Organic Frameworks with Cobalt(II)-Phthalocyanine Sites for Efficient Electrocatalytic Carbon Dioxide Reduction, *J. Am. Chem. Soc.*, 2021, 143, 7104–7113.
- 208 S.-Y. Chi, Q. Chen, S.-S. Zhao, D.-H. Si, Q.-J. Wu, Y.-B. Huang and R. Cao, Three-dimensional porphyrinic covalent organic frameworks for highly efficient electroreduction of carbon dioxide, *J. Mater. Chem. A*, 2022, **10**, 4653–4659.
- 209 B. Han, Y. Jin, B. Chen, W. Zhou, B. Yu, C. Wei, H. Wang, K. Wang, Y. Chen and B. Chen, Maximizing Electroactive Sites in a Three-Dimensional Covalent Organic Framework for Significantly Improved Carbon Dioxide Reduction Electrocatalysis, *Angew. Chem., Int. Ed.*, 2022, 61, e202114244.
- 210 Y. R. Wang, H. M. Ding, X. Y. Ma, M. Liu, Y. L. Yang, Y. Chen, S. L. Li and Y. Q. Lan, Imparting CO<sub>2</sub> Electroreduction Auxiliary for Integrated Morphology Tuning and Performance Boosting in a Porphyrin-based Covalent Organic Framework, *Angew. Chem., Int. Ed.*, 2022, 134, e202114648.
- 211 M. Liu, Y.-R. Wang, H.-M. Ding, M. Lu, G.-K. Gao, L.-Z. Dong, Q. Li, Y. Chen, S.-L. Li and Y.-Q. Lan, Selfassembly of anthraquinone covalent organic frameworks as 1D superstructures for highly efficient CO2 electroreduction to CH4, Sci. Bull., 2021, 66, 1659–1668.
- 212 M. D. Zhang, D. H. Si, J. D. Yi, S. S. Zhao, Y. B. Huang and R. Cao, Conductive Phthalocyanine-Based Covalent Organic Framework for Highly Efficient Electroreduction of Carbon Dioxide, *Small*, 2020, 16, e2005254.
- 213 H. J. Zhu, M. Lu, Y. R. Wang, S. J. Yao, M. Zhang, Y. H. Kan, J. Liu, Y. Chen, S. L. Li and Y. Q. Lan, Efficient electron transmission in covalent organic framework nanosheets for highly active electrocatalytic carbon dioxide reduction, *Nat. Commun.*, 2020, 11, 497.
- 214 Q. Wu, M.-J. Mao, Q.-J. Wu, J. Liang, Y.-B. Huang and R. Cao, Construction of Donor–Acceptor Heterojunctions in Covalent Organic Framework for Enhanced CO<sub>2</sub> Electroreduction, *Small*, 2021, 17, 2004933.
- 215 N. Huang, K. H. Lee, Y. Yue, X. Xu, S. Irle, Q. Jiang and D. Jiang, A stable and conductive metallophthalocyanine framework for electrocatalytic carbon dioxide reduction in water, *Angew. Chem., Int. Ed.*, 2020, 132, 16730–16736.

- 216 M. Lu, M. Zhang, C.-G. Liu, J. Liu, L.-J. Shang, M. Wang, J.-N. Chang, S.-L. Li and Y.-Q. Lan, Stable Dioxin-Linked Metallophthalocyanine Covalent Organic Frameworks (COFs) as Photo-Coupled Electrocatalysts for CO2 Reduction, Angew. Chem., Int. Ed., 2021, 60, 4864-4871.
- 217 H. Liu, J. Chu, Z. Yin, X. Cai, L. Zhuang and H. Deng, Covalent Organic Frameworks Linked by Amine Bonding for Concerted Electrochemical Reduction of CO2, Chem, 2018, 4, 1696-1709.
- 218 G. C. Dubed Bandomo, S. S. Mondal, F. Franco, A. Bucci, V. Martin-Diaconescu, M. A. Ortuño, P. H. van Langevelde, A. Shafir, N. López and J. Lloret-Fillol, Mechanically Constrained Catalytic Mn(CO)3Br Single Sites in a Two-Dimensional Covalent Organic Framework for CO2 Electroreduction in H<sub>2</sub>O, ACS Catal., 2021, 11, 7210-7222.
- 219 S. An, C. Lu, Q. Xu, C. Lian, C. Peng, J. Hu, X. Zhuang and H. Liu, Constructing Catalytic Crown Ether-Based Covalent

- Organic Frameworks for Electroreduction of CO2, ACS Energy Lett., 2021, 6, 3496-3502.
- 220 Y. Song, J.-J. Zhang, Z. Zhu, X. Chen, L. Huang, J. Su, Z. Xu, T. H. Ly, C.-S. Lee, B. I. Yakobson, B. Z. Tang and R. Ye, Zwitterionic ultrathin covalent organic polymers for highperformance electrocatalytic carbon dioxide reduction, Appl. Catal., B, 2021, 284, 119750.
- 221 H. Dong, M. Lu, Y. Wang, H.-L. Tang, D. Wu, X. Sun and F.-M. Zhang, Covalently anchoring covalent organic framework on carbon nanotubes for highly efficient electrocatalytic CO2 reduction, Appl. Catal., B, 2022, 303, 120897.
- 222 Y.-L. Yang, Y.-R. Wang, L.-Z. Dong, Q. Li, L. Zhang, J. Zhou, S.-N. Sun, H.-M. Ding, Y. Chen, S.-L. Li and Y.-Q. Lan, A Honeycomb-Like Porous Crystalline Hetero-Electrocatalyst for Efficient Electrocatalytic CO2 Reduction, Adv. Mater., 2022, 34, 2206706.